Galloping, Bounding and Wheeled-Leg Modes of Locomotion on Underactuated Quadrupedal Robots

James Andrew Smith

Department of Mechanical Engineering
McGill University
Montreal, Canada

November 2006

A thesis submitted to McGill University in partial fulfillment of the requirements for the degree of Doctor of Philosophy.

2006/11/09

Your file Votre référence
ISBN: 978-0-494-32240-6
Our file Notre référence
ISBN: 978-0-494-32240-6

"*Life is like riding a bicycle. To keep your balance you must keep moving.*"
- Albert Einstein

Dedication

Cette thèse est dédiée à ma belle Michelle.

Abstract

This thesis presents advances in the state-of-the-art in legged locomotion through the development of bounding and galloping gaits as well as new modes of hybrid wheeled-leg modes of locomotion. Two four-legged running robots, Scout II and PAW, are examined, the latter of which is distinguished by actuated wheels at the ends of its legs.

First, hybrid modes of locomotion are demonstrated which use legs to dynamically reposition wheels at specific locations with respect to the body. These modes improve the stability and tire-wear of turning and braking manoeuvres and allow pitch-controlled slope ascent and descent in a wheeled-leg vehicle such as the PAW robot.

Second, through hip actuation, passive leg compliance and controlled wheel action it is possible to make the same vehicle run using a *dynamically stable legged gait* called the *bound.* Experimental evidence of this is presented and compared to similar experiments on the same robot with mechanically blocked wheels, a 3D simulation of the same, as well as bounding on a completely different quadrupedal robot, Scout II. While a casual observer finds no difference in blocked-wheel and active wheel control modes, detailed examination of the gaits reveals lower speeds and efficiency as well as decreased repeatability when the wheels are actively controlled.

A new method of forward speed control is presented for the bounding gait using liftoff, as opposed to touchdown, leg angles. The liftoff angle method of speed control is shown to be particularly suited to fine-tuning of certain gait performance indices.

Third, the underactuated bounding gait is extended to demonstrate, for the *first time*, that robotic *galloping* is possible and that it can be achieved in two underactuated quadrupedal robots and with varying levels of decoupled control. In the Scout II robot the front leg pair and rear leg pairs function independently, while in the PAW robot galloping is achieved with no controlled coupling between any of the four legs. The rotary gallop gait demonstrated by both robots is characterized by a significant yaw component and is compared to another bound-derived turning gait which uses liftoff angles to produce yaw. In particular, the correspondence of lead leg to yaw direction in both cases is found to match results from biology. In contrast, while it is thought that animals pivot about their lead leg to turn, the rotary gallop demonstrated by these robots shows that yaw occurs primarily in the leg *behind* the lead leg.

Résumé

Les travaux exposés dans cette thèse portent sur l'étude de trois formes de locomotion de robot : le roulement qui conjugue pattes et roues, le bond et le galop. Plusieurs centaines d'expériences ont été réalisées avec deux robots à pattes, Scout II et PAW. Ce dernier est équipé de jambes munies de roues actionnées.

Premièrement, le roulement, dans cette allure les pattes sont utilisées pour situer les roues à plusieurs endroits par rapport au torse du robot PAW. Ainsi, le robot tourne et freine d'une manière plus efficace et stable. Un système de commande incluant une centrale inertielle (Inertial Measurement Unit) a été développé pour garder le corps du robot à niveau lors de la montée ou de la descente de pentes.

Deuxièmement, le bond, une allure qui permet aux robots Scout II et PAW de courir, est démontré. Il est important de préciser que ces robots courent d'une manière rapide et stable avec un degré de liberté limité. Pour chacune des pattes, il n'y a qu'une hanche motorisée ainsi qu'un genou muni de deux ressorts. Ces résultats sont d'abord répétés en simulation et, par la suite sur le robot PAW avec des roues motorisées. Cette dernière forme de bond a été jugée moins efficace que le bond à pied non-actionnè. De plus, une nouvelle méthode de commande de vitesse est introduite; celle-ci sert à l'angle de décollage au lieu de l'angle d'atterrissage de la patte. Cette méthode de commande est aussi utilisée pour changer la direction du bond du robot.

Troisièmement, la commande du bond est modifiée pour démontrer, pour la première fois, que le galop est possible avec des robots sous-actionnés. Le galop est démontré sur les deux robots, Scout II et PAW. De plus les résultats prouvent qu'il est possible de réaliser cette allure avec un système de commande à accouplement élémentaire, ou même sans accouplement du tout. Finalement, contrairement aux animaux qui amorcent un mouvement de lacet autour d'une jambe antérieure, le robot utilise une jambe postérieure comme pivot.

Acknowledgments

I would like to thank my two co-supervisors, Inna Sharf and Martin Buehler, for sharing their insight and for their patience and perseverance. In particular I would like to thank Martin for giving me the ARL "bug" and showing me what innovation is in an up-close-and-personal way. I am also hugely indebted to Inna for instilling a sense of discipline and order in my research – it cannot be overstated how important she has been to helping me get my work done. Her persistence in hammering home important lessons and her attention to detail have truly been amazing.

Ioannis Poulakakis, a fellow graduate student and good friend, has been instrumental, throughout my time at McGilll, in opening my eyes to the realities of academia. Thank you, Ioannis, for the great conversations!

I really need to thank Aaron Saunders for being an amazing sounding board for all sorts of ideas, engineering and otherwise. You've been, and continue to be, a great supporter and friend.

Dave McMordie and Don Campbell: you guys have been inspiring examples of great electrical engineers. From the day I interviewed to get into the lab and throughout our time outside the lab I've been astonished at what you guys are able to do.

Many thanks are in order for Neil Neville who helped me put together the MSC.ADAMS simulation.

Shane Saunderson and Chris Prahacs have been tremendous resources in the ARL and MLL. Thanks for helping me with drilling out set screws, gluing stuff together and debugging all manner of electro-mechanical problems.

Alessio Salerno: thank you for the great talks, the proof-reading, the suggestions and being an overall great guy.

François Deschênes: Un gros merci! J'ai vraiment apprécièe nos discussions! Merci M. Brassens, maître de Quake! Yiiiiô!!

Thank you to Felix Grimminger and Matt Smith for the mechanical engineering advice while I worked on both Scout II and PAW. Also, I would like to extend a big thank you to other ARL/MLL lab members, past and present: Ned Moore, Neil Wyper, Evgeni Kiriy, Aki Sato, David Cowan, Nicola Plamondon and Christine Georgiades.

An appreciative thank you goes out to Carl Steeves who did the original simulations and design work, and first portion of the construction of the PAW platform.

Thank you to the great undergrads that have passed through the lab. Enrico Sabelli and John Sheldon: you've been outstanding – top notch! – people to work with. Thank you, also, to Julien Marcil and Mike Tolley for your work on PAW.

Thanks to Robert Battaglia, Anca Cocosco, Martin de Lasa, Nadim El-Fata, Geoff Hawker, Sami Obaid, Didier Papadopoulos, Shervin Talebi and Ken Yamazaki who worked on Scout II prior to my arrival in the ARL. The work that both Ioannis Poulakakis and I conducted would not have been possible without your contributions to Scout II. Your work on Scout II also helped lead to further work on the PAW project.

Greg Dudek, Ioannis Rekleitis, Philippe Giguère and the rest of the crew in the MRL: thanks for all the help you've given me with respect to threads and general coding and CS questions.

Thank you to Frank Ferrie and the Faculty of Engineering's Dean's Office. Frank: you're unwavering support for the students in the lab and the work we do has been second-to-none. Thanks!

To Terry Tobin and the wonderful folks at the Faculty of Engineering Development Office: thank you so much for helping us get the word out about legged locomotion!

Merci beaucoup to the Mechanical Engineering and CIM support staff: Cynthia Davidson, Marlene Gray, Lili Misztal, Mary Fiorilli, Joyce Nault, Jean Millikin, Melissa Brown, Gen Vinois, Irene Cartier, Jan Binder and Danny Chouinard. Without all of you it would be next to impossible to get things done around here. Thanks for being such great resources!

I also want to acknowledge the support of DRDC / RDDC - Suffield. Thank you for getting behind the ANT and PAW projects prior to my arrival at the ARL and for the continuous support while I was involved in the PAW project. Specifically I would like to thank Mike Trentini, as well as Blake Beckman, Chris Brosinsky, Greg Broten, Bruce Digney, Doug Hanna, Clément Laforce, Steve Penzes, Sean Verret and Isabelle Vincent.

Thank you to Prof. Kabal, of McGill's Electrical Engineering Department for the LaTeX template used for this thesis.

I would like to thank my family for supporting me throughout my time at McGill. Merci à ma famille ici à Montréal, à Lévis et à Sainte-Foy. J'ai bien aimé le temps qu'on à pu passé ensemble. Merci Serge, Jean-François, Marcelle, et Louise! Merci d'avoir été si interessé dans mes projets. Un gros merci Benoît de m'avoir aidé à traduire le résumé. Thanks to the Huth clan in Vancouver for listening to my robot stories. Thank you, Dad, for the feedback, the suggestions and the constant support. Thanks, Mom, for patiently

listening to me, even when my yammering about galloping didn't make any sense at all. Thank you, Tom, the greatest brother anyone could ask for, for inspiring me to be a better engineer (who knew helping me with that Lego robotics project was going to lead to, eh?).

Finally, I couldn't have done this without my wife's unwavering support... thanks so much Michelle for your patience and understanding!!

Contents

List of Figures

List of Tables

Symbols

φ	Leg/hip angle with respect to body.
$\dot{\varphi}$	Leg/hip angular velocity with respect to body.
φ_{td}	Leg/hip angle at leg touchdown event.
φ_{ftd}, φ_{rtd}	Front and rear leg/hip angle at leg touchdown event.
φ_{lo}	Leg/hip angle at leg liftoff event.
φ_{flo}, φ_{rlo}	Front and rear leg/hip angle at leg liftoff event.
φ_{swl}	Leg/hip commanded sweep limit. Ideally equal to φ_{lo}.
φ_{L1}, φ_{L2}	Leg/Hip angles for the first and second member of a lateral leg pair.
$\dot{\varphi}_{L1}$, $\dot{\varphi}_{L2}$	Leg/Hip angular velocities for the first and second member of a lateral leg pair.
ϵ	Desired angular difference between lateral legs.
γ	Leg/hip angle with respect to gravity vector.
τ_j	Applied joint torque.
τ_j	Applied joint torque with motor, gearhead and pulleys but not amplifier saturation.
τ_{jd}	Desired joint torque.
τ_{sjd}	Desired synchronizing joint torque.
τ_{MAX}	Maximum rated (stall) joint torque.
τ_m	Applied motor (bare motor; i.e. no gearing, etc.) torque.
τ_{md}	Desired motor (bare motor; i.e. no gearing, etc.) torque.
A	Slope of joint speed/torque curve.
ω	Motor speed.
n	Gear ratio.
η	Gear efficiency.
α, β	Gearing conversion factors related to n and η.
K_T	Motor torque constant.

K_ω	Motor speed constant.
K_A	Amplifier feedback voltage-to-current gain.
R_a	Motor armature resistance.
R_b	Internal battery resistance.
V_b	Battery voltage, at the terminals.
$\bar{V}_b$	Average battery voltage, at the terminals.
V_{bn}	Nominal battery voltage.
V_{Ai}	Amplifier i signal voltage.
i_b	Battery current.
i_{MAX}	Maximum motor amplifier current.
i_d	Desired current corresponding to a desired bare-motor torque, τ_{md}.
ϑ_j	Joint angle (PD Controller).
ϑ_{jd}	Desired joint angle (PD Controller).
$\dot{\vartheta}_j$	Joint angular velocity (PD Controller).
$\dot{\vartheta}_{jd}$	Desired joint angular velocity (PD Controller).
k_P	PD controller proportional constant.
k_D	PD controller derivative constant.
m	Body mass.
I	Body inertia matrix.
L	Half the spacing between front and rear hips.
k	Leg spring constant.
ψ	Body roll angle used during inclined turns.
H	Desired COM height used during inclined turns.
l	Maximum leg length.
$\hat{l}$	Leg length from hip to wheel axle.
W	Body width (midway between front and rear toe-to-toe widths).
h	Inner leg hip height during inclined turns.
w_R	Wheel radius.
r_C	Turning radius of the ground-projected COM during inclined turns.
r_I, r_O	Turning radii of the inner and outer wheels during inclined turns.
x_I, x_O	x-coordinates of the inner and outer wheels used during inclined turns.
y_I, y_O	y-coordinates of the inner and outer wheels used during inclined turns.
v_I, v_O	Velocities of the inner and outer wheels during inclined turns.

v_C	Velocity of the COM during the inclined turn.
v_{fI}, v_{fO}	Velocities of the front inner and outer wheels during inclined turns.
v_{rI}, v_{rO}	Velocities of the rear inner and outer wheels during inclined turns.
θ	Body pitch angle.
ξ	A gain used in IMU-assisted slope ascent and descent.
Δt	Elapsed time from one control cycle to the next. Generally about 1 ms.
$\varepsilon(v)$	Specific resistance, a function of forward speed.

Chapter 1

Introduction

This thesis presents advances in the state-of-the-art in legged locomotion through the development of bounding and galloping gaits as well as new modes of hybrid wheeled-leg modes of locomotion. The experimental work reported in this thesis was conducted on two quadrupedal robots, Scout II and PAW, designed and constructed at McGill University between 1998 and 2004. Design details, controller details, simulated and experimental gait development, and corresponding results are presented in the context of advancing the state-of-the-art in legged locomotion, especially within the context of advancing dynamically stable legged locomotion, especially for underactuated quadrupedal robots with minimal sensing and simple feedback control strategies. In the following we introduce the main topics discussed in this thesis.

1.1 Literature Review

A detailed survey of the relevant state-of-the-art in wheeled-leg systems and in dynamically stable legged locomotion is presented in Chapter 2. Traditional wheeled and tracked systems are briefly discussed and the transition to legged systems is made by way of hybrid wheeled-leg systems which contain elements of both mobility paradigms. Focusing specifically on legged systems, the topics of walking, running and biomimetics are discussed, which then leads to the topic of bounding and galloping systems. Finally, an outline of the specific contributions of this thesis is presented at the end of the chapter.

1.2 Robot Design

In Chapter 3 basic design details on the Scout II and PAW robots are given. Both robots are underactuated, minimally sensing robots, but PAW incorporates actuated wheels at the distal ends of the legs, while Scout II has conventional fixed toes. The PAW robot is smaller and more compact than Scout II, reflects design and implementation lessons learned on Scout II, and thus shares many features, including body shape and leg design, but also hip actuators, power source, computing and control hardware. The methods for basic actuator control are examined, taking into account the fact that neither the power source, nor the amplifiers or motors are ideal. While the Scout II robot is uniquely a dynamically stable running robot, the addition of wheels and wheel actuators on PAW enable it to replicate many of Scout II's running behaviours but also produce new hybrid wheeled-leg modes of mobility. The Spring Loaded Inverted Pendulum (SLIP) model is presented as an introduction to the concept of using compliant legs for running. The discussion on SLIP leads to the application of the φ-controller, in which touchdown angle is used as the primary control input, to the bounding and galloping gaits. A variation on this controller is presented and establishes the liftoff angle, φ_{lo}, as a second important control parameter for forward speed control in the bounding gait.

1.3 Simulation of PAW Robot Bounding

A three-dimensional MSC.ADAMS simulation of the PAW robot is presented in Chapter 4. The model is based on the geometric and mass properties established in the original design of the robot. The φ-controller is developed in Matlab and interacts with the MSC.ADAMS Solver via the MSC.ADAMS/Controls toolbox. While the simulated and actual experimental bounding gaits conducted on PAW are qualitatively similar, there are some small quantitative differences between parameters such as leg phase difference and duty cycle. Through the simulation it is found that the tendency to yaw counter-clockwise during the bound on the PAW and Scout II robots is due to asymmetric mass distribution in both robots. Lastly, a test of the hypothesis that liftoff angle can be used to regulate forward speed is conducted in simulation and the results are found to confirm results obtained later in experimental tests.

1.4 PAW Rolling Mobility Behaviours

Chapter 5 presents wheeled mobility work on the hybrid wheeled-leg PAW robot. Three rolling mode controllers are introduced which take advantage of the hybrid nature of the platform and improve stability. The inclined turning method illustrates how to improve turning over simple skid-steering by repositioning the wheels and lowering the centre of mass. The reduction in shear forces which wear down the tires is found to be immediately beneficial, whereas future benefits include better stability at higher speeds due to the lowering of the center of mass. An improvement to braking is made by placing the wheeled-legs in a sprawled position prior to braking and using the wheel motors to dissipate energy. The ability to reposition the wheeled-legs is then combined with inertial feedback to develop a controller for maintaining body pitch while climbing slopes. Rolling speeds of up to 2.0 m/s have been demonstrated on the robot, as has an operational range of over 2500 m.

1.5 Bounding Gait on Scout II and PAW

Experimental results for quadrupedal bounding, using the Scout II and PAW robots, are given in Chapter 6. While bounding forward speed control is achieved by using variation of *touchdown* angle, φ_{td}, on both robots, it is shown here, for the first time that *liftoff* angle, φ_{lo}, effected by the sweep limit, φ_{swl}, is a dominant parameter for speed control. The conclusion reached is that the φ_{td} and φ_{lo} control parameters are complementary, with φ_{td} and φ_{lo} yielding coarse- and fine-tuning capability, respectively. In addition, the bounding gait is explored using the wheels which are mounted on the distal ends of PAW's legs. These results are compared to fixed toe bounding gaits achieved on both Scout II and PAW, the latter with wheels mechanically blocked.

Power efficiency is found to be better at higher speed in both robots during the bounding gait, with notable decrease in efficiency in PAW when active wheel control is used. Finally, measures for gait success are presented and the bounding gaits for both robots are shown to have good rates of convergence, stable limit cycles and very good repeatability.

1.6 Gallop Gait on Scout II and PAW

Finally, Chapter 7 presents the first gallop gaits on non-simulated, mechanical artificial systems. The work on Scout II and PAW galloping shows that underactuated galloping can be achieved with leg compliance and only four hip actuators. This is significant because all previously proposed 3D gallop controllers have required a minimum of eight actuated degrees of freedom. Also, until now and without exception, no individual or group has achieved galloping on a real robot. The rotary gallop gait variant is demonstrated here on not one, but *two* robots.

The controller used to achieve galloping is derived from the φ-controller, and requires far less controlled coupling than has previously been suggested. On Scout II galloping is achieved by only coupling lateral leg pairs. In PAW, leg control is completely independent, with no coupling between any leg. The basic experimental results obtained on Scout II and PAW, which exhibit a significant yaw component, are given and contrasted with the results of the φ_{lo}-turn controller, which uses differential liftoff angles in lateral leg pairs to achieve yaw, as opposed to the gallop controller which uses differential touchdown angles. While it is easier to maintain higher forward speeds with the φ_{lo}-turn controller, the range of yaw rates is greater with the gallop controller. The relationship found in biology between yaw direction and the "leading" leg in the gallop gait is found to also occur in the two artificial systems used in this thesis. Finally, stability of the galloping and φ_{lo}-turn gaits is examined and the gaits are found to have good rates of convergence, good repeatability and low stride frequency standard deviation.

Chapter 2

Literature Review

This thesis describes work conducted on two quadrupedal robots, Scout II and PAW, which use a low number of actuated and passive compliant degrees of freedom to run. While running gaits are widely used in nature they are rarely seen in robots. The bounding gait has been demonstrated on only a select number of robots, while the gallop has *only* been demonstrated on *two* robots, Scout II and PAW, shown in Figs. 2.1 and 2.8 (see p. 17). PAW can also be configured to use actuated wheels at the distal ends of its compliant legs in both bounding and wheeled modes of locomotion.

What follows is a survey of the relevant state-of-the-art in wheeled-leg systems and in dynamically stable legged locomotion. To begin with, in Section 2.1, traditional wheeled and tracked systems are discussed. The transition to legged systems – the main focus of this thesis and the topic of Section 2.3 – is made by way of hybrid wheeled-leg systems which contain elements of both mobility paradigms, in Section 2.2. In addition to a general discussion on running and biomimetics, in Sections 2.3.1 through 2.3.3, attention is focused, in Section 2.4, on relevant work conducted on the bounding and galloping gaits. Finally, Section 2.5 outlines the specific contributions of this thesis.

2.1 Small/Medium Wheeled and Tracked Mobile Robots

Designers of ground-based mobile systems tend to create vehicles which use wheels or tracks for locomotion for a number of reasons. These vehicle designs can take advantage of a large accumulated knowledge base, very good performance characteristics, and established methods for maintenance, construction and manufacturing, [1, 2, 3, 4]. These vehicles

offer an efficient and often rapid method of ground traversal, especially in conditions where the terrain is flat. Of particular relevance to the mobile robotics community, a number of studies have been performed on relatively small tracked or wheeled platforms (e.g. [5] and [6]), of which iRobot's PackBot [7] (see left of Fig. 2.1) is one of the more successful and widely deployed examples. One of the keys to its success is the use of foot-like tracked paddles. The modification of wheeled and tracked vehicles with leg-like features is expanded upon in the next section.

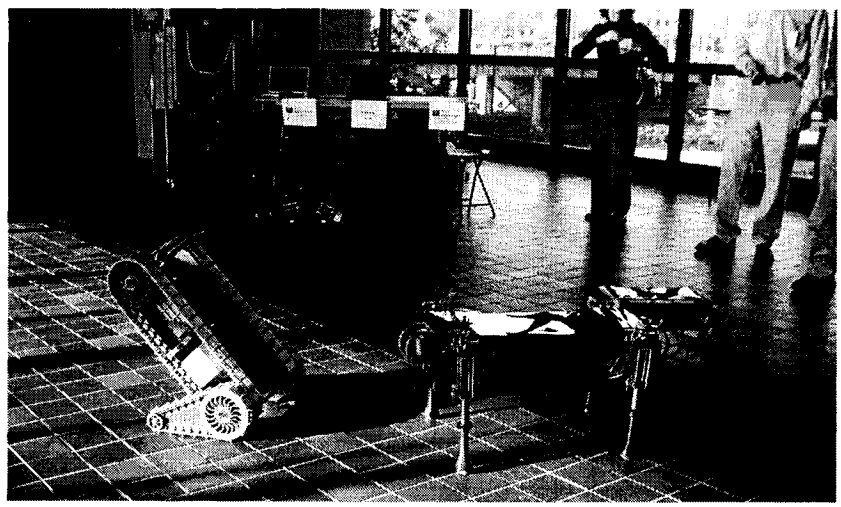

Fig. 2.1 iRobot's tracked PackBot (left) and the McGill's legged Scout II robot (right) at a demonstration at Department of National Defence Headquarters, Ottawa, Canada. The PAW and RHex robots are in the background.

2.2 Wheeled-Leg Systems

As mobile robots are required to operate outside the laboratory, the limitations of traditional wheeled and tracked vehicle designs become increasingly apparent: their simple and robust design does not provide sufficient versatility and adaptability for many real-world terrain conditions. Generally, these vehicles have difficulty overcoming obstacles higher than half the diameter of the wheel and are prone to problems such as detracking (or detreading). Design modifications, which add passive or active degrees of freedom with or without compliance, can be made to make the vehicles better suited to rough terrain. PackBot's active foot-like tracked paddles [7] (see Fig. 2.1) and Sojourner's passive bogies

(a) NASA's Sojourner

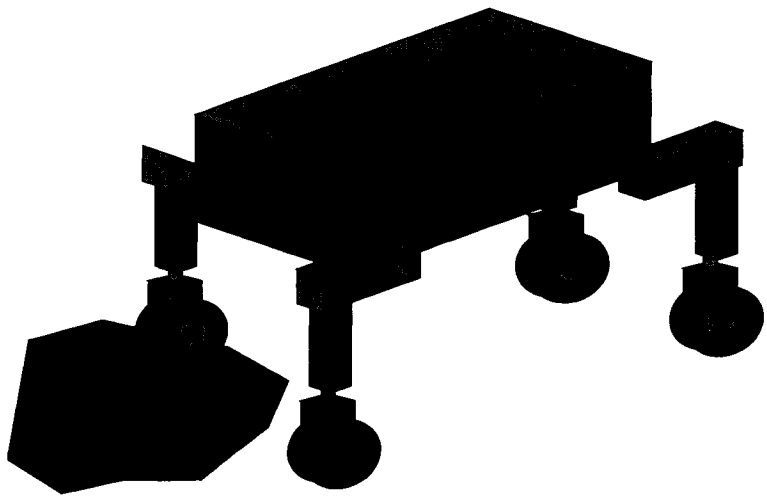

(b) Hylos-like Robot

(c) RHex

Fig. 2.2 Wheeled vehicles typically have difficulty traversing large obstacles. The addition of passive bogies, such as those found on Sojourner (a) help but are not always sufficient. The use of actuated legs like those found on some Hylos-like hybrid wheeled-leg robots (b) (adapted from [8]) or the the recirculating variety found on RHex (c) can make traversing large obstacles much easier. [*Sojourner photo courtesy of Jet Propulsion Labs.*]

[9] (see Fig. 2.2a) are examples of modifications made to traditional tracked and wheeled vehicles that have enabled greater mobility. From an opposite perspective, one model of the legged RHex robot uses a second actuator to move the pivot point on its half-circle fibreglass legs to allow selection of more leg-like or more wheel-like modes of locomotion, depending on the encountered terrain, [10] (see Fig. 2.2c).

It is possible to obtain many of the advantages of both traditional wheeled and legged systems by combining aspects of these into a single articulated suspension platform. The Roller-Walker robot, [11], has demonstrated that passive wheels attached to the distal ends of actively-controlled legs can allow a vehicle to roll along a surface. The Shrimp system negotiates terrain with actuated wheels and a passive adaptation mechanism, [12]. In contrast, the Hylos system, similar to the adaptation in Fig. 2.2b, uses active posture control to adapt to irregular terrain in order to maintain stability and traction, [8].

2.3 Legged Systems

As more robots are designed to operate in the real world, the limitations of traditional wheeled and tracked vehicular designs have become increasingly apparent. To overcome these limitations one branch of the mobile robotics field has turned to biological inspiration for other possible solutions including legged systems, which promise a versatility and mobility unparalleled in more traditional designs.

Early attempts to implement legged designs resulted in slow moving *statically stable* systems; these manipulator-derived designs are still the most prevalent today, [13, 14, 15, 16]. However, in this thesis attention is restricted – with the exception of PAW's complementary wheeled behaviours – to *dynamically stable* legged robots. To date, the most significant research on dynamic legged locomotion occurred at the CMU and MIT Leg Labs in the 1980s and 1990s pioneered by M. Raibert, [17]. Raibert's research revolved around simple fundamental principles for controlling hopping height, forward speed and body posture, making complex gaits possible on monopedal, bipedal and quadrupedal robots. His three-part controllers, although very simple, resulted in high performance running with different gaits. Recent research, [18], conducted at McGill University's Ambulatory Robotics Lab has shown that even simpler control laws, which position the legs at a desired touchdown angle, without requiring task-level or torso-state feedback, can achieve stable running at speeds up to 1.3 m/s in Scout II (Fig. 2.1), despite the absence of active control over leg

length, and with only one actuator per leg, [19].

This thesis focuses on the implementation of the bounding and galloping gaits, two forms of dynamically stable gait. The galloping results are *especially significant* since they have *never before been studied* in non-simulated artificial quadrupeds. Although galloping has been studied in biological systems, [20, 21], and in simulation, [22, 23, 24, 25, 26, 27], the gallop gaits (rotary and transverse gallops, as well as the little-known toelt) and the related half-bound had not been implemented on any mechanical system until recently, [28, 29], first with Scout II and then with PAW.

Regardless of the potential advantages of legged systems, wheeled and tracked systems continue to outperform their legged counterparts, as demonstrated in the recent trials at the Southwest Research Institute, headquartered in San Antonio, Texas, USA, [6]:

> [iRobot's tracked] PackBot is generally faster, can climb steeper slopes and higher curbs, and travels more meters per watt-hour of energy. [The legged] RHex appears to have better mobility and higher speed in certain types of rough terrain ... and to have similar power efficiencies for on- and off-road terrains. We note that the PackBot has over four years of focused development and testing under its tracks, while the [Rugged RHex] vehicle has just begun the hardening and optimization cycle.

In general, legged systems are more complex, less efficient, have smaller operational ranges, and have higher peak energy and torque requirements than wheeled and tracked systems. Their payloads and sensors also must be designed to withstand or compensate for oscillatory motion. These factors lend credibility to detractive statements such as that made by Colin Angle, CEO of iRobot, that "Legs in my mind are for Hollywood." [30]

For all of these disadvantages legs still have potential advantages, whether they are used in strictly legged systems like Scout II or hybrid wheeled-leg systems like PAW. Biological examples of legged systems that all readers are familiar with reinforce the notion that legs provide versatility, redundancy and potential adaptability that traditional wheeled and tracked systems can not. For instance, the compliant elements in the legs of robots such as Scout II and PAW act to decouple the payload and center-of-mass of the robot from the ground, effectively acting as suspension; this is a useful, potentially energy-saving feature if the terrain is rough. Furthermore, unlike many other legged systems, the hexapedal RHex robot (as well as similar systems presented in [31] and [32]) does not attempt to

exactly determine the toe placement of its compliant recirculating legs with respect to its environment. Its control is effectively feed-forward, relying on *mechanical intelligence* [33]. Practically speaking this requires the use of passive compliant elements that react to disturbances in a *preflexive* rather than deliberate, actuated *reflexive* manner. This is a key paradigm shift with respect to traditional, rigid, manipulator-derived legged systems and is key to improving the performance of legged and wheeled-leg systems with respect to their strictly wheeled counterparts.

Underactuated systems such as the quadrupedal Scout II [18] and hexapedal RHex [34] have allowed researchers to examine fundamental elements of legged locomotion which were not easily studied in earlier systems with more actuated degrees of freedom. From these systems new capabilities have been discovered and new lessons have been learned, opening up new directions for research. Platforms descended from RHex such as AQUA [35] and RiSE, [36], are demonstrating versatility with respect to real-world mobility by adding amphibious and scansorial (climbing) features that are unparalleled in traditional wheeled and tracked systems. Wheels (and tracks) and legs are not mutually exclusive: systems such as the Scout II-derived PAW, [37], are approaching the issue of ground mobility by combining wheeled and legged aspects – somewhat similar to the notion of adding bogies and tracked feet in Sojourner and PackBot.

2.3.1 Running Versus Walking

Legged systems, regardless of the number of legs, are capable of two basic types of locomotion: walking and running. Intuitively, the distinction between walking and running is generally based on running having an aerial phase while walking does not.[1] Exceptions to this intuitive definition exist, such as [25], and so a more rigourous definition has been illustrated in [39] and summarized by McMahon and Cheng in [40] as:

> A better criterion[2] for distinguishing between walking and running is the one put forward by Cavagna *et al.* [41]. On the basis of observations in humans, they

[1] Definitions of running such as those put forward by Hildebrand [38] which propose that running gaits have step duty cycles of less than 50% or that put forward by Raibert which requires a body ballistic flight phase [17, p. 14] are not used in this thesis even though the author has experimentally demonstrated gaits, such as Scout II's rotary gallop, which meet both these requirements [29].

[2] A better criterion than "in running, all feet are in the air at some point in the gait cycle, whereas in walking there is always at least one foot on the ground".

pointed out that in walking, the center of mass is highest in mid-step, when the hip of the stance leg passes over the ankle. In running, by comparison, the center of mass is lowest at mid-step. Thus in walking but not in running, gravitational potential energy is stored in the first half of the walking step as the center of mass rises, and returned in the form of kinetic energy during the second half of the step as the center of mass falls.

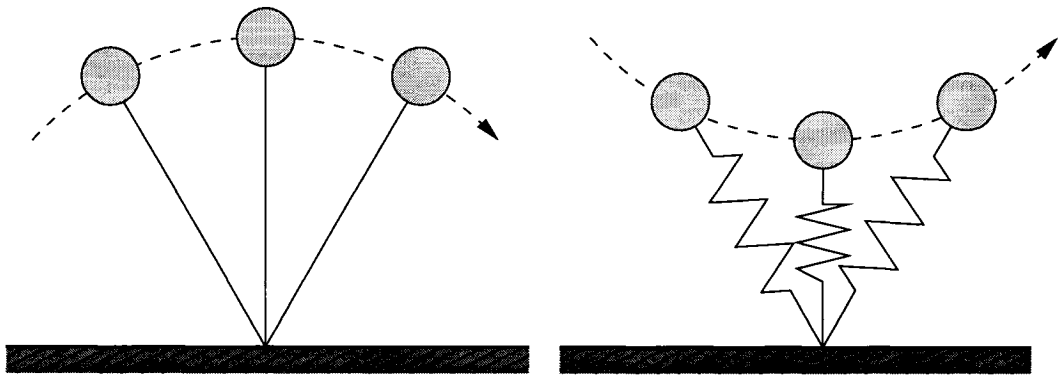

(a) Walking (b) Running

Fig. 2.3 The rigid inverted pendulum (a) is used to represent walking, while the Spring-Loaded Inverted Pendlum (SLIP) (b) is used to represent running.

The essence of the above description can be captured by two simple inverted pendulum mathematical models for walking and running, as illustrated in Fig. 2.3. The stiff inverted pendulum model is used to describe walking results, whereby at mid-stance the hip is at its highest point, travelling at its slowest speed, and one can observe a simple exchange between kinetic and gravitational energy occurring during stance. In contrast, for the spring-loaded inverted pendulum model of running the slowest point (as with walking it is at mid-stance) corresponds to the lowest hip height. The spring stores energy from the kinetic and gravitational potential components during the first half of the stance phase, and returning them during the second half. For an inverted pendulum system which does not contain compliance, the maximum speed at which it is able to move is $\sqrt{gl}$, where g is the gravitational constant and l is the leg length, [39]. The most famous examples of legged robots which use springs to achieve running are those developed by Raibert in the 1980's at the CMU and MIT Leg Labs, [17]. Robots derived from this pioneering

work, the controllers for which simplified by taking advantage of the spring-mass *natural* or *passive dynamics*, are generally classified as *dynamically stable legged robots* and are further described in Section 2.3.3.

2.3.2 Biomimetics

The physical and control designs of many legged and non-legged robots have and continue to be guided by *biomimesis*, the mimicking of biological systems. This section explores the application of biomimetics to robot design. Biomimetics can be found in many fields related to robotics, from artificial intelligence (e.g.artificial neural networks, [42]) to control (e.g. central pattern generators, [33]) to mechanical design.

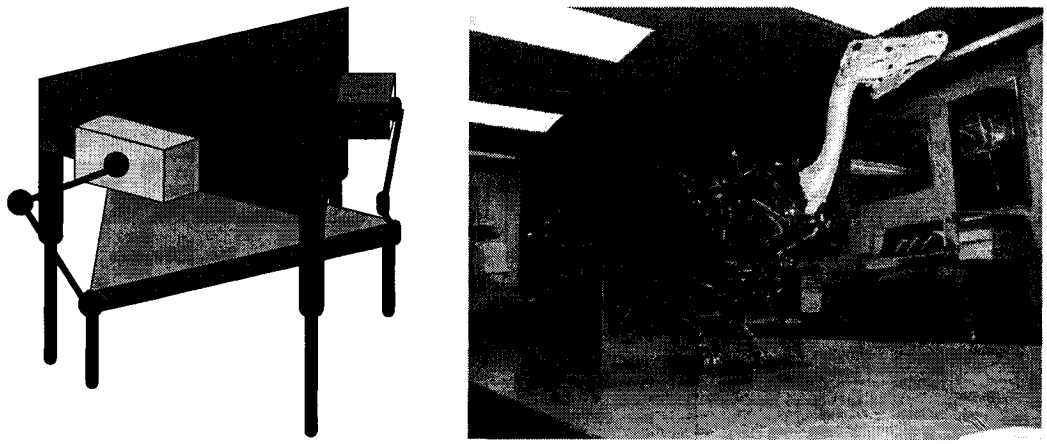

(a) Parallel Walker (b) Dilworth's Troody

Fig. 2.4 Examples of walking robot kinematics that accept or reject morphological biomimesis. The kinematic design of (a), similar to Parawalker2 [43], explicitly rejects the *morphologically biomimetic* paradigm, whereas the Troody "dinosaur" robot (b) is explicitly morpholocially biomimetic, [44]. [*Photo of Troody used with permission of Peter Dilworth.*]

At the same time, mechanical designs for legged systems do not necessarily have to be routed in the biomimetic paradigm. Many designs, such as Hirose and Yoneda's Para-Walker or Hyperion platforms [43], see Fig. 2.4a, are explicitly non-biomimetic in order to avoid poor performance resulting from the large mass generally associated with designs which mimic the kinematics of animals. Specifically, these designs reject *morphological biomimesis*, or the nearly one-to-one copying of animal morphological design parameters.

Adopting the *morphological biomimetic* paradigm, in which the mechanism is deliberately made to look like an animal, can be useful in applications where successful performance is not measured directly in terms of speed, power efficiency or accurate trajectory tracking. In the case of entertainment robots, where an emotional connection must be made between the audience and the robot, morphological biomimesis is an asset. Examples include Dilworth's Troody [44] (see Fig. 2.4b) and the Sony AIBO [16]. These systems, as with the non-biomimetic systems described earlier, often have no compliant mechanisms and are often over- or reduntantly-actuated.

Through careful examination of the task which is to be performed one can mimic biological designs without blindly copying unnecessary morphological elements. For example, in the case of locomotion, the objective is to get from point A to point B in a generally efficient, robust and rapid manner. From the *functional morphological* point of view, the mechanism which is to accomplish this goal must capture the most important task-oriented features of the biological analogue. In other words, the designer's task is to "develop analogies at the appropriate level of abstraction" [33]. Because of its relevance to biological running, concepts associated with sagittal plane *Spring Loaded Inverted Pendulum*, or *SLIP* [45, 39], can be applied to the design of running robots. For instance, running generally requires compliant mechanisms in the leg and speed can be regulated through control of leg angles prior to ground impact. This is the case for robots such as MIT/CMU Leg Lab monopod, biped and quadruped [17], the ARL's two monopods [46] and the Scout II quadruped [47], as well as the RHex series of robots [48] developed in collaboration by McGill University, the University of Michigan, the University of California at Berkeley and Carnegie Mellon University. Unlike over-actuated walking systems such as the Sony AIBO, many of these systems use minimal actuation (sometimes only a single actuator per leg) in conjunction with passive compliant elements. Because the number of actuators is less than the total number of degrees of freedom, these systems can be said to be *under-actuated.*

2.3.3 Dynamically Stable Legged Locomotion

This thesis focuses on dynamically stable legged robots which use modes of locomotion such as the bounding and galloping gaits, in contrast to slow-moving, statically stable walkers such as those illustrated in Fig. 2.4. As is discussed in [50] the term "dynamic stability" is taken to be, within the context of legged locomotion, the ability of characteristic state

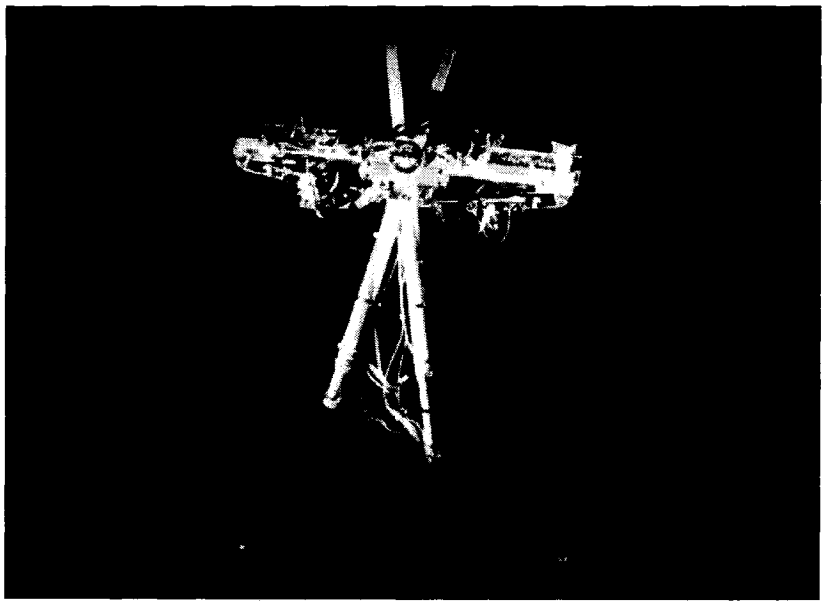

Fig. 2.5 Raibert's biped: one of the first examples of a fast moving, dynamically stable robot based on a Spring Loaded Inverted Pendulum model. [*Photo used with permission of MIT Press.*]

variables of the system (e.g., body pitch) to return to steady-state periodic motion (e.g. a bound or gallop gait) after the application of perturbations. In addition, the system often lacks or has marginal static stability, that is, the ground-projected COM falls close to the boundaries of the support polygon formed by the legs which are in contact with the ground. The reader is referred to Fig. 2.6 for a graphical overview of the various flavours of stability in legged locomotion.

Raibert's early research, [17], on *actively-balanced legged locomotion* revolved around fundamental principles for controlling hopping height, forward speed and body posture, making various gaits possible on monopedal, bipedal and quadrupedal robots equipped with compliant legs, see Fig. 2.5. His controllers, aided by Sutherland's "virtual leg" concept [51], resulted in fast and stable dynamic running with different paired-leg gaits, such as the trot, pace and bound. These concepts have been applied to a number of other robots, including the Scout II and PAW robots discussed in this thesis. Specific discussion on examples of dynamically stable quadrupedal robots is presented in Section 2.4.

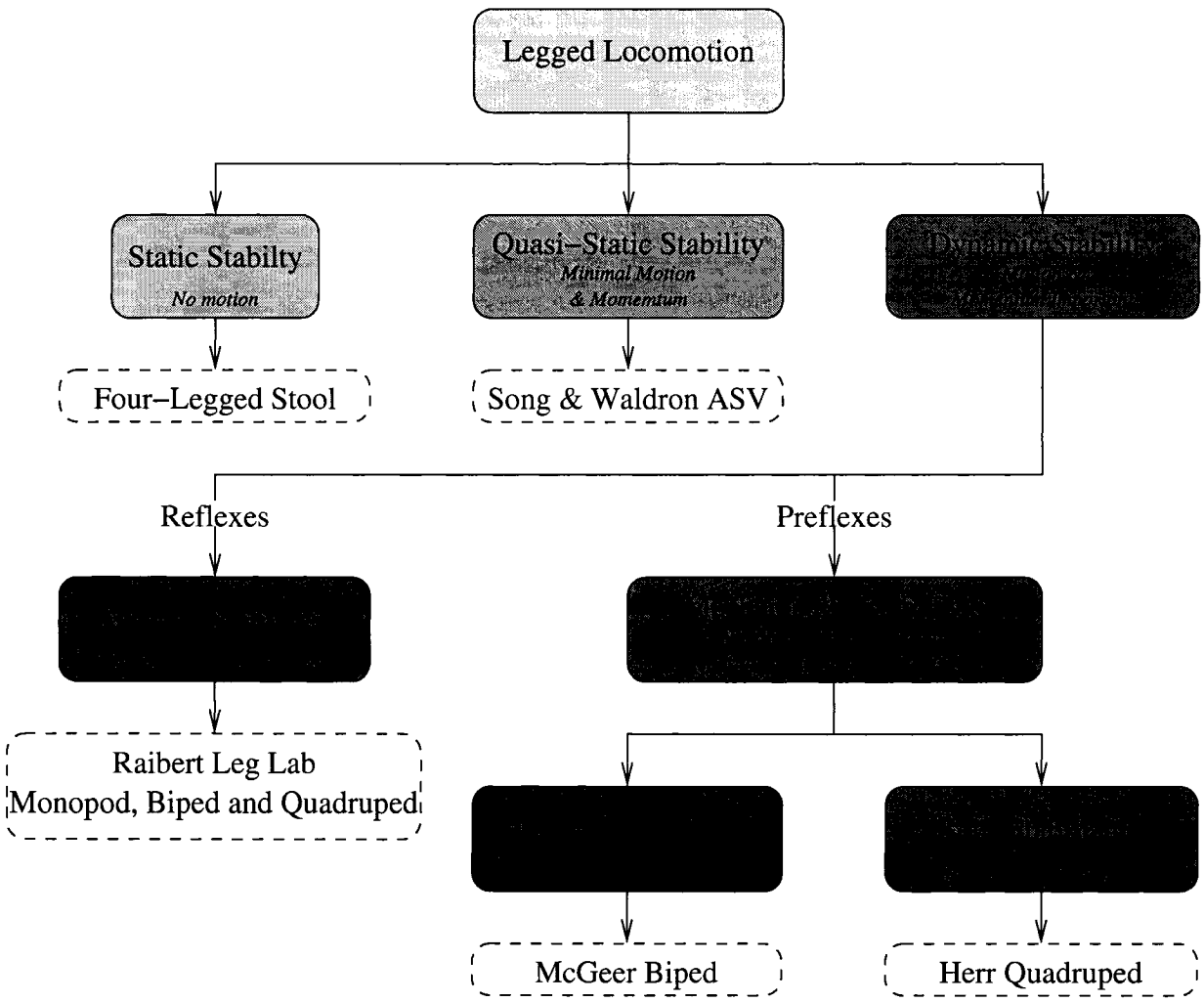

Fig. 2.6 Static vs. Dynamic Stability, in the context of legged locomotion. Adapted from [49, p. 14].

2.4 Quadrupedal Running: From Bounding to Galloping

In this section, work relevant to running in four-legged systems is discussed. In particular, the bounding and galloping gaits are examined with a particular focus on work that is relevant to the Scout II and PAW research.

Quadrupeds can run using multiple gait types, which are often classified by the order of ground contact of individual legs. One-beat gaits such as the pronk require that all legs touchdown together. Two-beat gaits such as the pace, trot and bound require touchdown to be conducted in pairs (right and left sides, diagonal or front and rear, respectively). Three-beat gaits, such as the half-bound and the canter require that one leg pair contact the ground at once, while the remaining legs contact the ground in an out-of-phase manner. In four-beat gaits such as the transverse and rotary gallop, as well as the toelt, the four legs touchdown at separate times. Some of these gaits, including the bound and rotary gallop, are illustrated in simplified form in Fig. 2.7. In this section we begin by examining paired two-beat gaits, primarily the bound, as a precursor to an examination of the related gallop gait.

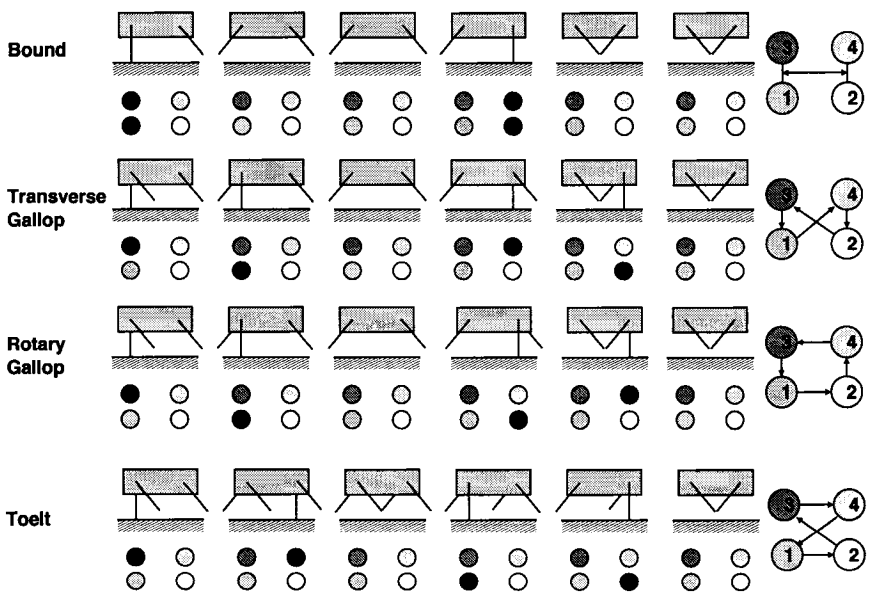

Fig. 2.7 Simplified footfall patterns bounding, galloping and toelting. Progression is left to right. The bound is a two-beat gait while the transverse gallop, rotary gallop and toelt are four-beat. These basic gait patterns also hold if multiple legs are in contact with the ground, as shown in Fig. 6.3 on p. 83.

2.4.1 Bounding

Other leg, body and controller designs for dynamically stable robots have been proposed since Raibert's work, noted in Section 2.3.3, including the articulated-knee Scamper bounding quadruped by Furusho *et al.*, [52]. Scamper's controller divided one running cycle into eight states and switched the two joints per leg between three control modes: free rotation, position control and velocity control. Following a different approach, Kimura *et al.* implemented bounding by transitioning from pronking in the Patrush robot based on principles from neurobiology, [53]. They combined explicit compliance with a neural oscillator network, whose frequency matched that of the spring-loaded mass, hopping vertically on a compliant surface. Patrush's three Degree-Of-Freedom (DOF) legs each featured an actuated hip and knee, and an unactuated, compliant foot joint while the robot was physically constrained to move in the sagittal plane by overhead beams.

(a) Scout II (b) PAW

Fig. 2.8 The Scout II (left) and PAW (right) robots are shown demonstrating the bounding gait. The PAW robot is using active wheel control during this bound gait.

A variety of leg designs have also been proposed, most involving more actuators than Scout II. One such recent design, currently being implemented, is the OSU-Stanford KOLT quadrupedal robot which houses all of the leg actuators at the hip or on the body, [54]. Engineers at Boston Dynamics have also begun field trials of a new hydraulically-actuated quadruped, BigDog, [55], which is capable of dynamically stable locomotion, using paired

gaits such as the trot.

Unlike these other designs, the Scout II robot houses only a single actuator per leg and uses one of the simplest controllers proposed to date, [18]. It has been demonstrated experimentally that dynamic running on flat ground via a bounding gait is possible by merely positioning the legs at a fixed desired touchdown angle during flight (not modified during successive strides), and commanding a motor torque during the stance until a sweep limit angle is reached. The most striking feature of the controller is that it only requires touchdown/lift-off detection and local feedback of the leg angles relative to the body. These are available from leg potentiometers and motor encoders respectively, which are the only sensors needed. The resulting motion is largely caused by the interaction between the actuators and the natural dynamics of the mechanical system. In a similar minimalist vein, speed regulation has recently been demonstrated on a hip-actuated quadruped with compliant legs using a single control parameter, [56]. Rather than use the touchdown angle for speed control, as is the case for Scout II and the Raibert Quadruped, this quadruped specifies either stride frequency or leg phase difference. In this thesis another, complementary, method of speed regulation is presented, using the liftoff, rather than the touchdown angles.

The bounding gait has not only been studied on robot platforms, like Scout II and PAW shown in Fig. 2.8, it has been examined using numerical models. Various mathematical models have been proposed to study dynamically stable quadrupeds. Murphy and Raibert studied bounding and pronking using a model with kneed legs whose lengths were controllable, [57]. They discovered that active attitude control in bounding is not necessary when the body's moment of inertia is smaller than the mass times the square of the hip spacing. The relationship between the mass, the pitch moment of inertia and the hip spacing is referred to as the *dimensionless moment of inertia.* Following up on their work, Berkemeier showed that this result applies to a simple linearized running-in-place model and that it can also be extended to pronking, [58]. Brown and Raibert investigated the conditions for obtaining passive cyclic motion, [57]. They studied two limiting cases of system behaviour – the grounded and the flight regimes – and found that the system in either regime can passively trot, gallop or bound if provided with the proper initial conditions. More recently, from a minimalist open-loop perspective – that is, with very little actuation and no task-level feedback – passively generated stable bounding of a conservative model of the Scout II quadruped was shown to be possible under appropriate initial conditions and sufficiently

high speeds [47, 59].

Through continued study of the bounding gait on Scout II, experimental validation of the dynamics model for Scout II in a bounding gait has been conducted in order to advance the state-of-the-art in modeling and simulation of dynamically stable legged systems. Although many models for open or closed loop dynamic legged locomotion have been studied (e.g. [23], [57], [58], [60], and [61]), and many simulation techniques have been proposed for efficient integration of the dynamic equations and visualization of the resulting motion (e.g. [62]), until recently no models existed in the literature, which were experimentally validated down to the actuator torque level. In [18], Poulakakis *et al.* proposed and tested various modeling assumptions for the Scout II quadrupedal robot and showed that power autonomous legged robots like Scout II typically operate at the torque-speed limits of their actuators, and that their simulated analogues require a model of the actuator dynamics and their interaction with the power source. Some of the modeling details are also presented in Chapter 3, while experimental measurements illustrating operation along these limits are shown in Fig. 6.13.

2.4.2 Galloping

Paired, two-beat gaits such as the pronk, the trot and the bound have all received a fair amount of experimental and numerical study [17, 28]. Although these gaits have been studied in biological systems [20, 21] and in simulation [23, 24, 25, 63, 27, 22], the gallop (as well as the half-bound) had not been implemented on any mechanical system until recently [28, 29], using the Scout II robot, in spite of the desire by at least two research groups to do so [64, 65]. This thesis is a continuation of the work introduced in [28, 29].

The gallop is a four-beat gait – that is, each of the four legs touches down on the ground sequentially. Two variations of the gallop are generally admitted to exist in the animal world: the transverse, in which the footfall pattern connects the front and rear lateral legs diagonally, and the rotary, in which the footfall pattern alternates between longitudinal and lateral throughout the stride, see Fig. 2.7. A galloping dog is shown in Fig. 2.9. A third four-beat gait, similar to the two gallops also exists and is referred to alternatively as the canter [66, p. 21], toelt[3] [67] or "backward cross type" [68]. At its extreme, when the phase differences between leg pairs in the gallop approach zero, the gait

[3]Toelt: alternatively, tölt

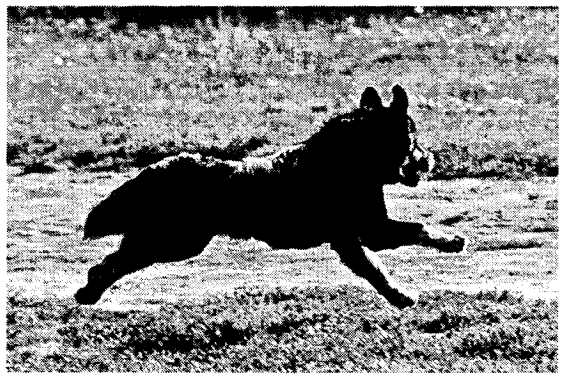

Fig. 2.9 A galloping dog.

becomes a bound, a trot or a pace.

Some choose to make further distinctions of galloping gaits based on terms such as "cursoriality", [69] and [70], claiming that some forms of gallop are cursorial and others, are not. The use of this term is controversial, especially with respect to the assumed straightforward relationship, complete with clear-cut categorical delineations, between morphology and gaits, [71]. Therefore, cursoriality is herein simply considered to refer to running (as opposed to walking) and therefore encompasses all forms of galloping, regardless of morphology.

At present, the next most relevant work on robotic galloping is being conducted at Ohio State and Stanford Universities on the KOLT robot and related simulated models. A number of simulations, mostly concentrating on the transverse gallop in the sagittal plane, [72, 24] have been conducted. To the author's best knowledge, no results of any galloping implementation based on this group's research have been published as of the time of this writing.

Forward Speed and Energetics

The gallop is widely acknowledged [73, 60, 74, 25] to be the fastest quadrupedal gait in nature. Although the gallop is considered to be the fastest gait, there are possible exceptions in some animals. The Icelandic horse can use the two-beat "flying pace" at speeds rivaling the gallop [75, 76], [4] while some animals tend to the bound and half-bound from the gallop as speed increases, as is discussed in [21, p. 144]. The juvenile crocodile may also select

[4]The flying pace may, in fact, be a four-beat gait, as described in [77].

the gallop gaits at the slowest speeds, [68].

In addition to generally being rapid, the gallop has been found, at least in horses, to be the most efficient gait at high speed [20]. The researchers found that the "minimum oxygen cost[5] to move a unit distance was almost the same in [walking, trotting and galloping] gaits" when the horse was allowed to select its gait at a given speed. At the slowest speed, horses tend to select a walking gait, at moderate speeds the trot is often selected, while at the highest speeds the gallop is chosen. This energy-gait relationship could be exploited in legged robots to make locomotion more efficient. While the current galloping results on Scout II and PAW show that the gallop is less efficient than the bound for these two robots, results for the half-bound (which is arguably also a half-gallop) in PAW show an improvement in efficiency, as shown in Fig. 7.10. The decreased gallop efficiency is due in large part to lack of actuated knees and the need for large apex heights to achieve the necessary gallop footfall phasing. With optimization of the mechanical and controller designs it may be possible to mirror the biological efficiency results.

In [74] Muybridge hints of a belief that transverse galloping horses may be made to run faster if trained to use the rotary gallop. This is based on his observation of a small hound (using the rotary gallop) being able to locomote faster than larger animals. This belief is echoed by Hildebrand in [21]: "The rotary sequence tends to be preferred to the transverse sequence by the fastest and most maneuverable cursors [animals with a preference for running], and limited evidence indicates that some *artiodactyls* may tend to change from the transverse to the rotary gallop as speed increases". This thesis deals uniquely with the rotary gallop, having found that the two robots, Scout II and PAW, tend to converge on the rotary gallop footfall pattern using the gallop control method introduced in Chapter 3. While the transverse gallop has occasionally resulted, it is generally transitory and the data have been insufficient to comment on the speed claims made by Muybridge and Hildebrand, as noted above.

Stability and Manoeuvrability

Although Schmiedeler *et al.* state that there is "no obvious preference for transverse over rotary gallops"[72],[6] others assert that the rotary gallop is more maneuverable, while the

[5]Oxygen usage indicates energy expended.

[6]Schmiedeler *et al.* suggest that that there may be an advantage to using the rotary gallop in animals with flexible backs, but do not elaborate or cite a reference, [72].

transverse is more stable in general [68, 78]. Ashley-Ross states that this is because at the slowest speed, the gallop can have three legs on the ground at any given time. In the transverse gallop, the ground-projected centre of mass falls within the leg support triangle, while in the rotary gallop it falls near the edge, indicating that it is easier for the latter to destabilise. The possibility that the rotary gallop is less stable than the transverse is briefly discussed in [49, p. 102], leading Ringrose to conclude that the rotary gallop favours yaw, to the point where his simulated quadrupeds would turn in circles.

Hildebrand discusses that the galloping leading leg plays a role in maneuverability, with cheetahs often switching leading legs in order to change direction while chasing prey [79, p. 488]. Depending on the flight phase, it may be easier to switch leading legs while using a rotary gallop than the transverse gallop, and the leading leg switch may be used to make changes to yaw. In the end, as with the relationship between forward speed and gait selection among the gallops, any correlation between manoeuvrability or relative stability and gallop gait type is largely speculative.

Regardless of the *relative* stability between these gaits, it has been shown that both rotary and transverse gallops are, in fact, stable. Herr and McMahon have conducted studies and simulations of transverse galloping systems [23, 25]. Some of their observations include that their models' postural orientation does not need to be explicitly measured or controlled to exhibit mechanical behaviour similar to galloping animals. That postural stability is an emergent characteristic of galloping is important because it can potentially make the control of the system much simpler and efficient.

In this thesis, it is shown that both the Scout II and PAW robots tend to gallop in circles, similar to the results obtained by Ringrose. And, as Hildebrand observed, the leading leg in Scout II and PAW's rotary gallop is a consistent indicator of the direction of yaw. Both robots also have demonstrated an overwhelming tendency to prefer rotary over the transverse gallops. While occasional transverse gallop footfalls have been observed on both robots, the control method used to generate four-beat footfall patterns have nearly always resulted in stable rotary gallops, as shown in Chapter 7, which demonstrate emergent postural stability, as was shown in the work by Herr and McMahon, [23].

Passive and Actuated Degrees of Freedom

Nanua presented two- and three-dimensional simulations which illustrated transverse galloping using one rotary and one prismatic actuator per leg, [27], which, unlike Ringrose, [49], did not require a specific toe shape. Simulations using Nanua's controller, perhaps the first controller specifically designed to produce a simulated gallop gait, result in stable gallop gaits, including yaw control [27, pp. 93 - 96]. All research on the gallop to date has assumed the requirement of at least two actuated degrees of freedom per leg [23, 27, 60, 80], if not three, [81, 82]. In addition to these actuated degrees of freedom all of these models contain at least one prismatic or torsional, unactuated spring-damper in each leg. Some of these models have also included neck or spinal degrees of freedom, either passive or actuated. Both Nanua and Herr have argued, [27, 83], that flexible spines and even necks are important features of at least the transverse gallop because of their presence in biological systems. In a minimal gallop system which is *functionally* and not *morphologically* biomimetic, though, these are not necessary, as is demonstrated by the results found within this thesis.

2.5 Contributions of This Thesis

This section contains short descriptions of the main contributions to the field of robotics, and in particular to legged robotics, that the author has made. These contributions are described in greater detail within this thesis.

Braking and Turning Strategies for PAW To the author's knowledge relevant works such as [8, 12, 9, 4] have not examined the application of reconfigurable leg design of a system such as PAW to turning and braking manoeuvres. The author has executed, on the PAW platform, both banked turning and sprawled braking which have improved stability characteristics, especially at higher speeds. Details regarding this work are presented in Chapter 5.

Bounding in a Wheeled-Leg Quadruped This thesis conclusively demonstrates, in Chapter 6, that dynamic gaits such as the bound are possible in systems that are not strictly legged. Of particular importance is the fact that a stable bounding gait is possible given the fact that the wheels, while actively controlled and not mechanically

blocked, rotate a non-negligible amount during the stance phase. This is the first time that such experimental results have been presented in the literature to date, opening up the possibility of hybrid legged and wheeled behaviours, such as those proposed in [37].

Regulation of Forward Speed and Turning via the Takeoff Angle It is shown in simulations in Chapter 4 and experiments in Chapter 6 that, in contrast to the control method established by Raibert, forward speed can be also regulated using the liftoff angle, via a stance-brake action, while maintaining the same touchdown angles.

Underactuated Galloping Unlike previous work in the field, this thesis demonstrates, in Chapter 7, that a four-beat running gait such as the rotary gallop can be achieved using a single actuated degree of freedom on a passive, compliant leg.

Decoupled "Monopod" and "Biped" Gallop Controllers The author presents the first experimental evidence of robotic galloping using the Scout II quadrupedal robot. The gallop controllers described in Chapter 3 and implemented in Chapter 7 alternatively use separate controllers for the front and rear hip pairs (Scout II), as well as four separate controllers for all four individual legs (PAW). In addition, the mechanical design rigidly couples the hips together. This is in contrast to Herr, whose simulated gallop controller and simplified models presented in [23], required coupled control of all four legs or Ringrose's simulated gallop controller and simplified models, presented in [49], which used revolute joints to couple the two hip pairs to the rigid spine of his model.

Improving Galloping Results Via Bounding Transition Although it is possible to achieve a stable rotary gallop gait from a standstill as shown by the author in [28], many of the best, most repeatable galloping results in Chapter 7 have been achieved by transitioning from another gait. In the particular case of Scout II and PAW this has meant starting with a bound and transitioning to a rotary gallop by adding asymmetry to the leg touchdown angles.

Turning Strategies Via Galloping Touchdown Pattern The dynamics of the gallop are rich, and have important three-dimensional properties. One of the most striking results of Scout II's rotary gallop is that the overall result of the gait, which has

important pitch and roll characteristics, is to force the robot to yaw. Not only can the robot now yaw by varying hip torque during the stance phase of the bound but it can also yaw through selection of the touchdown order of its legs during the rotary gallop. These results are contrasted in Chapter 7 with the use of liftoff angles to generate yaw as well. Demonstrating that the footfall order, including consistent location of the lead leg, is an important determinant of yaw direction is another important contribution of this thesis.

Effect of Gait Selection on Leg Strain, Gait Efficiency and Speed Although it is a widely held belief that the gallop is simply a more efficient gait at higher speed, [20], the author examines performance characteristics such as leg strain, efficiency and speed in both the bound and the rotary gallop with the goal of providing a more holistic comparison. This is the first time that this has been done on experimental robotic platforms, with results presented in Chapters 6 and 7. It is shown here that galloping leads to asymmetric leg compression and that it does not necessarily lead to more efficient motion at the speeds investigated.

Chapter 3

Quadruped Robot Design and Gait Controllers

The two quadrupedal robots studied in the course of this dissertation, Scout II and PAW, were designed and constructed at McGill University between 1998 and 2004, [84, 37, 85]. This chapter summarizes the basic design features of Scout II in Section 3.1.1 and PAW in Section 3.1.2. While the PAW robot is smaller and more compact that Scout II it applies many of the design and implementation lessons learned on Scout II, and thus shares many features, including body shape and leg design, but also hip actuators, power source, computing and control hardware, as discussed in Section 3.2. The methods for basic actuator control are examined in Section 3.3, taking into account the fact that neither the power source, nor the amplifiers or motors are ideal. Scout II is uniquely a dynamically stable running robot, while the use of wheels and wheel actuators makes PAW the first robot to demonstrate quadrupedal running behaviours in addition to hybrid wheeled-leg modes of mobility. In Section 3.4 the Spring Loaded Inverted Pendulum (SLIP) model is presented as an introduction to the concept of using compliant legs for running. The discussion continues in Section 3.4.2 in which the touchdown angle, φ_{td}, is the primary control input for φ-controller used in bounding and galloping. A variation on this controller is given in Section 3.4.2 and establishes the liftoff angle, φ_{lo}, as a second important control parameter for forward speed control in the bounding gait.

3.1 Robot Design Concepts

3.1.1 Scout II

The design of Scout II (refer to Fig. 3.1a, as well as [84] for details) is an exercise in simplicity. Reducing the complexity of the mechanical and electronic components results in minimizing the major sources of failure, thus increasing the reliability and robustness of the platform, while considerably decreasing the cost. Furthermore an essential feature for real-world tasks is power autonomy. Power autonomy imposes very strict design constraints and is often impossible to achieve with simple modifications to a platform otherwise designed for tethered operation. These features underline the importance of designing a platform using a minimum number of actuators and deriving controllers that share minimum reliance on sensing. Further details regarding the original design requirements, as well as machine drawings, of the Scout II robot are discussed in [84].

Scout II consists of a rigid body with four compliant prismatic legs. The most striking feature of Scout II is the fact that it uses only a single actuator per leg, located at the hip joint, which provides leg rotation in the sagittal plane. Each leg assembly consists of a telescoping lower and upper leg pair, connected by a spring and a pair of bushings to form a compliant prismatic joint. Thus, each leg has two degrees of freedom: the hip's actuated rotational DOF, and the passive compliant prismatic DOF. This configuration allows for the realization of different dynamically stable running gaits such as dynamic walking [86], pronking [87], bounding [88, 18] and galloping, [29].

It is important to mention that the design paradigm behind Scout II focuses less on morphological imitation and more on functional biomimetic representation. The fact that Scout II possesses legs with only one actuated DOF, which do not share more than a passing resemblance to those of quadrupedal animals, is not critically important. Rather, the design has focused on the task of relocating the robot in a manner similar to what is seen in biological analogues while also matching the basic footfall patterns. The functional biomimetic paradigm has been successfully used in other robots, among them those constructed by Buehler and his collaborators: most notably the RHex series, [34], which uses recirculating legs – unheard of in the animal world – to move in a manner similar to a cockroach.

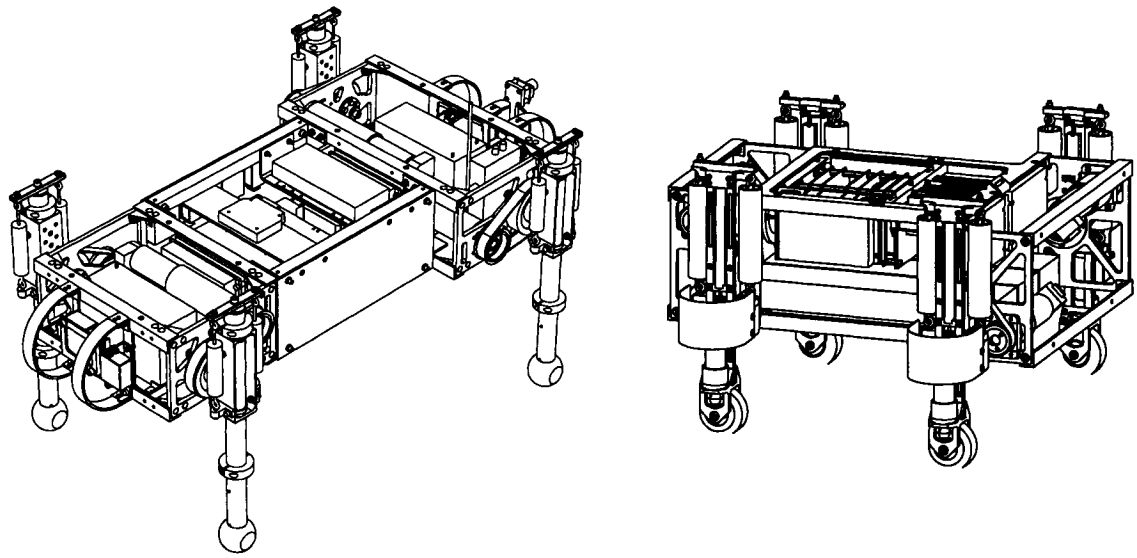

(a) Scout II (b) PAW

Fig. 3.1 Scout II and PAW CAD Models

3.1.2 PAW

The PAW (Platform for Ambulating Wheels) robot, as pictured in Fig. 3.1b, combines many aspects of the Scout II robot, with which it shares a T-shaped body (albeit lighter and more compact) and compliant legs. Two notable improvements over Scout II include the use of tightly toleranced double row bearings rather than simple bushings in the hips, as well as a caged ball slider and matching rail rather than the bushing pair found on Scout II's legs. PAW also bears resemblance to articulated suspension systems, [8, 11, 12], described earlier in Section 2.2, combining aspects of legged and wheeled locomotion in order to achieve greater mobility. Unlike Scout II, PAW's legs are equipped with actuated hard rubber wheels instead of fixed toes. In wheeled modes of operation the four hip motors can reposition the wheels with respect to the body of the robot. Many of PAW's wheeled behaviours are primarily kinematic, but they have implications for high-speed locomotion in which vehicle dynamics play a role, such as in braking and high-speed turning. In legged modes, the wheels may be actively controlled, allowing dynamic behaviours such as jumping and bounding, similar to Scout II. Original design details of the PAW robot are discussed in [37], while updated machine drawings and an operation guide are presented in [85].

3.2 Electro-Mechanical Hardware

The two robots share many of the same design features and hardware components. However, there have been a number of improvements implemented on the PAW robot based on lessons learned using Scout II. The following describes the commonalities, as well as the differences.

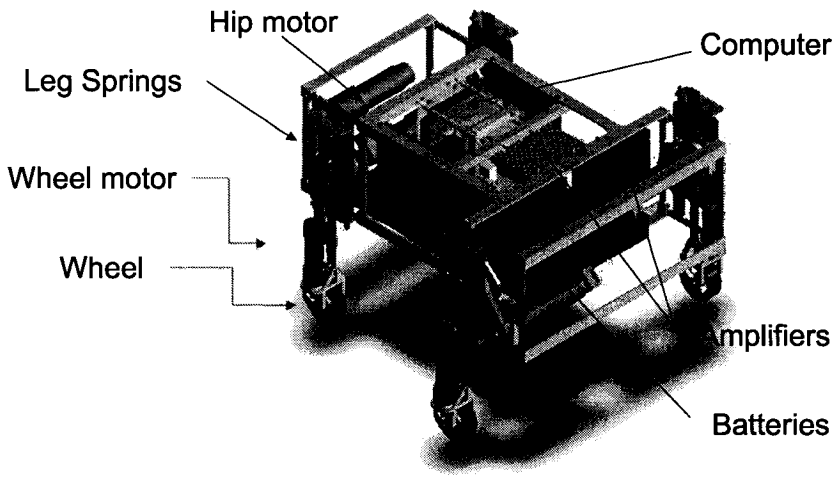

Fig. 3.2 Labelled PAW components. Scout II component layout is identical save for the lack of wheels and wheel actuators.

The chassis of both robots is T-shaped, with three distinct sections, the torso and the two hip modules. The torso forms a structure that houses a PC/104 computer stack with various I/O boards. On the PAW robot all batteries are housed within the torso, while one of Scout II's three batteries is slung under the torso. Scout II's other two batteries are located in the two hip modules. On both robots, the front and back hip assemblies house the hip actuation mechanisms. The reader is directed to Fig. 3.2 to see a labelled layout of parts on PAW; Scout II's parts layout is similar. A list of inertial, geometric and actuation parameters for Scout II and PAW is found in Table 3.1.

Each hip is actuated by a Maxon 118777 brushed DC motor, a Maxon three-stage planetary gearbox (110404 for Scout II and 203123 for PAW). A timing belt and toothed pulley pair further amplify the torque and isolate impact forces from the motor shaft. On Scout II the pulley ratio is 24:17, while on PAW it is 4:3, as shown in Figs. 3.3 and 3.4a, respectively. Each motor is equipped with 2000 counts-per-revolution effective resolution quadrature encoders.

On both robots selection of the hip motor, planetary gearbox, as well as sprocket com-

Table 3.1 Scout II and PAW Inertial, Geometric, Actuation and Leg Compliance Parameters

Parameter	Scout II	PAW
Body Length	0.837 m	0.494 m
Front Body Width	0.335 m	0.366 m
Rear Body Width	0.250 m	0.240 m
Front Leg-to-Leg Width	0.498 m	0.478 m
Rear Leg-to-Leg Width	0.413 m	0.352 m
Hip Separation	0.552 m	0.322 m
Body Height	0.126 m	0.168 m
Body Mass	20.9 kg	15.7 kg
Body Moments of Inertia (I_{xx}, I_{yy}, I_{zz})	1.3 kg m^2 (I_{zz}, pitch only)	(0.170, 0.470, 0.372) kg m^2
Body Products of Inertia (I_{xy}, I_{xz}, I_{yz})	*not available*	(0.00061, -0.00064, 0.00665) kg m^2
Leg Length	0.323 m	0.212 m
Leg Mass	0.97 kg	1.3 kg
Leg Spring Constant	3520 - 4300 N/m	2000 - 3200 N/m
Hip Gear Ratio	72.38:1	73.5:1
Hip Gear Efficiency	68%	72%
Hip Pulley-Belt Ratio	24:17	4:3
Hip Pulley-Belt Efficiency	96%	96%
Hip No-Load Speed	69 RPM	74 RPM
Hip Stall Torque	63 Nm	64 Nm
Wheel Gear Ratio	*not applicable*	4.3:1
Wheel Gear Efficiency	*not applicable*	80%
Wheel Bevel Gear Ratio	*not applicable*	3:1
Wheel Bevel Gear Efficiency	*not applicable*	n/a
Wheel No-Load Speed	*not applicable*	715 RPM
Wheel Stall Torque	*not applicable*	<2.5 Nm

bination was made to maximize available hip torque while also allowing reasonable hip velocities. The availability of high hip torque is especially important when the robot stands up or carries a payload. The motors are driven by four Advanced Motion Controls 25A8 PWM servo amplifiers. The amplifiers control the current to the motor, thus delivering predictable torques at the motor shaft as long as the motors are not saturated. While the motors are rated to 30 VDC, they are driven slightly higher, at between 36 and 40 VDC, enabling higher speeds without damaging the motor windings. This voltage is provided by three battery packs, each consisting of ten Sanyo HR-D NiMH cells.[1]

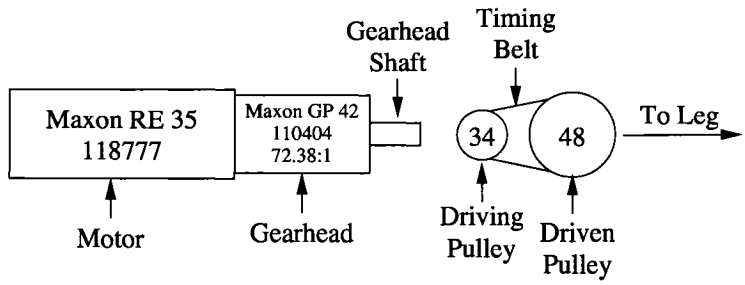

Fig. 3.3 Scout II hip transmission diagram.

As can be seen in Figs. 3.3 and 3.4, both the hip motor gearhead and the hip pulley pair act as speed reducers. PAW's overall gear ratio for the hips is 98:1 (73.5:1 in the motor gearhead and 4:3 in the pulley pair), with an assumed efficiency[2] of 69%, [89], while Scout II's combined ratio is 104:1 with an assumed efficiency of 65%, [90] and [18]. The small difference in efficiencies is due to the more recently designed gearheads on PAW. Given a bare-motor rated stall torque of 0.949 Nm, PAW's maximum hip stall torque is therefore 64 Nm, which is approximately the same as on Scout II.

The electrical subsystem is designed to allow for continuous modifications and improvements, to ease quick implementation and debugging of new locomotion controllers, and integration of new sensors. The PC/104 stack houses a Lippert Cool RoadRunner 2 CPU board with a 300 MHz National Semiconductors Geode (Intel Pentium II class) processor. Together with multiple I/O boards the computer collects data from the sensors and performs all the necessary computations for implementing the various controllers.

[1]PAW also uses a set of Saft VH D battery packs with slightly higher charge capacity ratings.

[2]Actuator efficiency values are estimates only since manufacturer-specified data is only provided for a single speed-torque value whereas it should be given for the entire actuator speed-torque variable space.

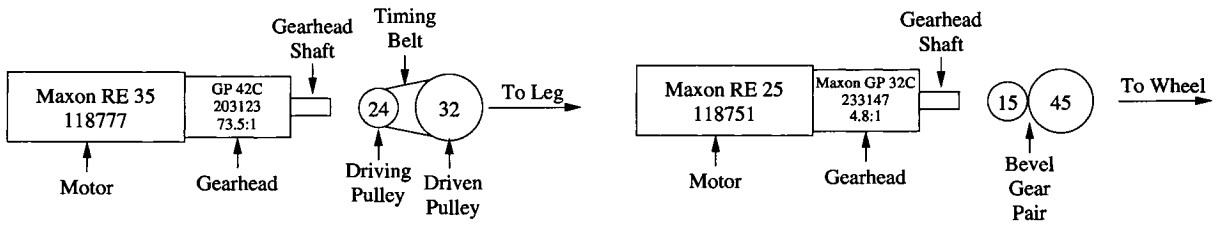

(a) Hip Motor (b) Wheel Motor

Fig. 3.4 PAW hip and wheel motor configuration. Combined gear ratio on the hips is 98:1 (73.5:1 and 4:3 for the gearbox and pullies, respectively) with an assumed combined efficiency of 69%. The combined wheel motor gear ratio is

Various sensors are used to monitor the motion of both robots. Both robots have sensors to measure the battery voltage and current. Current measurement in each of the hip amplifiers allows estimation of hip torque. Apart from incremental optical encoders, which are used to measure the angular displacements of the motor shafts, linear potentiometers measure the displacement of the lower part of the leg with respect to the upper part, and are only used to infer the state, flight or stance, of the legs. On Scout II, a pair of high precision laser range finders (NAIS LM10) are used to measure the distance of the front and back ends of the robot from the ground, and thus to provide a relatively accurate estimate of the body's hopping height and pitch. While the range finders are effective for sagittal plane motion, they cannot be used once the assumption of planar motion fails, as is the case for the galloping results presented herein. For this reason, the PAW robot houses a high accuracy, low-drift Inertial Measurement Unit (IMU). This particular IMU, a BAE SilMU-01, is currently used to transmit roll, pitch and yaw information to the PC104 stack via an RS-232 line. This factory-calibrated IMU was chosen for its high angular velocity and linear acceleration ratings, high update rate, relatively small size, and *very* low drift rate, as shown in Table 3.2. The IMU also performs onboard integration of sensor readings on each of the three rotational and three linear axes, yielding incremental angular displacements and incremental linear velocities. The latter measurements have not been utilized in the experiments reported in this thesis.

Note that although various sensors are used to study the properties of the bounding and galloping motion of both robots, the controllers, which will be presented in detail in Section 3.4, do not rely on all of them. For instance, the implementation of the φ-controller

Table 3.2 BAE SilMU-01 IMU Parameters. Only the angular data from the three gyroscopes are used in the context of this thesis.

Parameter	Angular Value	Linear Value
Measurement Range	600-1000 deg/sec	50 g
Scale Factor	500 ppm 1 σ	2000 ppm 1 σ
Bias Instability	5 deg/hr 1 σ	-
Bias Repeatability	100 deg/hr 1 σ	10 mg 1 σ
Random Walk	1.0 deg/ $\sqrt{}$ hr	1.0 m/s/ $\sqrt{}$ hr
Bandwidth	75 Hz	75 Hz
Update Rate	200 Hz	200 Hz

used in bounding and galloping gaits on both robots relies only on measurements from the encoders and the potentiometers.

The wheel motors on PAW have no analogue on Scout II. Each of PAW's legs has a 20 Watt Maxon 118751 brushed DC motor with a 4.8:1 Maxon 233147 planetary gearbox and a custom 3:1 ratio bevel gear pair connected to a 0.066 m diameter wheel. The wheel motors' quadrature encoders are identical to those of the hip motors. The motors are driven by six (two redundant) Apex SA60 amplifiers on a custom-made device, the RHex Motor Driver Board (MDB), originally developed for the RHex hexapod robot project, [91].

Power and signal wires to the wheel motors and sensors on each leg are passed through a hollow hip axle. This prevents the cables from becoming entangled in the legs and results in a simpler and more compact solution than that which can be provided with conventional commercial slip rings. Unfortunately, while this provides for larger leg sweep angles than are possible on Scout II, it still prevents the legs from continuously recirculating, as is the case in robots such as RHex.

3.3 Actuator Control

In this section the control of hip motors (for both robots) and wheel motors (PAW only) is examined. In addition, the fact that the motors, amplifiers and power source are non-ideal is addressed in this section and the effect that this plays is explained.

At the heart of the control for each joint of the robot is a proportional-derivative (PD) controller which is responsible for either maintaining a desired position or a desired velocity

at that joint. Because the steady-state error obtained with the PD controller is minimal, an integration error term is not included here. The equation for position control of a particular joint (hip or wheel) is described as:

$$\tau_{jd} = k_P(\vartheta_j - \vartheta_{jd}) + k_D(\dot{\vartheta}_j - \dot{\vartheta}_{jd}) \tag{3.1}$$

where τ_{jd} is the desired joint torque, $(\vartheta_j - \vartheta_{jd})$ is the error between actual and desired joint position/angle, $(\dot{\vartheta}_j - \dot{\vartheta}_{jd})$ is the error between actual and desired joint angular velocities, and k_P and k_D are the proportional and derivative gains, respectively.

In the case of controlling a desired position, such as during braking, a desired position value is given and the desired velocity is set to zero. In the case where the controller is required to maintain a particular velocity, a constant desired velocity is set and a matching desired position trajectory is computed. Alternatively, PD controllers can be set up using joint velocities and accelerations but this has the disadvantage of using a double derivative in the form of the motor acceleration, which is susceptible to large transient values due to time measurement errors. Transitions between one set of desired velocities and/or positions and another is resolved using cycloidal functions, [92], which provide smooth motion and are relatively computationally efficient.

The desired joint torques, τ_{jd}, computed on the PC/104 computer stack, are converted into control signal voltages which are then fed into one of two types of amplifiers. AMC 25A8 amplifiers are used in closed-loop current/torque control mode for the hips (both robots), while an amplifier board housing Apex Microtechnology SA60 amplifiers is used to drive the wheel motors (PAW only). The control signal voltage for the hip amplifiers is set to be proportional to the desired amplifier current using the manufacturer-specified conversion factor, while the resulting amplifier current is directly related to the motor shaft torque using conversion factors and efficiency values provided by Maxon Motors. The SA60 amplifiers are essentially open-loop PWM amplifiers, unlike the AMC 25A8s. By estimating current draw by the motors driven by these amplifiers it is possible to obtain a reasonable estimate of the applied torque at each wheel. Details on motor current estimation without direct measurement, using a motor model, battery voltage measurements and motor speed measurements, are explained in [93].

Because in wheeled/rolling modes, the PAW robot is redundantly actuated, it is not possible to have overly high gains on all joints because there is no coordination between

individual motor controllers. High gains are set on the hip actuators to ensure that the wheels are properly positioned with respect to the body and lower gains are used at the wheels, resulting in relatively compliant wheel motion. This active compliance tends to smoothen wheel velocity transitions. Gains must also be sufficiently small to not drive the wheels to instability during the flight phase when they are effectively unloaded. During PAW's legged modes, such as bounding with actively controlled wheels, the PD gains cannot be arbitrarily large (which would yield stiff response during stance) therefore, the wheel will react compliantly as a relatively soft torsional spring and damper during the stance phase of motion. This is reflected in the wheel response observed in Fig. 6.6 of Chapter 6. While gain scheduling could limit the oscillation of the wheel during the flight phase, it adds unnecessary complexity since the effect of the low-mass wheel on the robot's flight phase dynamics is negligible. In addition it would delay reaction of the wheel to ground contact while the leg compressed sufficiently to change the leg state.

Stance Torque With and Without Actuator Model

In both robots, the control method selected during flight-protraction and stance-brake servos primarily on error in position since the primary objective is to hold the leg at a particular angle in both cases. During stance retraction, one of two methods is used for control. The first, and simplest, is to command a constant desired torque. This is the method used on PAW in both bounding and galloping. The hip motor amplifier, an AMC 25A8 in the case of Scout II and PAW, is given a desired torque value (in terms of the proportional electrical current output) and regulates its output to comply. Due to actuator, amplifier and power supply dynamics a constant output torque rarely results, however. The second method, used on Scout II, varies the desired torque based on a model of the actuator. Its inclusion does not improve or worsen actual performance of the robot. It is particularly useful, however, when applying the results to model validation, as was done in [18]. What follows is the method used to apply this model to torque control.

During Scout II's stance-retraction, the controller sweeps the leg backwards, until a sweep limit angle, φ_{swl}, is reached. Actuator constraints are the dominant feature in the stance-retraction phase. The motors have to be capable of not only supporting the robot's weight, but also of imparting significant accelerations to the body, and of supporting large dynamic loads. Therefore, they often operate at their limits, characterized by their

torque/speed curve. While this curve is well known, it is rarely taken into account in robot modeling and control, as discussed in [18]. To include motor saturation in the controller, desired joint torques are commanded according to

$$\tau_{jd} = \tau_{MAX} + A\dot{\varphi} \tag{3.2}$$

$$\tau_{MAX} = \alpha\frac{K_T\bar{V}_b}{R_a}, \quad A = -\beta\frac{K_T K_\omega}{R_a} \tag{3.3}$$

where τ_{MAX} and A are the offset and the slope of the torque/speed line at the hip joint of the leg and $\dot{\varphi}$ is the leg's rotational speed. In Eq. (3.3) K_T and K_ω are the torque and speed constants of the motor, respectively, and R_a is its armature resistance. The parameters α and β in Eq. (3.3) are used to relate variables at the motor shaft (prior to the gearbox) to the corresponding ones at the leg (after the gearbox), and are given by

$$\alpha = (n_G\eta_G)(n_P\eta_P), \quad \beta = (n_G^2\eta_G)(n_P^2\eta_P), \tag{3.4}$$

where n_G and η_G correspond to the ratio and the efficiency of the gearbox and n_P and η_P to the pulley combination and efficiency, respectively.

In Eq. (3.3), $\bar{V}_b$ represents the average voltage at the motor terminals. Note also that according to the robot sign conventions, during stance-retraction the motors operate in the first quadrant where both the torque and speed are positive. There are two additional constraints that must be imposed on the desired hip torques τ_{jd},

$$\text{if} \quad |\tau_{jd}| > \alpha K_T i_{MAX} \quad \text{then} \quad \tau_{jd} = \alpha K_T i_{MAX}, \tag{3.5}$$

$$\text{if} \quad \tau_{jd} \leq 0 \quad \text{then} \quad \tau_{jd} = 0. \tag{3.6}$$

The constraint of Eq. (3.5) ensures that the commanded torque will not exceed the maximum value predicted by the amplifier current limit i_{MAX}. The constraint (3.6) prevents the commanded torque from becoming negative, thus decelerating the robot. Note that Equation (3.5) arises when $\dot{\varphi}$ is too small. In that case excessively large torques are predicted from Eq. (3.2), which cannot be applied by the motors due to high current requirement and resulting saturation of the PWM amplifiers. Equation (3.6) occurs when

the legs spin at speeds large enough to result in a sign change of the desired torque.

Modeling Batteries and Amplifiers with Actuators

In this section we present simple models for the motor driving system, including the battery, PWM amplifier, actuator, and gearbox units. As shown in [18], these models must be included in simulations to improve their accuracy. Even if these models are not used in directly controlling the robot, they play a significant role in the performance of the actuators. This is in contrast to other studies on quadruped locomotion, such as in [60], which assume that impulsive actuation is possible.

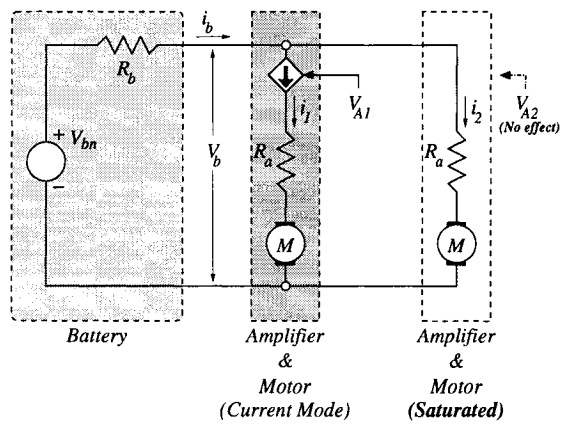

Fig. 3.5 Model of the motor, amplifier and battery. Here, one motor is being driven by the amplifier (diamond) in current mode, whereby current, i_1, is internally regulated by modulating the pulse width of the voltage across the motor terminals. The other motor, originally driven in current mode as well, is saturated and the current, i_2, is so high that the amplifier essentially acts as a closed switch to the battery.

Since electrically actuated autonomous robots draw significant peak power and operate from non-ideal voltage sources, the variation of the supply voltage as a function of the total load current must be considered. As shown in Figure 3.5, the battery model is composed of a resistance, R_b, in series with an ideal voltage source, V_{bn}. The equation that describes the output voltage is

$$V_b = V_{bn} - i_b R_b. \tag{3.7}$$

To determine the parameters in Eq. (3.7), namely V_{bn} and R_b, the current i_b and voltage

V_b were measured during a set of experiments, and then the model described by Eq. (3.7) was fit in a least-squares sense to the experimental data, resulting in the values $V_{bn} = 37.17$ V and $R_b = 0.13\ \Omega$.

We assume that the PWM switching signal may be completely removed from the motor input. When the motor is not saturated, the amplifier operates in current mode and achieves the desired motor current by appropriately adjusting its terminal voltage via an internal current monitoring feedback loop, as shown in the left-hand motor-amplifier pair in Fig. 3.5. In this regime, the amplifier can be approximated by an ideal voltage-controlled current source whose output current is directly proportional to its input voltage signal, denoted as V_{Ai}, i.e.:

$$i_i = \frac{\tau_{mi}}{K_T} = K_A V_{Ai} \tag{3.8}$$

where the i subscript designates one of the four motor-amplifier pairs, and $K_A = 4.3\ \text{AV}^{-1}$ is the voltage-to-current gain of the AMC 25A8 hip amplifier. Note that the amplifiers peak current is limited to $i_{MAX} = 20$ A by internal circuitry to prevent the motor from being critically overdriven. This limit is taken into account by Eq. (3.5) of the stance-retraction controller. As the motor shaft accelerates under a desired bare-motor (i.e. no gearhead or pulley) torque, $\tau_{md} = K_T i_d$, its rotational speed ω, increases until the back EMF $K_\omega \omega$ becomes larger than the available power supply voltage $V_b - i_d R_a$. Therefore, the current mode applies only up to a speed limit, ω_{MAX}, given by:

$$w_{MAX}(i_d) = \frac{V_b - i_d R_a}{K_\omega}, \tag{3.9}$$

after which the motor enters its saturation regime, where we assume that the amplifier operates as an ideal conductor, as shown in the right-hand motor-amplifier pair of Fig. 3.5. In this regime the applied bare-motor torque τ_m is given by

$$\tau_m = \frac{K_T}{R_a}(V_b - K_\omega \omega), \tag{3.10}$$

in which the motor inductance has been neglected. Combining Eq. (3.8) and Eq. (3.10) we obtain the equation describing the torque τ_m applied by the motor in both the saturation and nonsaturation regimes. The applied joint torque $\hat{\tau}_j$ that takes into account the motor, gearhead and pulleys, but not the amplifier saturation can be calculated

$$\hat{\tau}_j = \begin{cases} \alpha K_T i_d & \text{for } |\omega| \leq |\omega_{MAX}| \\ \alpha \frac{K_T V_b}{R_a} + \beta \frac{K_T K_\omega}{R_a} \dot{\varphi} & \text{for } |\omega| > |\omega_{MAX}| \end{cases} \tag{3.11}$$

which is valid in the first quadrant of the torque/speed line (stance-retraction). In Eq. (3.11) the velocity ω_{MAX} is given by Eq. (3.9), the parameters α and β are given by Eq. (3.4), and the following sign conventions have been applied: positive torques and velocities represent motion of the leg from front to back. Finally, the joint torque τ_j that is delivered at the hip and that includes both the motor and amplifier saturation is given by

$$\tau_j = sgn(\hat{\tau}_j) \min\{|\hat{\tau}_j|, \quad \alpha K_T i_{MAX}\} \tag{3.12}$$

where i_{MAX} is the amplifier's peak current. Equations 3.11 and (3.12) constitute the motor model in the first quadrant and, with the appropriate sign changes, can be extended to the third quadrant of the torque/speed curve.

These new torque values are particularly useful in the work conducted on model validation in [18], and were used in the Scout II bounding trials. The simpler torque commands, in which no model is taken into account, are used in the PAW trials with the intention of using the PAW trials as a baseline for controller development in future PAW gait experiments.

3.4 Gait Controllers: From Monopods to Quadrupeds

While this thesis focuses on quadrupedal locomotion in two- and three-dimensions, it is useful to re-examine the original controller developed for a monopod operating in a plane. A monopod equipped with a spring can be reduced to the Spring Loaded Inverted Pendulum (SLIP) model when it is in contact with the ground. The concepts for controlling forward motion in the case of the SLIP, introduced in Section 3.4.1, are extended to operate on quadrupedal locomotion in Sections 3.4.2 through 3.4.3.

The reader will first be presented in this section with the method established by Raibert for speed control in the monopedal case, abstracted to the SLIP, [17]. This involves setting the angle of the monopod's leg so that it touches down about a "neutral point". While a neutral point is not explicitly determined in the cases of the quadrupedal Scout II and PAW robots, the φ-controller used, is based on the same concept of setting leg *touchdown* angles, φ_{td}. The φ-controller is presented here in the context of controlling both bounding

and galloping gaits.

While Raibert's method assumes no direct control over the *liftoff* angles, a variation of his controller, in which the liftoff angle, φ_{lo}, is used for speed control rather than the touchdown angle, is also presented here.

3.4.1 Spring-Loaded Inverted Pendulum

As discussed in Chapter 2 compliance in the leg is a key component to producing running. The simplest embodiment of a compliant legged system which is capable of exhibiting the essential dynamics of a running gait is a monopod. The contact point between the leg's "toe" and the ground is assumed to be a pin joint during the stance phase and, because the leg is assumed massless, there are no losses at impact. The spring-loaded inverted pendulum, SLIP, provides a useful template for modeling running even when the running machine involves more than one leg, as is the case with bounding and galloping.

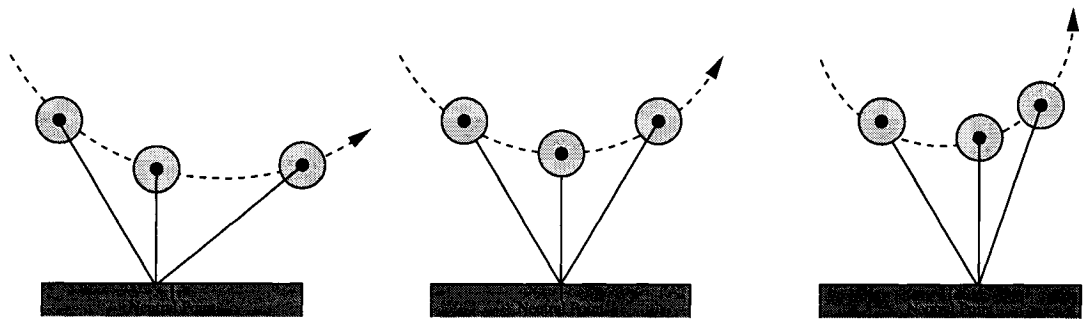

Fig. 3.6 SLIP speed control via touchdown angle. By varying the touchdown angle one can change the touchdown point with respect to Raibert's "neutral point." In the middle one can see symmetric touchdown and liftoff by landing on the neutral point. Landing in front of the neutral point slows the SLIP, while landing in back accelerates it.

Forward Speed Control: Touchdown Angle and the Neutral Point

As described by Raibert in [17], the forward speed of a SLIP can be adjusted by having the leg touchdown in front or in back of the so-called "neutral point." If the leg lands on the neutral point the resulting trajectory during the stance phase of motion will be symmetric, leading to the liftoff angle equalling the touchdown angle, as shown in Fig. 3.6. Landing

in front of the neutral point will accelerate the SLIP, while landing in back of it will slow it down. The neutral point is calculated at a distance $x_{f0} = \frac{\dot{x}T_s}{2}$ in front of the ground-projected centre of mass, where $\dot{x}$ is the forward speed and T_s is the stance phase duration. The stance phase duration is dependent on the spring constant, with longer stance phases resulting from more compliant leg springs.

Liftoff Angle to Vary Forward Speed

As shown above, the concept of varying the touchdown angle to explicitly control forward speed is not new. Varying the touchdown angle so that the leg touches down in front of or in back of the neutral point does, in turn, affect the forward speed. It also *indirectly* varies the liftoff angle as a result, as shown in Fig. 3.6.

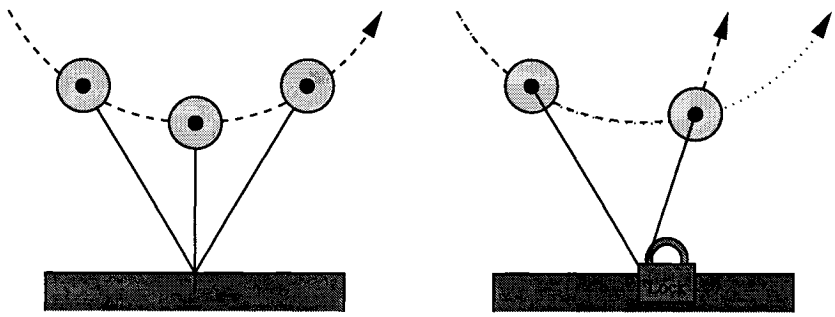

Fig. 3.7 SLIP speed control via liftoff angle. By locking the toe-ground pin joint prior to the usual liftoff angle the forward speed can be reduced in exchange for increased vertical motion.

Here, it is shown that the *deliberate* selection of *liftoff* angle, φ_{lo}, directly affects forward speed. By assuming that the passive pin joint between the toe and the ground of the SLIP can be locked one can limit the sweep angle (the range of angles between touchdown and liftoff) of the leg during stance.[3] By locking the rotation of the toe prior to liftoff the sweep angle is limited, and the SLIP model is forced to extend prior to liftoff in a more vertical direction. As shown in Fig. 3.7, holding the SLIP at this "sweep limit" angle is equivalent to setting the liftoff angle and results in a deceleration of the SLIP in the forward direction. Since the sweep limit retards forward motion it is not possible to use it to accelerate the

[3]This example is used for illustrative purposes only. Of course, for a monopod with a point mass and no actual control of the pin joint this is not possible.

SLIP, only to reduce its speed.

In the next sections the control of forward speed for quadrupedal locomotion is discussed. As in the SLIP case, the traditional method of speed control, via the touchdown angles, is presented first and is referred to as the φ-controller for bounding. In Section 3.4.2 the reader is once again presented with using the liftoff angle, φ_{lo}, to control forward speed, this time in the context of quadrupedal bounding.

3.4.2 Bounding with a Quadruped

In this section the bounding gait is discussed, using concepts introduced with the monopod earlier. First, simplification of the quadruped is introduced based on symmetry of the robot, next the basic state machine used to control the robot is discussed. Speed control of the robot is presented using both touchdown and liftoff angles.

"Planarizing" the 3D Quadruped

The bound gait is a *two-beat gait* in which there is a large degree of symmetry in both control and overall motion along the *sagittal* plane. A simplified bound footfall pattern, with comparison to other gaits, is shown in Fig. 2.7 in Chapter 2. Because of this symmetry, control can be simplified using the concept of the *virtual leg*, [17], illustrated in Fig. 3.8a. A schematic of the sagittal plane representation of the Scout II and PAW robots is found in Fig. 3.8b. System parameters and variables include the mass and pitch moment of inertia (m and I), the leg spring constant (k), the half hip spacing (L), the leg length (l) and the leg angle with respect to the body (φ). The f and r subscripts refer to front and rear ends of the robot, respectively. Since the dominant control parameter described for the bound controller used on both robots relies on the leg angle, this controller is referred to as the φ-controller.

In order to enforce the virtual leg paradigm two actions can be taken during bounding. The most important of these is to only allow retraction of a leg during stance when both legs have contacted the ground. This is applied to Scout II and PAW bounding gaits.

To further enforce the virtual leg paradigm an optional PD controller can be applied overtop of the existing stance-retraction controller (described below). This modifies any current desired hip torque to compensate for any asymmetry in leg angle between members of a leg pair, effectively making sure that both legs are lined up with one another. This new

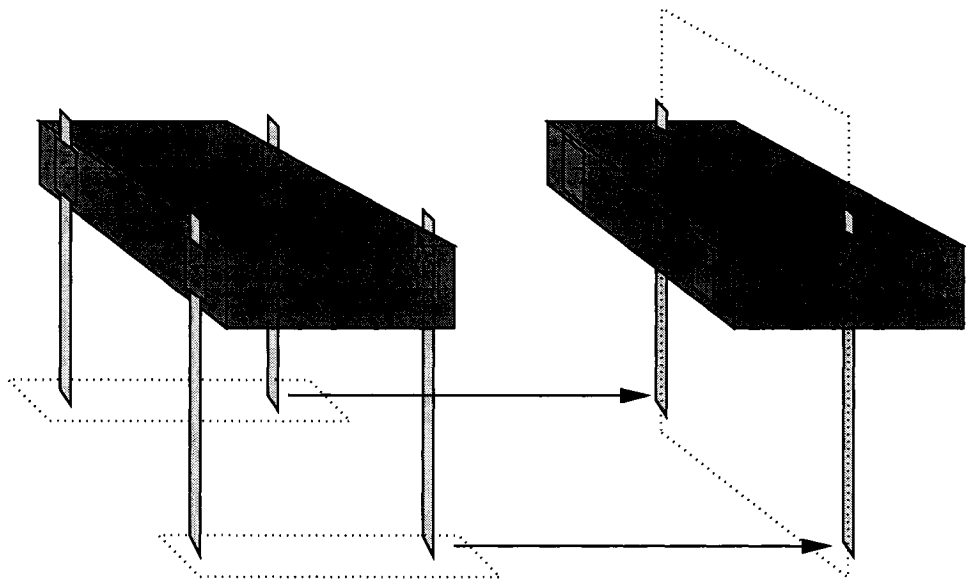

(a) Virtual Leg in Sagittal Plane

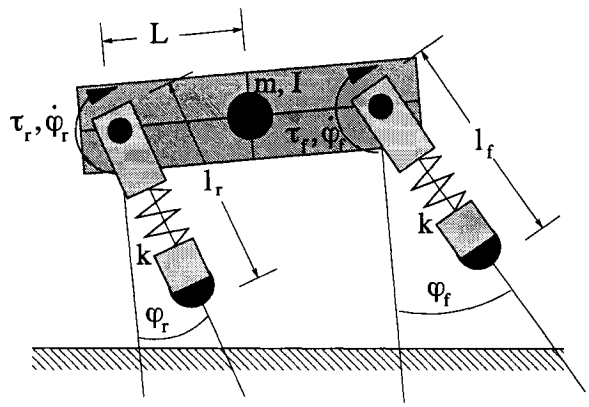

(b) Sagittal Plane Variables

Fig. 3.8 Bounding control is simplified by planarizing the problem via the virtual leg concept, [17]. Regarding sign conventions, the hip torques, τ, and velocities, $\dot{\varphi}$, are shown in the positive sense. Leg angles, φ, are considered negative when pointed forward, as they are in this case.

desired hip torque, τ_{sjd}, aids in synchronizing left and right legs and replaces the previously set desired hip torque, τ_{jd}, of Eq. (3.1) as follows:

$$\tau_{sjd} = \tau_{jd} + k_P(\varphi_{L1} - (\varphi_{L2} + \epsilon)) + k_D(\dot{\varphi}_{L1} - \dot{\varphi}_{L2}) \tag{3.13}$$

where k_P and k_D are proportional and derivative constants and ϵ is the desired touchdown angle difference between left and right legs. In the bound ϵ is zero, whereas it is non-zero in galloping, as explained in Section 3.4.3. While this synchronization action is applied to the Scout II bound and gallop controllers, it was not found to be necessary to apply to PAW. This is due to PAW's shorter legs, which reduced the effect of any misalignment between lateral legs.

State Machines Divide the Bounding Control Task

The gait is controlled by two separate state machines, one for the rear *virtual* leg pair and one for the front, illustrated in Fig. 3.9. The state machines affect the transitions between three robot states: flight, stance-retraction and stance-brake. When leg touchdown occurs the stance-retraction action is engaged. When liftoff occurs the leg enters the flight phase in which it protracts until it achieves the touchdown angle, φ_{td}, which it then holds until the transition to stance-retraction. A third action, that of the stance-brake, occurs when a sweep limit angle, φ_{swl}, is detected. If the leg passes φ_{swl} then the stance-brake action attempts to hold the leg at that angle until the liftoff event occurs. The angle at which liftoff occurs, φ_{lo} is ideally equal to φ_{swl}. It should be noted that stance-brake can be bypassed if the liftoff condition is detected during stance-retraction.

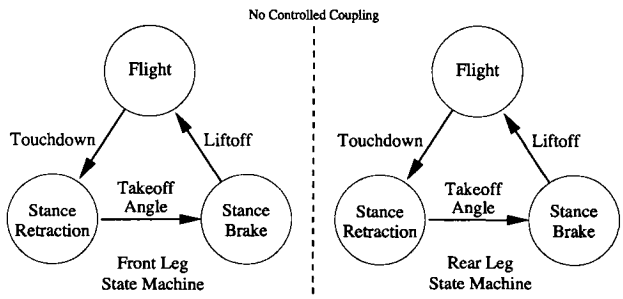

Fig. 3.9 Scout II & PAW's bounding state machine

To initialize the bounding gait, both robots begin from a standing position, proceeded

by a combination of lean-back and kicking motions. During lean-back, the legs are servoed to -25° using the hip position control described earlier in Eq. (3.1). After a fixed period of time the legs are rapidly servoed to 0°. This rapid sweep of the legs from one position to another, due in large part to the stiff control gains, launches the robot into the air, allowing the robot to then servo the legs in preparation for its first touchdown state change. Little leg compression occurs during the lean-back and kick. One particular advantage of this method of initiating the bound is that it is relatively independent of the legs' spring constants, working equally well with softer and harder springs.

Quadruped Bounding Using the φ-Controller

The concepts presented above regarding velocity control of the SLIP model are extended here to the case of the quadruped running in a plane. Here, the φ-controller, based on Raibert's concept of forward speed control via touchdown angles, is applied to quadrupedal bounding. It is shown how bounding control is simplified in Scout II and PAW by assuming motion to be constrained to the sagittal plane. The control task is shown to be broken up using a state machine that examines whether legs are in flight or not to determine appropriate control actions.

Varying φ_{lo} in the φ-Controller for Velocity Control

As explained earlier in the case of the monopod, if one varies the liftoff angle of the front and rear legs of a bounding quadruped it is also possible to control the forward speed. Rather than assume a lockable pin joint between the toe and the ground we take advantage of the fact that the mass of the robot body is not a point mass located at the hip. The hip joint is locked at a particular angle which corresponds approximately to the liftoff angle. While some pitch rotation of the body about the toe-ground interface results, forward motion that would otherwise occur if the leg was left to retract is retarded. As liftoff angle is made to be closer to the body's vertical reference the robot is forced to increase its apex height during the flight phase. Likewise, if the liftoff angle is increased, the robot is brought closer to the ground during ballistic flight and increases its forward speed proportionally. As can be seen in Fig. 3.10 the trajectory becomes shallower as the liftoff angle is increased. This proposed method of speed control is verified in the simulations and experiments of Chapters 4 and 6, respectively.

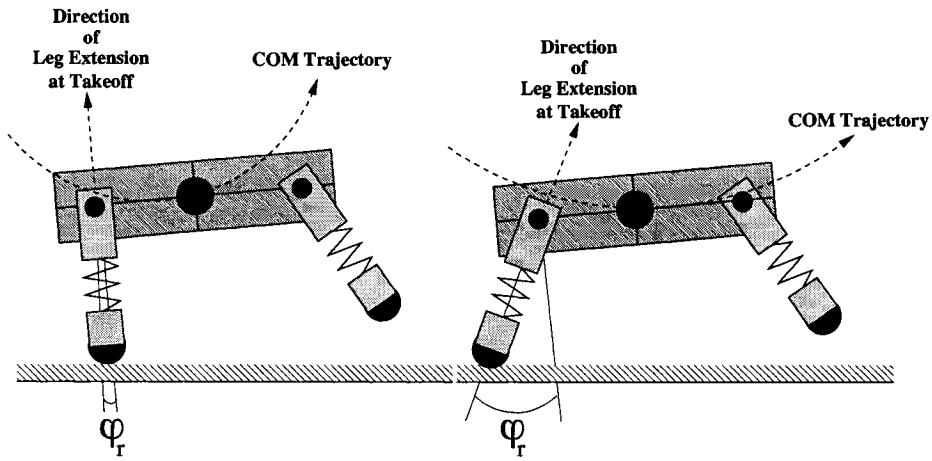

Fig. 3.10 Varying the liftoff angle allows a tradeoff to be made between maximum apex height and forward speed.

3.4.3 Quadruped Galloping Using the φ-Controller

The gallop is a *four-beat* gait, comprised of two members, the transverse and the rotary gallop, illustrated in simplified form in Fig. 2.7 in Chapter 2. The foot touchdown sequence of the rotary gallop follows a pattern which encircles the centre of the body, whereas the transverse gallop's pattern crisscrosses the centre of the body. In the transverse gallop, the lead leg of both front and rear leg pairs is on the same side, whereas in the rotary gallop they are on opposite sides.

The strategy for enabling the gallop hinges on the idea that the bound is essentially a limiting case of the gallop in which the lateral leg pairs have no phase difference. While this idea is not new, the method by which the galloping leg phase difference is introduced, is. In the cases of simulated gallopers discussed in Section 2.4.2, all used at least two actuated degrees of freedom per leg in the implementation of controlled gallops. Not only does this render the task of toe clearance during protraction easier, it also makes introducing the appropriate foot-impact phase differences relatively easy. Scout II and PAW with mechanically locked wheels only have one actuated degree of freedom per leg. Assuming the robot is engaged in a bounding motion, by adding an offset in the touchdown angles of a lateral leg pair, the bounding motion is perturbed and a new motion with a different footfall pattern emerges, such as the rotary gallop gait.

In order to obtain the rotary gallop gait, shown in simplified form in Fig. 2.7 in Chapter 2, the following strategy for setting the touchdown angles can be adopted. Within one

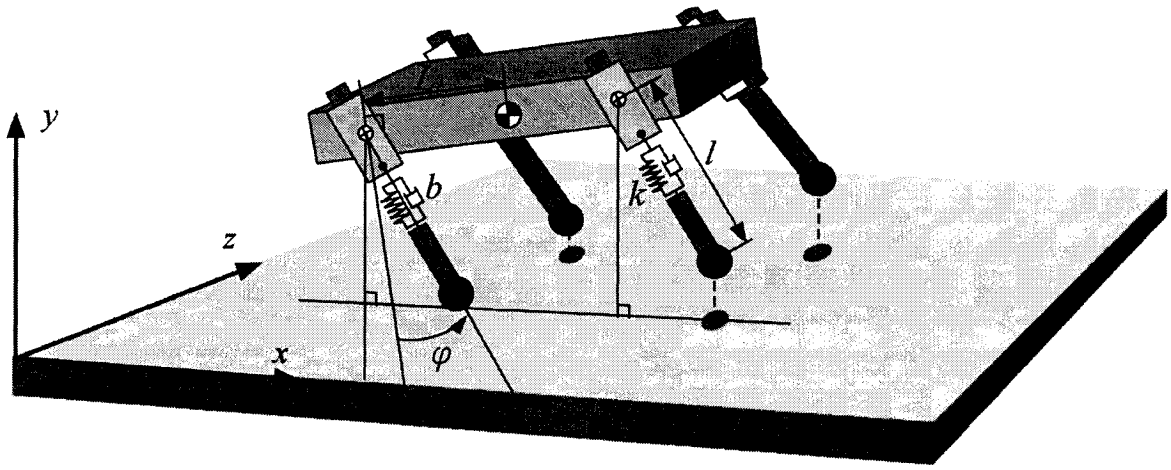

Fig. 3.11 3D schematic diagram of quadrupedal galloping with one leg on the ground, illustrating important variables and parameters.

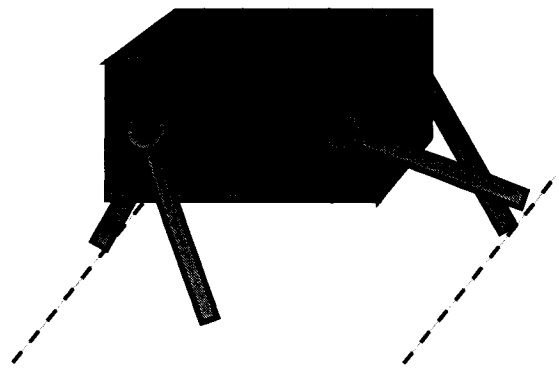

Fig. 3.12 Gallop via asymmetric touchdown angles.

lateral leg pair one chooses the touchdown angles of the first leg to be similar or identical to a successful bounding touchdown angle. The second leg's touchdown angle is set so that it is positioned *higher* than the first leg, as shown in Fig. 3.12. In this way the robot must roll to cause the second leg to contact the ground. In a similar fashion, the third leg (directly behind the second leg) is made to have a smaller touchdown angle than the fourth, so that it contacts the ground ahead of the fourth leg. This causes visible rolling motion, which is discussed in the experimental results of Chapter 7.

Appropriate selection of the offset angles results in the rotary gallop gait, without any significant additional control action beyond that of the bounding φ-controller. This reflects

the robots natural dynamics that depend on its physical properties. As with the bound, the successful use of the φ-controller agrees with conclusions made in [23] regarding horses not requiring vestibular sensing and knowledge of spatial orientation for gallop gait control.

Not only must touchdown angles be asymmetric, but another change with respect to the φ bounding controller must be made. The enforcement of virtual leg control, which only allows retraction of both legs in a pair to occur when both are in the same state, is reduced or eliminated in the case of the gallop. The PD controller, Eq. (3.13), which is used to synchronize leg retraction during the bound on Scout II is modified during the gallop to take into consideration the phase difference ϵ between legs in a lateral leg pair. On PAW this coupling is reduced even further, to the point where each leg functions independently of the others, so that the two state machines illustrated in Fig. 3.9 now become four. Therefore, while control of lateral leg pairs is tightly coupled in Scout II's bound, the coupling is relaxed during Scout II's gallop, and is completely gone in PAW's gallop. Finally, with the loosening or elimination of lateral leg pair coupling, the robot can no longer be assumed constrained to the sagittal plane, and must now be considered fully three-dimensional, as illustrated in Fig. 3.11.

3.5 Summary

This chapter presented the general design concepts behind the Scout II and PAW robots. While PAW is different from Scout II due to the actuated wheels at the ends of its legs the robots still share many features, including body shape and leg design, hip actuators, power source, as well as computing and control hardware. The effects of non-ideal batteries and amplifiers on basic control of electric actuators was presented in Section 3.3. In Section 3.4 the Spring Loaded Inverted Pendulum (SLIP) model was presented as a conceptual model useful for analysing running behaviours of robots with compliant legs. The discussion continued in Section 3.4.2 with respect to bounding in the planar case using the φ-controller, in which touchdown angle, φ_{td}, serves as the primary control input for bounding and galloping gaits. A variation on the φ-controller, as given in Section 3.4.2 establishes the liftoff angle, φ_{lo}, as a second important control parameter in addition to the touchdown angle, φ_{td}, for forward speed control in the bounding gait.

Chapter 4

Simulation of PAW Robot Bounding

In this chapter a three-dimensional simulation of the PAW robot performing bounding gaits is discussed. The numerical simulations permitted the study of this gait under more controlled conditions than were possible with the actual robot. Simulated trials allowed for leg angle parameter selections that would otherwise have been considered high risk on the robot. They also did not suffer from time consuming issues such as electromechanical component maintenance. The degree to which qualitative matches are found between these simulations and the experimental results presented in this thesis indicate that appropriate modelling parameters were used. The fidelity of the simulation allowed the examination of a bounding speed control using liftoff angles as well as an investigation of yaw bias.

The structure of this chapter is as follows. First, the model and software setup is introduced in Section 4.1. The model is largely based on information on PAW given in Chapter 3. Likewise, the φ-controller for this simulation is developed using details from Chapter 3. Second, in Section 4.2, general qualitative comparisons are made between the simulated bounding results and those achieved on the PAW robot. While the bounding gaits are qualitatively similar, there are some small quantitative differences between parameters such as leg phase difference and duty cycle. The tendency to yaw counter-clockwise during the bound on the PAW and Scout II robots is found to also occur in simulation. This is explained by asymmetric mass distribution in the PAW body, similar to Scout II. Lastly, in Section 4.3, an examination of the relationship between leg angles and forward speed is made. In addition to the effect of varying the touchdown angle, the effect of liftoff angles is also shown to be important with respect to regulation of forward speed, as previously

discussed in Chapter 3. These results reinforce results achieved on the actual PAW robot, which are discussed later, in Chapter 6.

4.1 Simulation using MSC.ADAMS and Matlab/Simulink

The simulation of the PAW robot is conducted in the MSC.ADAMS[1] mechanical simulation software package. The controller for the model is run in Matlab/Simulink, with communication between the two software packages taking place approximately every millisecond of "simulated time", similar to what occurs on the actual PAW robot. The Matlab control code is based on the C code developed for PAW, while the ADAMS model is based on the original Solidworks CAD model used in developing PAW. The simulation is conducted on a Pentium-IV desktop computer running at about 2GHz. Each bounding gait simulation, which lasts about 5.5 seconds in "simulated time" takes approximately five minutes to execute on the Pentium-IV.

The ADAMS model of PAW presented here is three-dimensional, as opposed to the two-dimensional model, referred to here as WM-2D-PAW, originally developed in [94] and shown in Fig. 4.1a. The previous model was developed in Working Model 2D to demonstrate proof-of-concept bounding simulations. In addition, several acrobatic manoeuvres were demonstrated. The parameters for this initial model reflect an early version of the PAW robot in which high-speed but low-torque actuation was desired at the hip joints. The version of the PAW robot discussed in this thesis uses higher torque hip actuators than the WM-2D-PAW model, which better reflects the actuators on the current version of the PAW robot. In addition, the three-dimensional nature of this simulation allowed for the investigation of the source of yaw visible in both the Scout II and PAW robots during the bounding gait through manipulation of the inertia tensor of the main body.

4.1.1 The 3D PAW Model and Simulator Setup

As noted earlier, the PAW model, shown in Fig. 4.1b. was developed in ADAMS, a popular commercial mechanical system simulation package. The geometric and inertial properties of the ADAMS model are based on a CAD model originally developed in Solidworks. The hand-coded, parametric ADAMS model matches the body and leg dimensions of the

[1]MSC.ADAMS and Matlab/Simulink are also referred to as ADAMS and Matlab, respectively, for brevity.

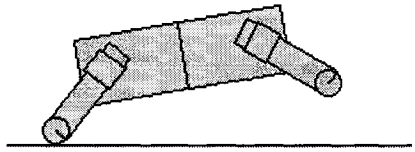

(a) WM-2D-PAW

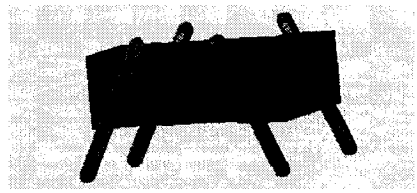

(b) MSC.ADAMS PAW

(c) The PAW Robot

Fig. 4.1 The bounding gait in simulation (a,b) and experiment (c).

Solidworks model as well as the aggregate mass distribution of these subassemblies. The masses match the real robot's total mass to within a few dozen grams. The inertia tensor derived from CAD model is assumed to be accurate based on accuracy of the total mass and component placement. The ADAMS model defines torque actuators at the four hip joints in addition to a passive prismatic joint within each leg. These torque actuators do not include gearing, therefore requiring that the gear and pulley-belt characteristics be included in the external controller when torque values are set. Parallel to the prismatic joints is a linear spring-damper. Hard stops at the ends of the joints help limit their travel. The link between the prismatic joint and the hip joint is referred to as the upper, sprung leg, while the distal end is referred to as the lower, unsprung leg. Like the version of PAW in which the wheels are mechanically blocked, no actuated wheels are used in the model.

The ADAMS/Control toolkit permits development of controllers within Matlab and provides Matlab-ADAMS interprocess communication. Once completed, the controller is run within Matlab while integration of the model dynamics occurs within the ADAMS Solver program. Once per millisecond (with respect to the model dynamics) model variables are transmitted to Matlab while torque commands determined by the Matlab controller are received by the ADAMS Solver.

The contact between the ground and the ends of the legs is modelled to be compliant with Coulomb friction characteristics. As shown in Table 4.1, the contact spring constant between the PAW model's toes and the ground is set to be very high, with little damping. To approximate the friction contact between the rubber wheels on PAW and the linoleum surface it generally runs on, the Coulomb friction coefficients are equivalent to those for between two dry rubber surfaces (or rubber and aluminum, steel, acrylic or nylon), as per the values suggested for ADAMS models in [95]. The contact model is assumed given that no specific model characterizations have been performed to confirm these values.

In the simulation results presented here, the ADAMS Solver is set to use the GSTIFF integrator with I3 equation formulation, [96]. The unit-sensitive integration error tolerance is set to 10^{-4}, where SI base units are used.

The important PAW model parameters are listed in Table 4.1.

4.1.2 Bounding φ-Controller in Matlab

The simplified block diagram for the ADAMS simulated PAW plant and Matlab controller is shown in Fig. 4.2. The plant inputs consist of four hip torques which are based on the desired torques set by the "Leg Trajectory Generator" block and modified based on realistic speed-torque constraints in the "Motor Torque-Speed Curve" block. These constraints, which take into account actuator and amplifier saturation as well as rigid torque transmission through the motor gearhead and a timing belt and pulley pair, are illustrated in Fig. 4.3. The speed-torque curve reflects the manufacturer-specified values for the actuators and amplifiers used on the robot, as described in Section 3.2. The plant outputs are the four hip angles, the four hip angular velocities, the four leg lengths, and the contact penetration into the ground of the four toes. In addition the ADAMS simulation outputs inertial information such as roll, pitch and yaw (and the three angular rates), and the x, y and z coordinates of the COM (as well as the three velocity components). The Matlab controller only uses the hip angles, hip angular velocities and contact penetration values for control. All other plant outputs are made available for analysis of results via the same Matlab analysis scripts used for the experimental PAW and Scout II results.

The bounding φ-controller, described earlier in Section 3.4.2, is implemented in the Matlab Controller section of Fig. 4.2. The bounding state machine, as described in Section 3.4, is implemented in the "Bound Controller" block. State switching is based on foot-

Table 4.1 Simulated PAW Parameters

Parameter	Value
Front Body Width	0.366 m
Rear Body Width	0.240 m
Front Toe-to-Toe Width	0.454 m
Rear Toe-to-Toe Width	0.328 m
Body Length	0.500 m
Hip Separation	0.322 m
Leg Length	0.210 m
Body Height	0.170 m
Max Body Clearance	0.125 m
Sprung/Upper Leg Mass (Each)	0.478 kg
Unsprung/Lower Leg Mass (Each)	0.814 kg
Body Bass	15.7 kg
M. of Inertia (I_{xx}, I_{yy}, I_{zz})	(0.170, 0.470, 0.372) kg m^2
Pr. of Inertia (I_{xy}, I_{xz}, I_{yz})	(-0.00061, 0.00064, -0.00665) kg m^2
Leg Spring Constant	2000 N/m
Leg Spring Damping Constant	20 N-s/m
Leg Spring Preload	-72 N
Leg Spring Free Length	0.123 m
Contact Stiffness	1E7 N/m
Contact Damping	20.0 N-s/m
Contact Penetration	1E-4 m
μ_{static}	0.8
$\mu_{dynamic}$	0.76
stiction trans. velocity	2 m/s
friction trans. velocity	3 m/s
No Load Actuator Speed (*Matlab Controller*)	600 deg/sec
Actuator Stall Torque (*Matlab Controller*)	50 Nm
Amplifier Torque Limit (*Matlab Controller*)	26 Nm

ground penetration in simulation, rather than the leg compression implemented on the robot. Selection of actuator control type is made in the "Leg Trajectory Generator" block. Velocity, position or torque control can be selected in this block, but only torque and position control are used. The Matlab code for these two blocks is nearly identical to what is implemented in C on the actual robot. The motor speed-torque curves, with the saturation components discussed in Chapter 3, are implemented in the third block, with actuator and amplifier limits listed in Table 4.1. The fourth "plant" block is a link between the Matlab controller and the separate ADAMS integrator, which accesses the parametric ADAMS model script. Simulations are run in manner similar to operation of the robot, with the exception that the gait is initialized by dropping the robot from a constant height in simulation, rather than by using a kickstart from ground level, as is done on the robot. The simulations last for 5.5 seconds. This is sufficient time to allow the PAW model to settle to steady-state bounding, as shown in Fig. 4.4.

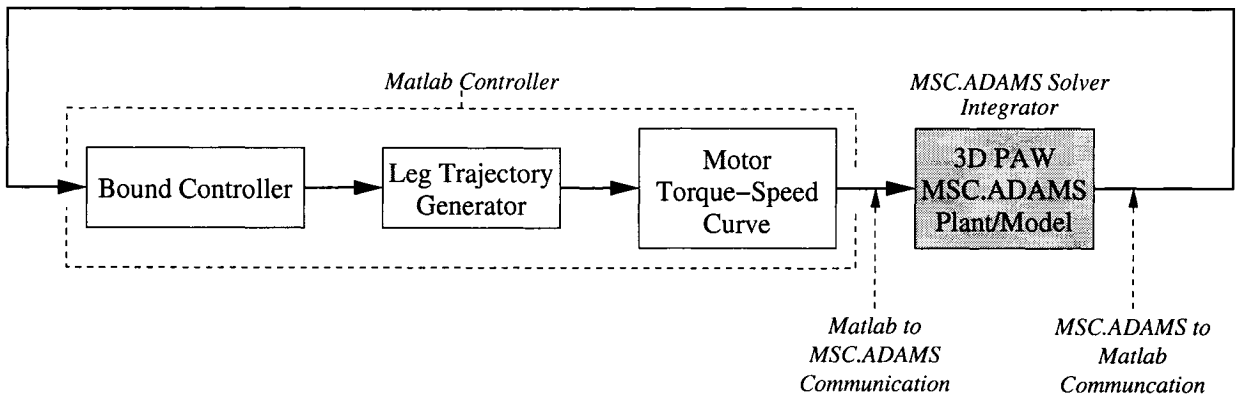

Fig. 4.2 Block diagram of the simulated PAW bounding controller and plant.

4.2 Simulation Results

By implementing the model of PAW in ADAMS as described above it is possible to examine basic characteristics of the PAW robot and qualitative trends of its locomotion free from experimental constraints. In particular, the relationship of touchdown and liftoff angles with respect to the forward speed of the robot is examined here. The results are broken up into two components, given in Table 4.2. In the first set, Simulations 1 - 4, the touchdown angles of the front and rear legs are set to -25 and -30, from vertical, respectively. In the

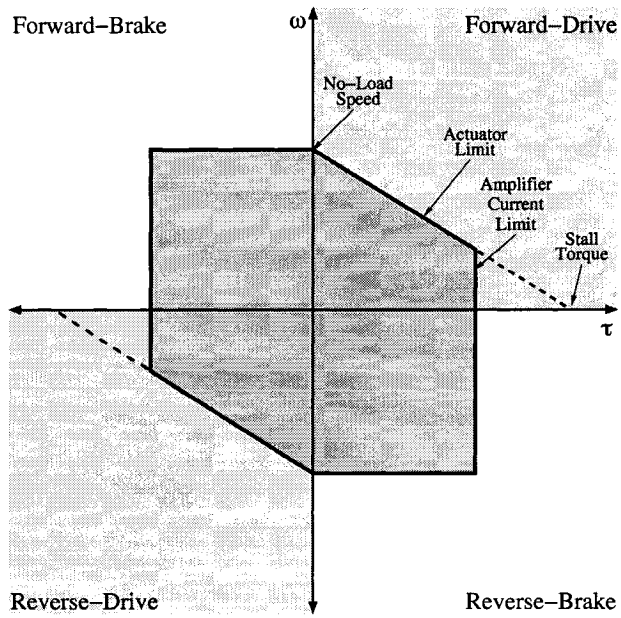

Fig. 4.3 Motor model in the ADAMS PAW simulation. The motor model implemented in the "Motor Torque-Speed Curve" block in Fig. 4.2 contains both actuator and amplifier saturation constraints.

second set, Simulations 5 - 8, the touchdown angles of the front and rear legs are set to -23 and -30, from vertical, respectively.

Prior to examining this relationship, however, it is important to first determine whether the simulated PAW model is a qualitatively valid representation of the PAW robot. This is done below.

4.2.1 Qualitative Similarity of the Simulation and the PAW Robot

In [18] it was demonstrated that accurate actuator modeling is essential for obtaining good agreement between simulated and experimentally measured parameters such as torques and displacement and orientation of the robot body. The PAW ADAMS model discussed here is not as complete as the Scout II model reported in [18] as it assumes rigid hip transmission characteristics and an ideal battery. The lack of these two items reduces the accuracy of the ADAMS PAW model but, as is discussed below, is sufficient for obtaining a qualitative sense of the characteristics of PAW's dynamics.

Table 4.2 Simulated PAW Results: Leg Angles vs. Fwd Speed and COM Apex Height.

Sim. #	Front Leg Angles $(\varphi_{ftd}, \varphi_{flo})$ [deg]	Rear Leg Angles $(\varphi_{rtd}, \varphi_{rlo})$ [deg]	Speed [m/s]	COM Apex Height [m]
1	(-25, 14)	(-30, 29)	1.30	0.246
2	(-25, 13)	(-30, 28)	1.28	0.247
3	(-25, 12)	(-30, 28)	1.24	0.248
4	(-25, 11)	(-30, 26)	1.20	0.250
5	(-23, 15)	(-30, 29)	1.31	0.242
6	(-23, 13)	(-30, 28)	1.31	0.242
7	(-23, 12)	(-30, 27)	1.29	0.243
8	(-23, 11)	(-30, 26)	1.24	0.245

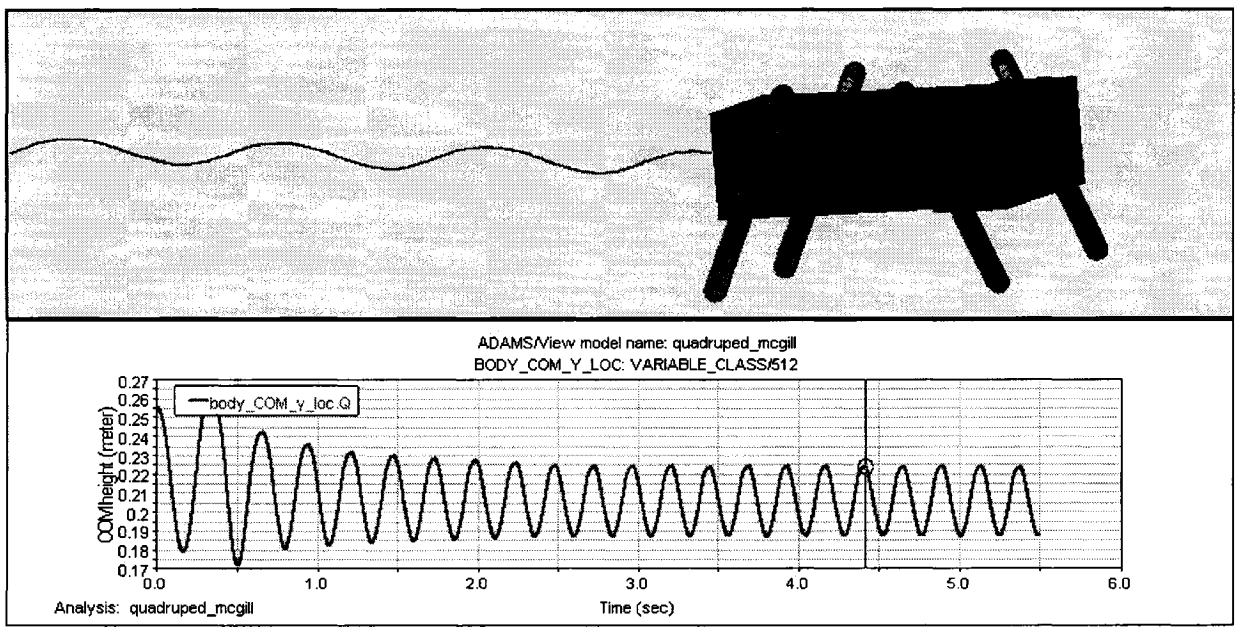

Fig. 4.4 Simulation of the bounding gait in ADAMS using the PAW model. The COM trajectory is shown trailing the PAW animation. The bottom plot illustrates the settling of the COM height in conjunction with PAW model achieving a bounding gait limit cycle.

Leg Angles Resulting in Bounding

While stable bounding gaits have been achieved using the 3D ADAMS model presented here, along with the 2D Working Model version in [94], the leg angle parameters which lead to stable solutions, as presented in Table 4.2, are not identical to those achieved on the real robot, as reported in Chapter 6. In both the 2D simulation of [94] and the ADAMS 3D simulation the legs sweep through a somewhat larger arc between touchdown and liftoff than on the real robot. For instance, in Simulation 5 of Table 4.2 the front legs sweep 38° while the rear legs sweep through 59°. The real robot, in Experiment 4 of Table 6.2 sweeps through 30° and 40° in the front and rear legs, respectively. This means that both the touchdown and liftoff angles, φ_{td} and φ_{lo}, used on the actual robot are smaller, in the absolute sense, than those seen in simulation, leading to slightly higher speeds in simulation (up to 1.3 m/s) than in reality (up to 1.2 m/s).

Leg Duty Cycles and Phase Differences

The phase difference between ground impacts of the front and rear leg touchdown is similar between the PAW robot and the ADAMS simulation. The ADAMS PAW model and PAW robot demonstrate phase differences in the neighborhood of 10% to 20% during the bound. The model tends towards values between 10% and 15%, shown in Table 4.3, while the PAW robot demonstrates phase differences between 15% and 20%. This means that the PAW model is demonstrating a more pronk-like bound than the actual robot. This is due to the larger, more horizontal touchdown angles used in simulation, since, when used on the robot, they also lead to reduced phase differences.

The duty cycle measures the time the leg spends on the ground versus its time in flight. The PAW robot and the ADAMS PAW simulation show some similarity in terms of the duty factor. In both cases the front legs tend to remain on the ground for less time than the rear legs, which is consistent with the notion that the rear legs are more important for thrust. While the PAW robot's front duty cycle, shown in Table 4.3, remains in the high thirties, the rear legs extend from the high thirties to the mid fourties. The simulated robot, on the other hand, shows front duty cycles in the low thirties and rear duty cycles in the low fourties, as shown in Table 4.3. This indicates that it is spending proportionally more time in flight than the real robot.

Table 4.3 Simulated & Experimental PAW Results: Footfall Phase Differences and Duty Cycles. See Table 6.2 on page 85 for more on the experimental results.

Sim. #	Phase Difference (mean) [%]	Front Duty Cycle (mean) [%]	Rear Duty Cycle (mean) [%]
1	11	32	41
2	11	32	41
3	12	31	41
4	14	33	41
5	15	34	41
6	14	34	41
7	14	34	43
8	14	34	42
Exp. #	Phase Difference (mean) [%]	Front Duty Cycle (mean) [%]	Rear Duty Cycle (mean) [%]
1	18	36	41
2	19	36	39
3	19	40	42
4	16	41	46

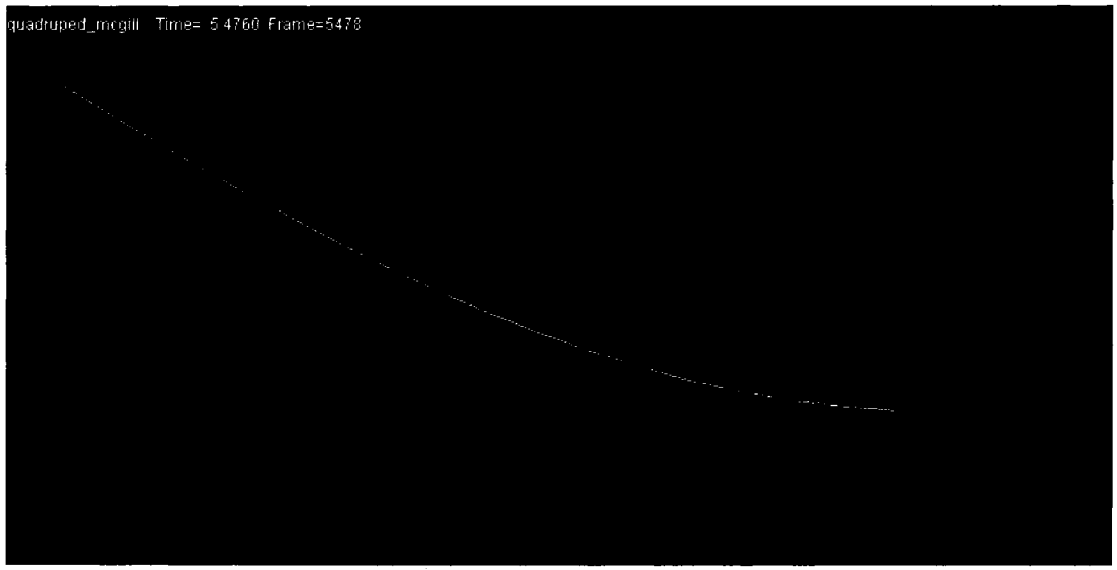

Fig. 4.5 The PAW model yaws during the bound. During bounding simulations the PAW model arcs in a counter-clockwise fashion, similar to PAW and Scout II. This is due to asymmetric mass distribution.

4.2.2 Source of PAW's Passive Yaw During Bound

Both the Scout II and PAW robots have a tendency to yaw in a counter-clockwise direction during the bound, even when all gait parameters are symmetric from left to right. Possible sources for this yaw are asymmetric motor or gearing characteristics, asymmetric mass distribution and variability in the leg spring constants. As can be seen in Fig. 4.5 this tendency extends to the ADAMS simulation. The model, however, is geometrically symmetric, and has identical actuation and compliance parameters between the four legs. The inertia matrix of the body of the PAW model, however, is non-diagonal due to asymmetric placement of the hip actuators on the robot.

By zeroing the off-diagonal terms in the inertia matrix the ADAMS model is made to bound in a straight line, as shown in Fig. 4.6. Therefore, one method to achieve a zero bias in yaw on the PAW or Scout II robots during the bound is through a new motor configuration or through the introduction of masses to achieve a diagonal inertia matrix for the robot. Given that the actuators, along with the batteries, are the largest and densest components on the robot, this is considered a non-trivial task. Alternatively, differential torques can be applied to correct for the yaw, as discussed in [88], or liftoff angles can be adjusted such as in the ϕ_{lo}-turn controller discussed in Chapter 7.

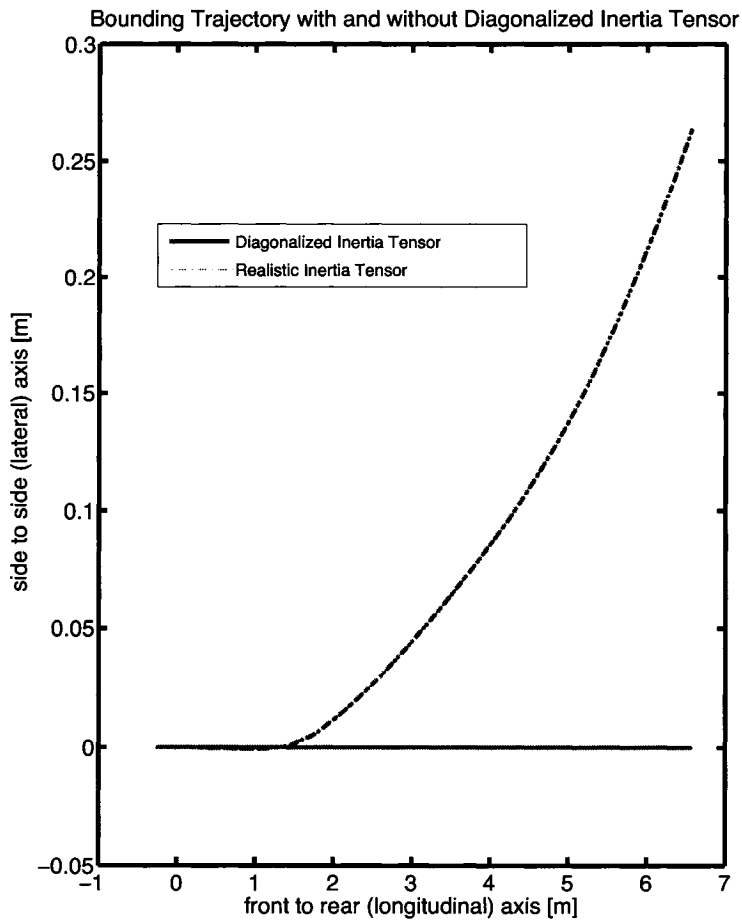

Fig. 4.6 Effect of the inertia matrix on the bounding trajectory. The bounding trajectory is affected by the off-diagonal terms of the inertia tensor. Here, the ground-projected COM trajectory is shown for bounding using the same leg angle parameters but with a realistic inertia tensor and an idealized one, with no off-diagonal terms.

4.3 Forward Speed Regulation

The eight simulation trials conducted on the ADAMS model, as shown in Fig. 4.4, illustrate the validity of implementing speed control through regulation of sweep limit angles, as originally proposed in Section 3.4. Table 4.2 illustrates that by alternatively making the front and rear sweep limits – and thereby, the liftoff angles – more vertical, the forward speed of the robot is decreased. In Simulations 1 - 4 a combined change in the φ_{flo} and φ_{rlo} liftoff angles of 6° yields a change in speed of 0.10 m/s, while in simulations 5 - 8 a 7° change yields a corresponding speed change of 0.07 m/s. This compares favourably to the 0.3 m/s change in speed for a combined change in liftoff angle of 12° obtained with PAW robot bounding, as shown in Experiments 2 - 4 of Table 6.2 in Chapter 6. In addition, as these liftoff angles become more vertical the ADAMS model develops a more significant flight phase, reflected in the increasing COM apex heights.

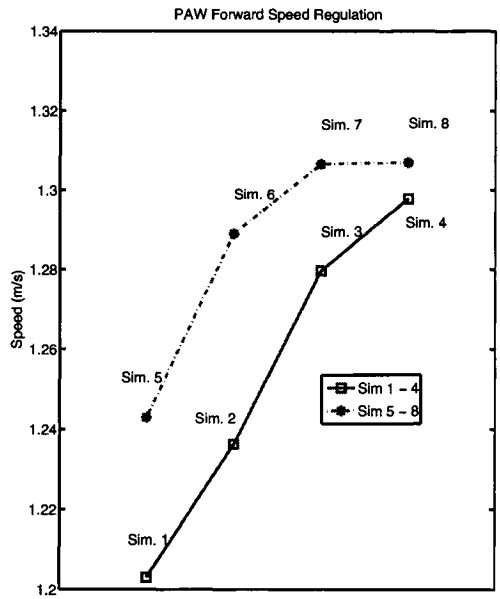

Fig. 4.7 Simulated PAW forward speed regulation. See Table 4.2 for details.

Exceptions to these trends exist at the boundaries of the results presented in Table 4.2. For instance, a plateauing of the speed and apex height is noticeable in Simulations 5 and 6. As shown in [17] increasing the touchdown angles beyond a certain value will result in braking rather than acceleration. This is also visible in the results presented in Table 4.2 and Fig. 4.7, where Simulations 1 - 4 have larger touchdown angles, but slower overall speeds than Simulations 5 - 8.

4.4 Summary

In this chapter, simulations involving a three-dimensional model of the PAW robot and a matching bounding controller were discussed to complement experimental work presented in later chapters. The simulation allowed for a study of the dynamics of the PAW model in more controlled conditions than are possible with the actual robot. In addition, the results can be obtained more rapidly than is possible on the robot and the effect of parameters such as the off-diagonal components of the inertia matrix could be studied with greater ease than is possible on the robot. The PAW model and the φ-controller were implemented in ADAMS and Matlab, respectively. The model of PAW and its robot analogue were found to bound in a qualitatively similar fashion. It is not surprising that a closer quantitative match was not obtained considering that even the more detailed models of [18] were only valid for a few strides. The counter-clockwise yaw found to occur in both Scout II and PAW also occurs in ADAMS model of PAW, leading to the conclusion that the yaw is due to asymmetric mass distribution, as opposed to other factors such as asymmetric motor or leg spring characteristics. Finally, the hypothesis that forward speed could be regulated via the liftoff angle, proposed in Chapter 3, was tested in simulation and found to be valid within certain limits. In Chapter 6 this hypothesis will again be tested on the real PAW robot.

Chapter 5

PAW Rolling Mobility Behaviours

This chapter, the first among the three dealing with experimental results for the two quadrupedal robots employed in the course of this research, is dedicated to the *wheeled* mobility of the PAW robot. In particular, controllers for rolling behaviours, which take advantage of the hybrid nature of the platform and improve stability of PAW are discussed. In Section 5.1 three rolling mode controllers are introduced. The inclined turning method of Section 5.1.1 illustrates how to improve turning of PAW over simple skid-steering by repositioning the wheels and lowering the centre of mass of the robot. An improvement to braking is made in Section 5.1.2 by placing the wheeled-legs in a sprawled position prior to braking and using the wheel motors to dissipate energy. The ability to reposition the wheeled-legs is then combined with inertial feedback of Inertial Measurement Unit (IMU) data in Section 5.1.3 to develop a controller for maintaining body pitch while climbing slopes.

Experimental results for wheeled modes of mobility on PAW are presented in Section 5.2. In Section 5.2.1 experiments are conducted to demonstrate rolling speeds of up to 2.0 m/s. The operational range is found to be over 2500 m in Section 5.2.2. In addition, a battery of experiments are conducted in Sections 5.2.3 to 5.2.5 demonstrate the successful operation of the turning, braking and IMU-assisted slope ascent and descent controllers.

5.1 Rolling Mode Controllers

Three types of controllers are introduced in this section. The first describes a method for turning, while the second describes a method for braking. Both controllers take advantage of the ability to reposition the wheels with respect to the body of the robot. The third

mode shows how to incorporate data from the IMU on the robot to maintain body pitch while climbing a slope.

5.1.1 Inclined Turning Controller

A new method is proposed here for achieving turns on the PAW robot. The method is based on the standard differential (skid) steering approach, but it also takes advantage of the hybrid mobility of PAW. Thus, rather than applying differential wheel speeds on either side of the robot with the legs fixed, the legs are used to reposition the wheels to reduce shear forces on them. Effectively, this means that while the legs on the outside of the turn are kept vertical with respect to the body, the legs on the inside of the turn are brought together, lowering the center of mass (COM) and leaning the robot *into* the turn. The delaminating effect of excessive shear forces during normal differential turning is shown in Fig. 5.1. In the following the derivation of the wheel speed setpoints is presented. These, in turn, are fed as inputs to the wheel motor controller described in Section 3.3 of Chapter 3.

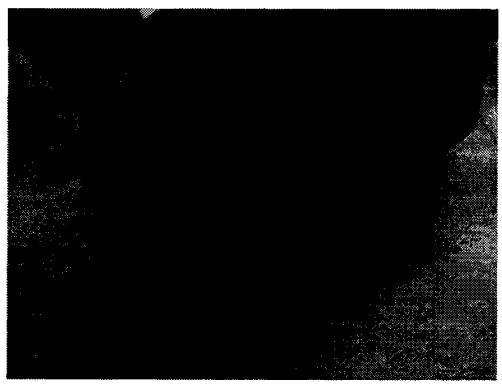

Fig. 5.1 Tire delamination due to regular differential (skid) steering. The inclined turning method reduces the shear forces which cause excessive tire wear.

To begin with, three concentric circles are defined. The first is the circle which defines the path that the ground-projected centre of mass follows. This corresponds to the origin of the reference frame in Fig. 5.2b. The other two circles define the paths along which the wheels will travel. The wheels on the outside travel along a larger circle than that of the COM, while the wheels on the inside of the turn travel along a smaller circle. The wheels on the smaller, inside curve (see the wheels in the foreground of Fig. 5.2a) will be set to

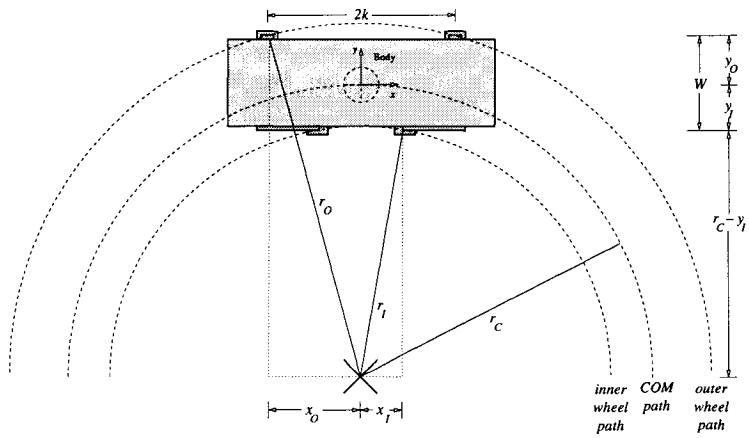

(a) Top View

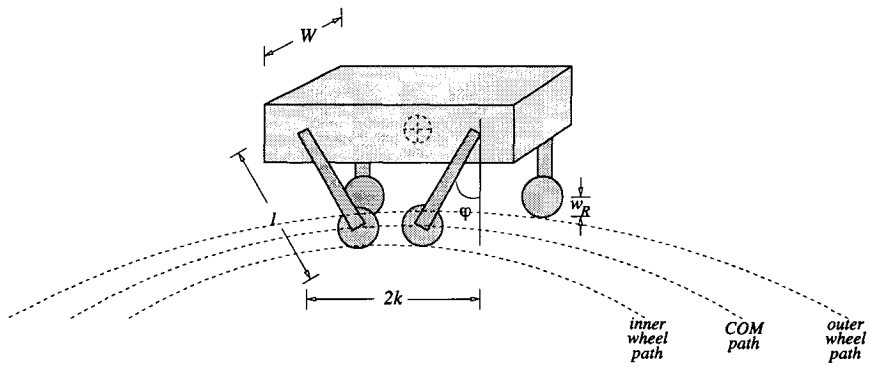

(b) Three-Quarter View

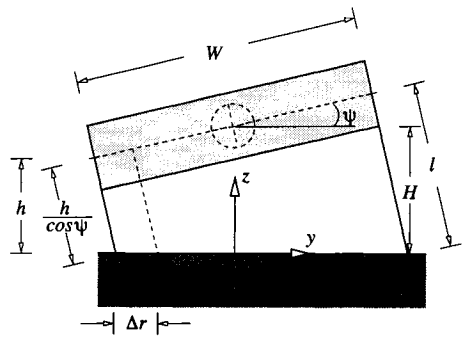

(c) Frontal View

Fig. 5.2 Simplified views of PAW illustrating some important variables used in calculating hip angles for the turning algorithm. Three concentric circles representing the main trajectories of the wheels and COM are shown with dashed lines.

spin slower than those on the larger, outside curve (see the wheels in the background of Fig. 5.2a).

As shown in Fig. 5.2, given a desired COM height H, a known maximum leg length l, a known body width W, and a requirement that one pair of legs must remain vertical with respect to the body's local coordinate frame, a roll angle of the body ψ, can be determined:

$$\psi = acos\left(\frac{H}{\sqrt{l^2 + \frac{W^2}{4}}}\right) + atan\left(\frac{2l}{W}\right) - \frac{\pi}{2}. \tag{5.1}$$

It is noted here that the body width W, is the value midway between the wheel-to-wheel width of the front legs and the wheel-to-wheel width of the rear legs. This simplifies the following calculations, by effectively making the front and rear widths of the robot identical. A small correction to final wheel velocities to compensate for this simplification is stated at the end of this section. Next, the height of the hips of the inner legs h, can be determined:

$$h = l\ cos(\psi) - W\ sin(\psi). \tag{5.2}$$

The angle φ, at which the hip joint is set with respect to the body can now be calculated:

$$\varphi = acos\left(\frac{\frac{h}{cos\psi} - w_R}{\hat{l}}\right) \tag{5.3}$$

where w_R is the radius of the wheel and $\hat{l}$ is the length of the leg from the hip to the wheel axle, $l - w_R$. The second hip's angle is simply set to $-\varphi$, resulting in the inner hips being in a gathered configuration, as seen in Fig. 5.2a.

In order to determine the inner and outer turning radii, one must determine the location of one of the wheels in the inner pair and one in the outer pair with respect to the COM of the robot, where the x and y axes form a plane parallel to the ground, whose origin is located directly below the COM:

$$x_I = -\hat{l}\ sin(\varphi) + k \qquad y_I = -\frac{W}{2}cos(\psi) + h\ tan(\psi) \tag{5.4}$$

$$x_O = k \qquad y_O = \frac{W}{2}cos(\psi) + l\ sin(\psi) \tag{5.5}$$

where k is half the hip spacing. Given a desired turn radius for the COM, r_C, the turn radius for the inner legs can be found as follows:

$$r_I = \sqrt{(x_I)^2 + (-y_I + r_C)^2} \tag{5.6}$$

while the turn radius for the outer legs is

$$r_O = \sqrt{(x_O)^2 + (y_O + r_C)^2}. \tag{5.7}$$

To set the speed of the wheels on the T-shaped layout of the real robot, the inner and outer radii are corrected by $\pm\Delta r$ to account for the offsets between front and rear wheels with

$$\Delta r = \frac{1}{4}\frac{\Delta W}{cos\psi} \tag{5.8}$$

where ΔW is the difference in front and rear "wheel-to-wheel" (or leg-to-leg) widths on the robot, as listed in Table 3.1 in Chapter 3. The individual wheel speeds are set proportionally to the corresponding radii to give the desired COM speed:

$$v_{fI} = \frac{r_I + \Delta r}{r_C} v_C \qquad v_{rI} = \frac{r_I - \Delta r}{r_C} v_C \tag{5.9}$$

$$v_{fO} = \frac{r_O - \Delta r}{r_C} v_C \qquad v_{rO} = \frac{r_O + \Delta r}{r_C} v_C \tag{5.10}$$

where v_C is the speed of the centre of mass, v_{fI} and v_{rI} are the velocities of the inner front and rear wheels, and v_{fO} and v_{rO} are the velocities of the outer front and rear wheels.

5.1.2 Braking Controller

Another important aspect of PAW's locomotion that must be considered is stopping. While driving forwards or backwards it is important to apply braking action in such a way as to prevent the robot from pitching over. Pitching motion can result from braking too suddenly or by angling the legs either vertically or in a gathered configuration. During forward and reverse driving the robot places its legs in a sprawled posture, at about $\pm 11.5°$ with respect to the body's vertical reference. When a brake command is issued the motors are used to

dissipate the kinetic energy of the robot through the use of low gain PD controllers, as described in Section 3.3, which also prevent wheel slip by not immediately locking up the wheels.

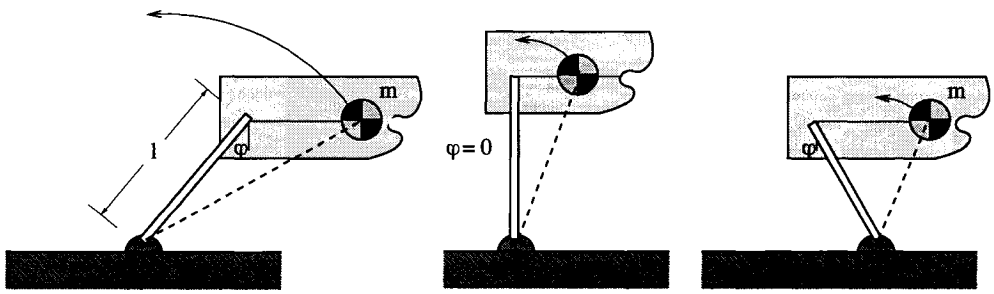

(a) Extended (b) Vertical (c) Gathered

Fig. 5.3 Front leg positions for different braking modes on PAW. Robot is travelling from right to left prior to braking.

To gain insight into the effect of leg position on braking, the front of the robot was modeled such that the distal end of the leg was considered to be a pin joint, and the rest of the robot an inverted pendulum, as shown in Fig. 5.3. The compliance in the legs is ignored in this analysis because the springs currently used on the robot are too stiff to show significant deflection during braking. The kinetic energy prior to braking was compared to the increase in gravitational potential energy required for the pendulum to pivot over the apex point. If the initial kinetic energy value is greater than the increase in gravitational potential energy, then the braking action fails. The maximum predicted forward speeds for given leg angles to ensure stable braking are given in Table 5.1. The increase or decrease in the *static stability margin* (the distance from the ground-projected center of mass to the support point) is also listed, using the vertical leg case as a baseline. The modeling shows that simply extending the legs yields a positive increase in the static stability margin and that it should be implemented on the PAW robot.

5.1.3 IMU-Assisted Slope Ascent and Descent

Using inertial sensing available on PAW it is possible to adjust the legs of the robot to maintain a desired attitude. For instance, while rolling up or down a hill, it can be desirable

Table 5.1 Braking: maximum forward speeds for given leg angles.

Type	Max Fwd. Speed [m/s]	Leg Angle [deg]	Change in Static Stability Margin [%]
Extended	1.28	-11.5	+26
Vertical	1.03	0	baseline
Gathered	0.79	+11.5	-26

to keep the body of the robot horizontal. Not only is this beneficial for potential sensors such as cameras or laser range-finders, it allows redistribution of wheel loading to maximize traction.

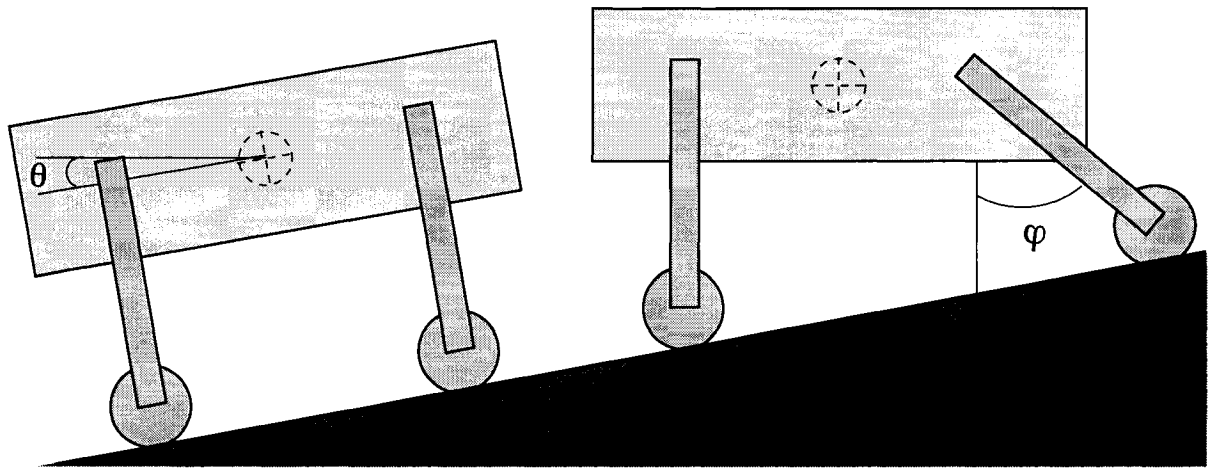

Fig. 5.4 Adjusting leg angle to maintain horizontal attitude.

A simple controller for adjusting the pitch of the robot is proposed here and illustrated in Fig. 5.4. Body pitch is adjusted by angle of the front leg hips when the IMU registers a pitch smaller than zero. When the pitch is greater than zero, it is adjusted by the angle of the rear hips. In both cases the lateral leg pair which is not used to adjust body pitch is held vertical with respect to the body's vertical axis. The desired hip angles are therefore defined with the following equations, where the desired hip angular velocity $\dot{\varphi}_{rd_n}$ or $\dot{\varphi}_{rd_n}$, (for the front or rear legs) is set to $\xi\theta$ where ξ is a gain in sec^{-1}. A desired hip angle, φ_{rd_n} or φ_{fd_n}, for the current control cycle n, is determined as follows, using the body's pitch angle θ, and the previously determined desired rear and front hip angles $\varphi_{rd_{n-1}}$ and $\varphi_{fd_{n-1}}$:

$$\varphi_{rd_n} = \begin{cases} \varphi_{rd_{n-1}} + \xi\theta\Delta t & \varphi_{rd_{n-1}} > 0, \theta > 0 \\ \varphi_{rd_{n-1}} + \xi\theta\Delta t & \varphi_{fd_{n-1}} \geq 0, \theta \leq 0 \end{cases} \tag{5.11}$$

$$\varphi_{fd_n} = \begin{cases} \varphi_{fd_{n-1}} + \xi\theta\Delta t & \varphi_{rd_{n-1}} \leq 0, \theta > 0 \\ \varphi_{fd_{n-1}} + \xi\theta\Delta t & \varphi_{fd_{n-1}} < 0, \theta \leq 0 \end{cases} \tag{5.12}$$

where $\varphi_{d_{n-1}}$ is the previous desired hip angle, Δt is the elapsed time since the last control action $(t_n - t_{n-1})$ was taken (approximately one millisecond). A PD controller, as described in Section 3.3 of Chapter 3, commands torque to the hip using the errors between the actual and desired values of hip angular position and angular velocity, calculated above, as inputs.

Two deficiencies of this controller are acknowledged. First, beyond a particular incline the controller will fail due to the bottom of the robot coming in contact with the ground. Secondly, this is strictly a pitch controller and does not take into account any roll component and, therefore, it is not suited to lateral slope traversal.

5.2 Experimental Results

In this section experimental results, demonstrating the rolling behaviours and controllers introduced in Section 5.1, are presented and discussed. Five basic results have been obtained. In Sections 5.2.1 and 5.2.2, the current maximum cruising speed of 2.0 m/s is established as well as the current operational range of over 2500 m obtained over the course of one hour. These results are included here for completeness, not to showcase a particular controller. In Section 5.2.3 the results of inclined turning tests with radii from 0.5 to 1 m are reported, while in Section 5.2.4 a demonstration of a sprawled braking is shown to help prevent tip-over. Finally, in Section 5.2.5, IMU-enabled slope ascent and descent are shown to function in both indoor and outdoor environments.

5.2.1 Cruising Speed

The highest straight-line speed attempted on the robot to date is 2.0 m/s, matching the predicted maximum rolling velocity discussed in [37].

For mobile robots to be of practical utility, they need to be energy efficient and be able to operate in a power autonomous fashion for extended periods of time. A standard

measure of vehicle efficiency is the specific resistance:

$$\varepsilon(v) = \frac{P(v)}{mgv} \tag{5.13}$$

where P is the power expenditure, m is the mass of the vehicle, g is the gravitational acceleration constant, and v is the vehicle speed. The specific resistance has been used to examine the efficiency of legged robots, [34, 97, 98] as well as traditional vehicles such as automobiles, ships and aircraft, [99, 100]. Alternatively, the "mechanical cost of transport", [101], has been proposed for biological running, which is similar to the specific resistance but without the gravitational term. Robot power consumption can be determined using onboard voltage and current sensors, as described in Section 3.2. The power and velocity values are *averaged* over the course of the experiment. While sitting with its body against the ground the robot has an average quiescent power consumption of 25 W. Comparatively, when placed on a 16 degree slope, with its legs locked perpendicular to its body and its wheels in active brake mode the robot consumes approximately 58 W.

Power consumption has been measured for the PAW robot rolling in a straight line at constant speed. For example, at a speed of 1.4 m/s its average power consumption has been found to be 51 W, while at 2.0 m/s it is 56 W. This corresponds to a specific resistance of 0.18 at 1.4 m/s and 0.14 at its current maximum speed, indicating that the robot runs more efficiently at the higher speed. In comparison, legged robots such as Scout II have an unsurprisingly higher specific resistance: 1.4 while bounding at 1.3 m/s, [18], and 1.47 while galloping at 1.4 m/s, [29]. Graphs comparing specific resistance values for various locomotion modes for Scout II and PAW are found in Figs. 6.16 and 7.10 in Chapters 6 and 7, respectively.

5.2.2 Operational Range

The robot uses three battery packs composed of a total of 30 NiMH D-Cells, as discussed in Section 3.2. At its current maximum speed of 1.4 m/s the robot draws approximately 1.36 A, yielding a peak theoretical run-time of over five hours using the Sanyo HR-D and nearly seven hours with the Saft VH D battery packs. On flat ground this translates to a maximum theoretical distance of 28 to 35 kilometres, respectively. To test the maximum range of the robot under somewhat more realistic conditions than non-stop straight line motion, the robot was made to move back and forth on a three metre track with a maximum desired

speed of 1.4 m/s until a critical (below 32 VDC) battery voltage was detected. Using a set of the VH D battery packs the robot travelled a total of 2.562 km in 59 minutes, with four brief interruptions to check motor temperature. The test was terminated when the battery voltage dropped suddenly from above 32 VDC to 21 VDC during a deceleration. In order to increase operational range, the frequency of direction-of-travel changes could be lowered, deceleration and acceleration phases could be increased in length to decrease maximum current draw in the wheels, and the legs could be positioned more vertically to reduce current draw to the hip motors. In addition, controller gains in the hips would have to be lowered to reduce the possibility of current spikes which would cause proportional drops in the effective battery voltage. Any drop in battery voltage below 25 VDC is likely to cause false sensor readings or undesirable behaviour. Because of this sensitivity to lowered voltage (which results from extended battery usage, even with moderate current draw), it may not be possible for the robot to exceed double or triple its current range, even with the controller modifications mentioned above.

5.2.3 Inclined Turning

A series of tests were conducted on the turning behaviour, as described in Section 5.1.1. Table 5.2 presents the results of 12 experiments for different settings of desired COM radii, COM speed and two settings of leg angles (seven laps were performed for each experiment). Experiments 1-4 test two different desired speeds (0.5 and 1.25 m/s) as well as two different leg angles (29.6° and 62.0°) for a 0.5 m turn radius. Experiments 5 - 8 are a repetition of these tests for a desired turn radius of 0.75 m. Likewise, Experiments 9 - 12 repeat the tests for a desired radius of 1.0 m. Note that Columns 3 and 4 of Table 5.2 represent percentages of the values found in Column 5, the desired forward speed. Inner wheels values are less than 100% while outer wheels are greater. Desired radii and speed of the COM were matched to within approximately 10% for all experiments.

Improvements to the turning results could be made through better coordination of the hip and wheel controllers. Currently, these are independently controlled and, even with relatively low gains on the wheel actuators, the transition from horizontal to inclined postures demonstrates some jerk due to mechanical coupling. This, in turn, may have an effect on good matches between desired and actual velocity and radius of curvature. In addition, the model used to establish desired wheel velocities in large part assumes that

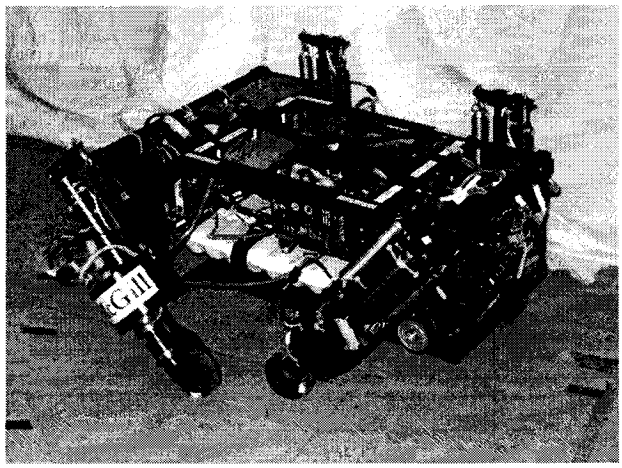

Fig. 5.5 The PAW robot executing an inclined turn.

front and rear legs lie in the same plane. While offsets are added in Equation 5.8 to take the non-planar nature, a more complete revision of the model may be beneficial.

The tires used in earlier differential steering tests, which demonstrated the delamination seen in Fig. 5.1, were not used in these trials. The older laminated rubber tires were replaced with solid rubber tires which are not susceptible to the type of wear seen in the earlier trials. However, earlier trials which used the laminated rubber wheels and an earlier version of this inclined turning controller demonstrated the effectiveness of the controller in reducing the wear due to shear loads.

Roll-over stability is an important factor in the design of many wheeled vehicles, [102]. It should be noted that increasing the roll-over stability of the robot via the implemented inclined turning algorithm is not critical at the speeds and radii of curvature it currently travels at, but it should become more important at higher speeds for this or a scaled-up version of the vehicle.

5.2.4 Braking

To demonstrate the positive aspects of the braking controller described in Section 5.1.2, experimental trials were performed with the robot driving at 1.5 m/s and with the legs gathered in and sprawled out, alternatively using high and low control gains for the wheel motors (the hip motors used relatively high gains throughout). A summary of the four

Table 5.2 Experimental Results: Inclined Turning. Note that Columns 3 and 4 represent percentages of the values found in Column 5. Inner wheels values are less than 100% while outer wheels are greater.

Exp #	Leg Angle [deg]	Outer Wheel Spds. [%]	Inner Wheel Spds. [%]	COM Speed Des'd [m/s]	COM Speed Ach'd [m/s]	Turn Radius Des'd [m]	Turn Radius Ach'd [m]
1	29.6	154, 141	56, 69	0.50	0.43	0.50	0.50
2	29.6	154, 141	56, 69	1.25	1.20	0.50	0.55
3	62.0	160, 147	58, 71	0.50	0.47	0.50	0.55
4	62.0	160, 147	58, 71	1.25	1.17	0.50	0.55
5	29.6	135, 127	70, 79	0.50	0.47	0.75	0.83
6	29.6	135, 127	70, 79	1.25	1.16	0.75	0.80
7	62.0	139, 131	72, 81	0.50	0.46	0.75	0.80
8	62.0	139, 131	72, 81	1.25	1.20	0.75	0.85
9	29.6	126, 120	78, 84	0.50	0.47	1.00	1.13
10	29.6	126, 120	78, 84	1.25	1.20	1.00	1.13
11	62.0	129, 123	79, 86	0.50	0.43	1.00	1.13
12	62.0	129, 123	79, 86	1.25	1.19	1.00	1.13

corresponding experiments is found in Table 5.3; ten runs were conducted for each setting and average braking distances were determined from these runs. In the first set of experiments the robot repeatedly tipped over while braking due to high gain wheel control and a gathered-in leg posture, as shown in Fig. 5.6a. In the second set of trials the wheel control gains were lowered and the robot did not tip over, but minor, non-critical, pitching is visible in video footage. A sprawled posture and high wheel gains, as conducted for the third set of experiments, resulted in wheel slip but a relatively short braking distance. In the fourth set of experiments, the wheel gains were lowered and a sprawled posture was used, as shown in Fig. 5.6, yielding stable braking with little noticeable slip or pitching but with an increased braking distance. For given leg angles the robot exceeded the maximum theoretical forward speeds, based on the inverted pendulum model and predicted in Table 5.1. This is due to the fact that the robot brakes over a non trivial distance, with kinetic energy dissipated through the motors and in wheel-ground friction.

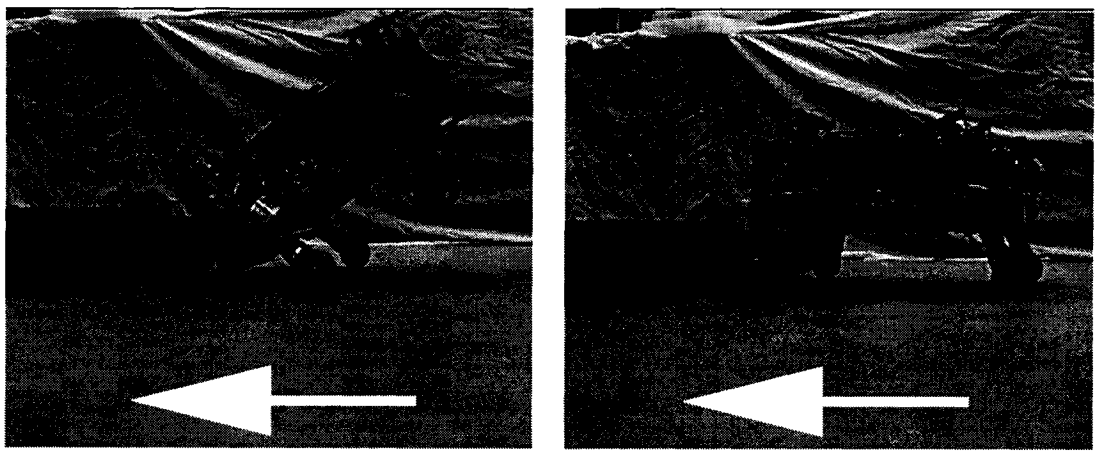

(a) Tipping over (b) Stable braking

Fig. 5.6 Two different braking methods, one which leads to tipping the other which is stable. The robot is travelling from right to left.

What these experiments demonstrate is that by simply decreasing the wheel control gains it is possible to reduce sliding and critical pitching motion during braking, while increasing braking distance. Using a sprawled posture further increases the stability of the robot, reducing pitching motion during braking in both low and high gain wheel control modes.

Table 5.3 Experimental Results: Braking

Exp. #	Speed [m/s]	Leg Angle [deg]	Leg Angle Description	Controller Gains	Brake Dist. [m]
1	1.5	$\pm$11.5	gathered	high	n/a
2	1.5	$\pm$11.5	gathered	low	0.24
3	1.5	$\mp$11.5	sprawled	high	0.15
4	1.5	$\mp$11.5	sprawled	low	0.23

5.2.5 IMU-Assisted Slope Ascent and Descent Experiments

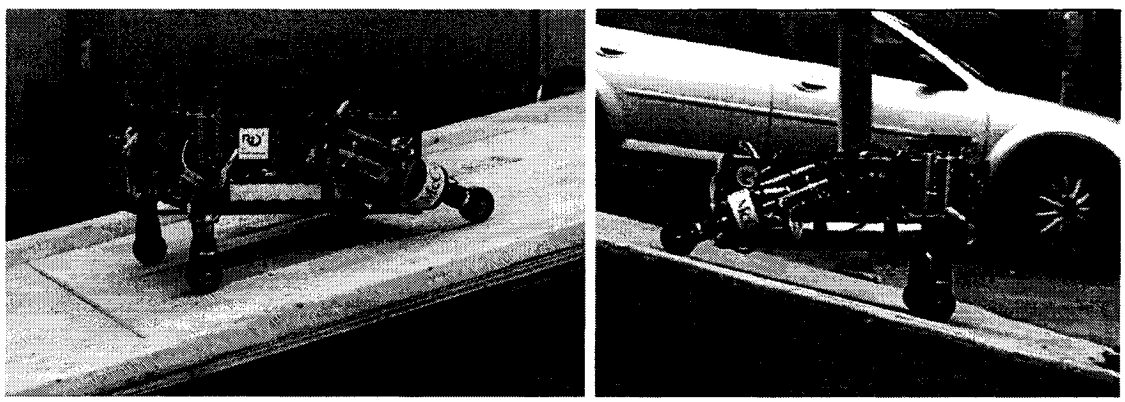

(a) Plywood Ramp (b) Concrete Ramp

Fig. 5.7 PAW climbing slopes both indoors (left, courtesy of DRDC – Suffield) and outdoors (right).

The robot has been made to ascend and descend a number of slopes, both indoors and outdoors, as is shown in Fig. 5.7. On a ramp with a 12 degree slope the controller discussed in Section 5.1.3 yields results such as those illustrated in Fig. 5.8, where the top plot shows the roll, pitch and yaw time histories measured by the IMU and the bottom plot shows the rear and front leg angles. The robot begins on a horizontal surface and is commanded to roll forward. The front wheels are initially stopped by the lip of the ramp, but overcome it at the 271.3 second mark. The rear leg wheels encounter the same problem, and overcome the lip at 274.4 seconds. With all wheels on the ramp, the robot finishes its adjustment of the front hip angles at 274.8 seconds, regulating the pitch of robot back to 0°. The final

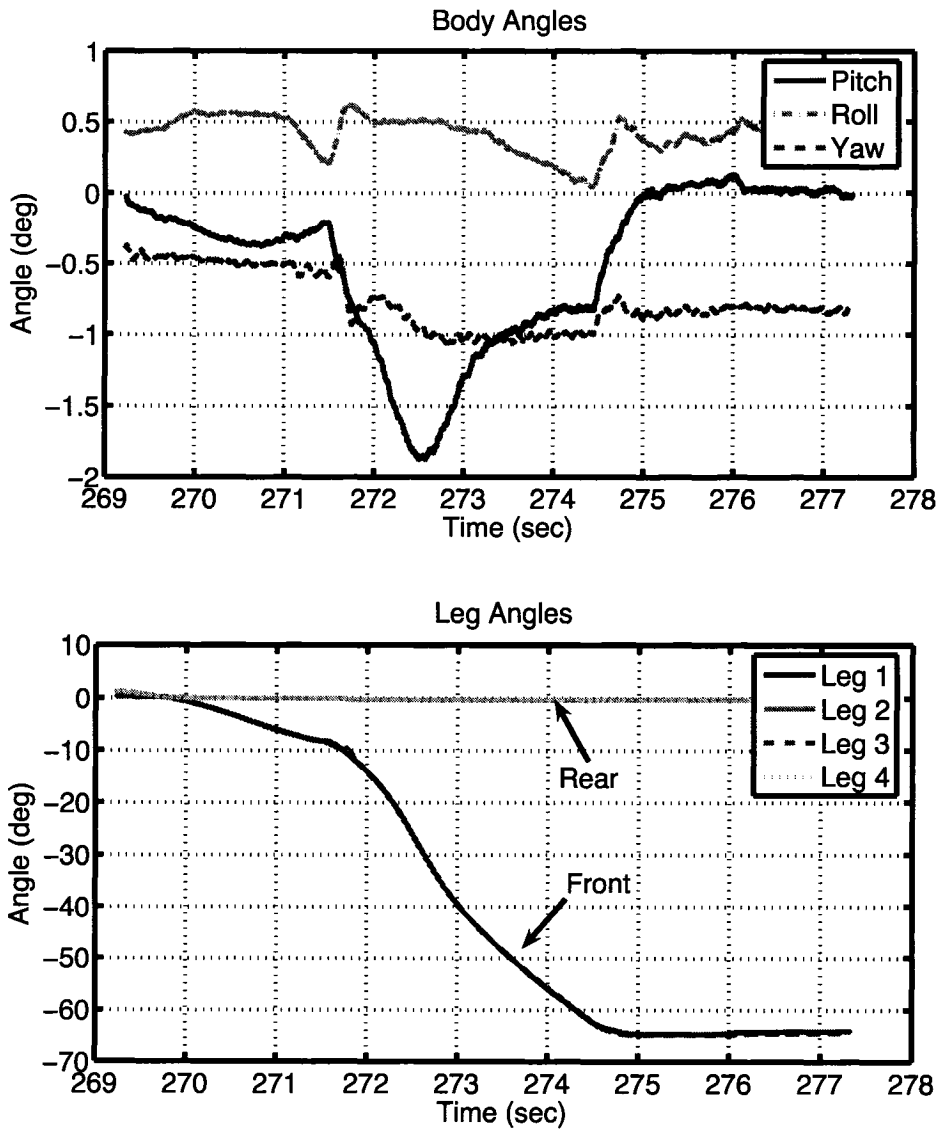

Fig. 5.8 IMU angular output as well as leg angles while climbing a ramp.

angle for the front legs is approximately -65° with respect to the body. Throughout the duration of the experiment the maximum pitch error does not exceed 2°. While the forward speed of the robot was kept to below 1 m/s throughout this experiment, other trials have been conducted, such as those during which the photos in Fig. 5.7 were taken, in which the forward speed of the robot was between 1.2 and 1.5 m/s and the slope of the ramps was between 10° and 15°. Regulation of the pitch was good in those cases as well, as is visible in the photos. The robot demonstrated the ability to brake while climbing the slope and changes in direction (ascent to descent and vice versa) worked consistendly. The failures of the slope ascent and descent controller occured when the slope exceeded about 20°. This is due to a disruption in the controller that occurs when the body of the robot contacts the ground. This can be compensated for in future implementations of the controller.

5.3 Summary

This chapter presented results of wheeled mobility research performed on the PAW hybrid wheeled-leg robot. The focus has been on developing control methods which take advantage of the legged capability of the robot to improve performance of certain basic rolling behaviours. Controllers for inclined turning and sprawled braking, as well as slope ascent and descent, which take advantage of the hybrid nature of the platform and improve stability were discussed. The robot demonstrated a controller which performed inclined turns by taking advantage of the ability to reconfigure wheel placement. Not only is this advantageous for stability in that it lowers the centre of mass, but it also reduces the wear on the wheels. In addition, through appropriate wheel placement and low controller gains the robot demonstrated the ability to brake without tipping over. The onboard inertial measurement unit was used for closed-loop control of body pitch for ascending and descending slopes.

Chapter 6

Bounding: Why Wheels & Liftoff Angle Matter

This chapter presents experimental results for quadrupedal bounding, using the Scout II and PAW robots, illustrated in Fig. 6.1. While a single type of bounding is discussed in Section 6.1 with respect to Scout II, *two variations of bounding* and a *new method of forward speed control* have been achieved on the PAW robot and are discussed in Sections 6.2 and 6.3, respectively. The bounding gait is explored using the wheels which are mounted on the distal ends of PAW's legs. The first bounding variation, presented in Section 6.2.1, uses unactuated, mechanically blocked wheels. This provides a baseline set of results using passive, fixed toes, similar to the results presented for Scout II. The second set of bounding results for PAW use actively controlled wheels and is discussed in Section 6.2.2. PAW is the *first robot* to achieve this *new* form of bounding and these results are compared to fixed toe bounding gaits achieved on PAW and Scout II.

While forward speed control is achieved using variation of touchdown angle φ_{td}, on both robots, it is shown here, for the first time that liftoff angle φ_{lo}, effected by the sweep limit φ_{swl}, is also a dominant parameter for speed control. A strategy for obtaining φ_{td} and φ_{lo} is given in Section 6.3. In Section 6.4 the effect of these two control parameters is examined with respect to gait parameters such as stride frequency, body pitch amplitude and leg compression. The conclusion reached is that the φ_{td} and φ_{lo} control parameters are complementary, with φ_{td} and φ_{lo} yielding coarse- and fine-tuning capability, respectively.

While the footfall patterns on both robots are found to be different due to their natural

dynamics, leg compression is found to be greater in the rear than the front legs, as reported in Section 6.5. The hip motor actuation is analysed for both Scout II and PAW in Section 6.6.1, while wheel actuation for PAW is presented in Section 6.6.2. Power efficiency, measured in terms of specific resistance ε introduced in Section 5.2.1, is shown in Section 6.7 to be better at higher speed in both robots during the bounding gait, with notable decrease in efficiency in PAW when active wheel control is used. Finally, measures for gait success are presented in Section 6.8 and the bounding gaits for both robots are shown to have good rates of convergence, stable limit cycles and very good repeatability.

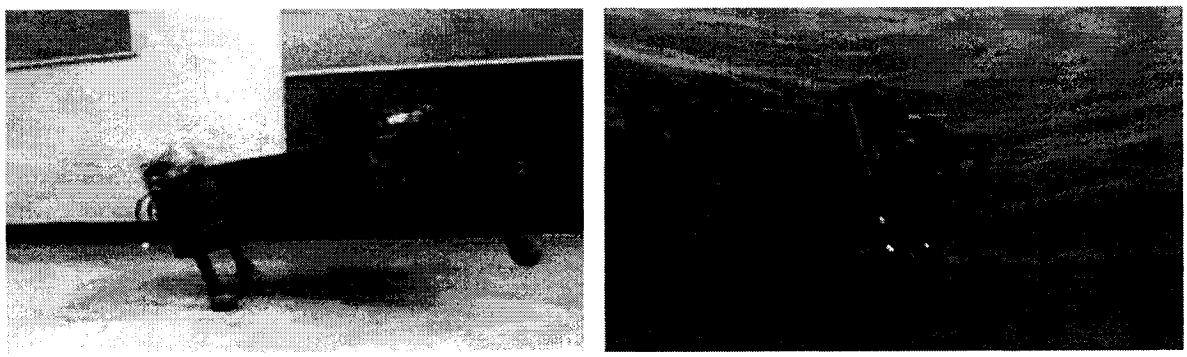

(a) Scout II (b) PAW

Fig. 6.1 Bounding video still frames of Scout II (a) and PAW (b). Here, Scout II has landed rear legs first, while PAW has landed front legs first.

6.1 Scout II Bounding Experiments

The bounding gait in Scout II has been studied previously in [47], [103], [86] and [87]; results from [18] are presented here in the context of making distinctions between the Scout II and PAW platforms. It is noted here that the Scout II and PAW robots perform the bounding gait in an underactuated sense because they accomplish this gait using fewer actuators than degrees of freedom of the robots. The number of unactuated degrees of freedom for different stages of the planar bounding robot are shown in Fig. 6.3 on p. 83.

As with previous bounding work on Scout II, in these experiments the touchdown angle of the front and rear legs was varied to primarily affect a change in the forward speed of the bounding gait. The desired liftoff angles of the legs were fixed at zero degrees throughout these experiments. Because this control method concentrates on hip angles referred to

the body frame, this is referred to as the φ-controller, as opposed to the $\dot{\varphi}$-controller, in which the hip stance-retraction velocity is also explicitly controlled, or the γ-controller, in which the hip angle is varied based on the pitch angle θ, [87]. Two major experiments were conducted, Exps. 2 and 3 of Table 6.1, each with a total of ten separate trials, in which the touchdown angles resulted in slow and fast bounds, respectively. Two additional experiments, Exps. 1 and 4 of Table 6.1, were carried out, each with only a single trial, for other touchdown angles. In all of these trials Scout II was made to accelerate prior to the timing of a steady-state bound over a distance of approximately four meters. During the acceleration routine the touchdown angle was increased from its initial value by one degree per stride over four strides. This enabled the robot to smoothly transition from standing to bounding, via an intermediate open-loop jump.

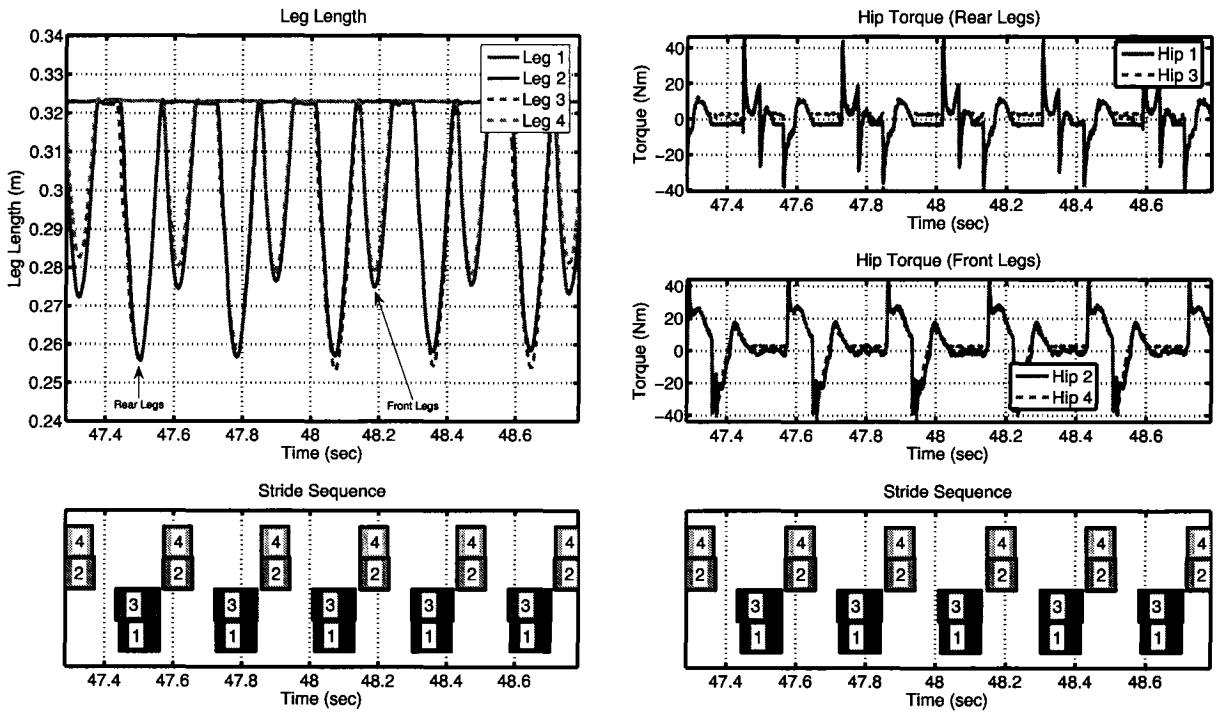

(a) Leg length (b) Hip torques

Fig. 6.2 Leg lengths (a) and hip torques (b) for *Scout II* during a fast bound (see Table 6.1, Exp 4.). Note the lack of common stance between front and rear legs.

The experimental data for Scout II bounding is presented here, starting with Table

Table 6.1 Experimental Results: *Scout II* Bounding. Italicized results (Exps. 1 and 4) represent isolated experiments with only a single trial. Experiments 2 and 3 were conducted with ten trials each.

Exp #	Front Touchdown & Liftoff Angles ($\varphi_{ftd}, \varphi_{flo}$) [deg]	Rear Touchdown & Liftoff Angles ($\varphi_{rtd}, \varphi_{rlo}$) [deg]	COM Speed [m/s]	Max Front Comp. (mean) [m]	Max Rear Comp. (mean) [m]	Stride Freq. [Hz]	Phase Diff. (mean) [%]	Front Duty Cycle (mean) [%]	Rear Duty Cycle (mean) [%]
1	*(-14, 0)*	*(-12, 0)*	*0.76*	*0.030*	*0.033*	*5.20*	*66.0*	*39.4*	*59.3*
2	(-16, 0)	(-14, 0)	0.86	0.032	0.038	4.82	65.0	36.7	56.3
3	(-21, 0)	(-19, 0)	1.26	0.044	0.064	3.50	49.8	28.8	42.3
4	*(-23, 0)*	*(-21, 0)*	*1.19*	*0.043*	*0.065*	*3.34*	*52.1*	*28.0*	*42.6*

6.1 and Fig. 6.2. Table 6.1 shows how, among other things, an increase in forward speed is obtained by making the legs more horizontal through higher touchdown angles, up to a certain limit (see Exp. 4), after which the braking action similar to that described by Raibert in [17] becomes apparent. Fig. 6.2 illustrates how regular the footfall pattern is during Scout II's bound. Greater leg compression is shown in Fig. 6.2a for the rear legs, than the front ones; this is similar to the results obtained with PAW. This supports the notion borrowed from biology that the rear legs are used primarily for thrust, while front legs are used for stabilization of the gait via their braking action. Hip torque profiles are also shown in Fig. 6.2b,[1] as measured by the current sensors of the hip amplifiers.

A simplified representation of the Scout II bounding gait is shown in the bottom portion of Fig. 6.3. The Scout II bounding results provide a *baseline* for evaluation of all of the PAW bounding results and also provide a baseline for comparison with the Scout II's gallop gait, which is discussed in the next chapter.

6.2 PAW Bounding Experiments

Inspired by the Scout II results, a number of bounding experiments was conducted on the PAW robot. These experiments, comprising several hundred individual trials, demonstrate

[1]Note that a non-zero bias is apparent in these hip torque plots, something which is also *occasionally* seen in PAW's amplifiers. This bias is likely due to the measurement circuitry and is not reflected in the actual motor current and resulting hip torque.

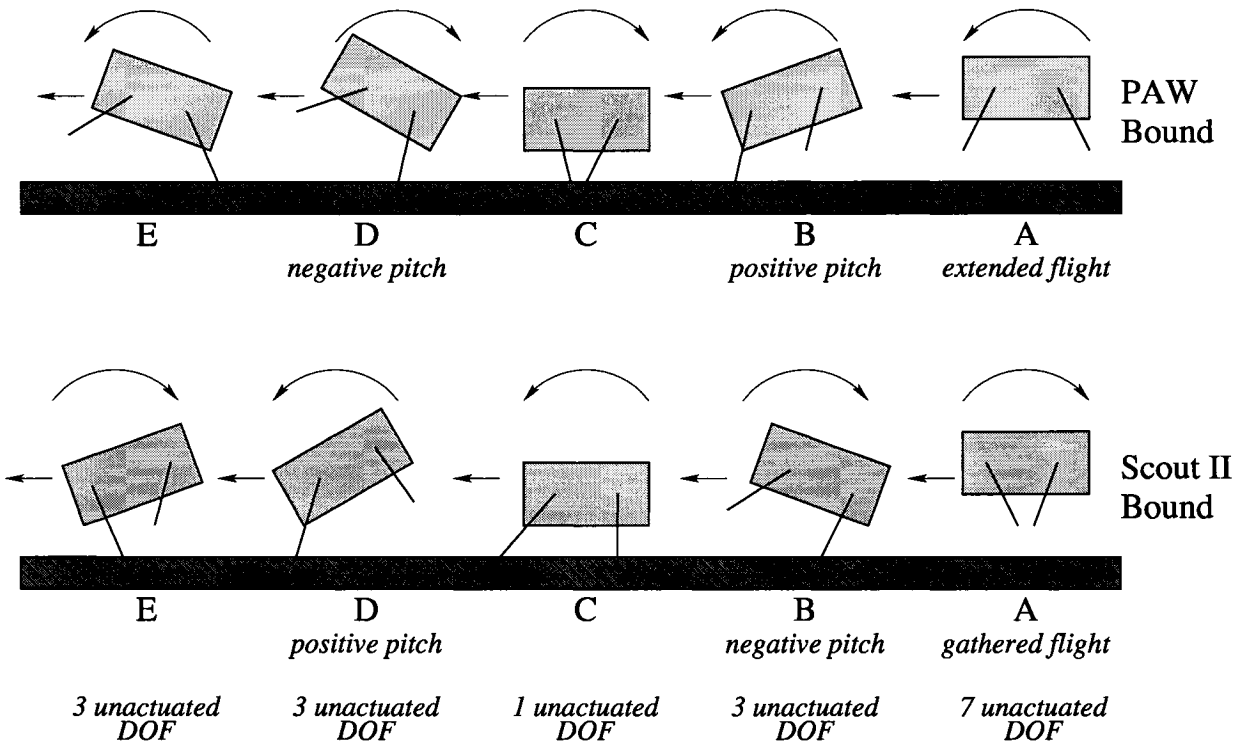

Fig. 6.3 Sagittal plane view of *Scout II*'s bound gait (bottom) versus *PAW*'s bound gait (top). Note that "double-support", shown in C, only occasionally occurs on Scout II. Direction of travel (right to left) as well as the pitch direction at different points in the gaits are shown. Degrees of freedom are calculated assuming pin joints at the hips and ground contacts and prismatic joints in the legs.

the possibility of bounding with both mechanically blocked and actively controlled wheels, and provide a baseline for the gallop gait on PAW.

Four *baseline* sets of experiments were performed on the robot using mechanically blocked wheels to approximate fixed toes. Five bounding experiments were also conducted using actively controlled wheels. In both cases the robot was made to run for three meters in an approximate straight line. After allowing the robot's pitch and roll motion to stabilize over the first meter (see IMU data in Fig. 6.18 on p. 107.), the speed of the robot was determined by measuring the elapsed time over the next two meters. For the results presented here, starting with Tables 6.2 and 6.3, approximately ten separate trials were performed for each experiment.

A simplified representation of the PAW bounding gait is shown in the top of Fig. 6.3.

Note the difference in the progression of the gait with respect to Scout II.

6.2.1 PAW Bounding Experiments with Mechanically Blocked Wheels

A set of bounding tests was performed using mechanically blocked wheels to help identify whether active control of the wheels had any significant effects on the bounding gait. To prevent the wheels from turning an adhesive was poured around and between the teeth of the bevel gears connecting the wheel and wheel motor. Triangular pieces of rubber were also wedged between the wheel and the wheel motor mount. A photo of a mechanically blocked wheel on PAW can be found in Fig. 6.4.

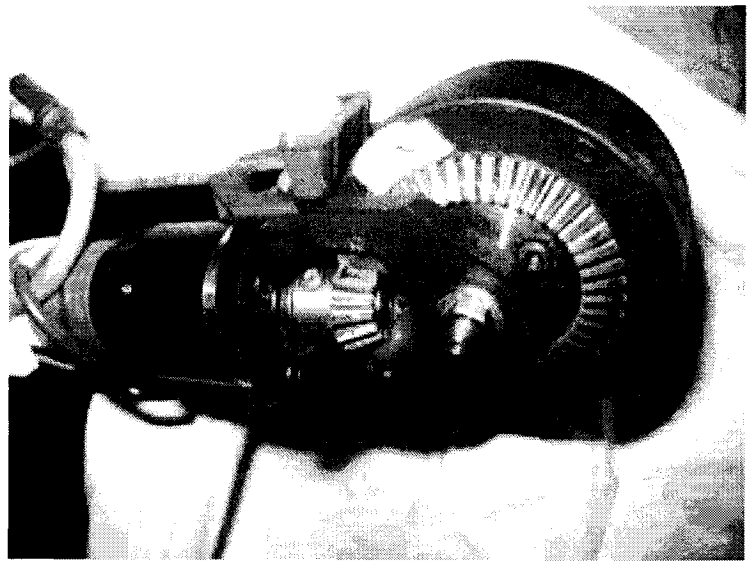

Fig. 6.4 The mechanically blocked wheel. Adhesive was poured into the teeth of the wheel bevel gears to prevent turning.

The touchdown and liftoff angle parameters as well as the results from the experiments are listed in Table 6.2. Note that by varying the touchdown and liftoff angles, it is possible to increase the speed of a stable bounding gait on PAW from 0.81 m/s to 1.18 m/s, nearly matching the maximum forward speed of Scout II. Further discussion of the other tabulated results are found in Sections 6.4 and 6.5.

As can be seen in the top two plots of Fig. 6.5a, mechanical blocking of the wheel limits measurable wheel rotations to below two degrees, peak-to-peak. Measured wheel rotation does not include components due to backlash in the motor gearhead and bevel gear pair coupling the wheel to the motor. The measured rotation is most likely due to the somewhat

compliant nature of the adhesive (commercial hot glue) and rubber wedges used to hold the wheels' bevel gears in place. The likelihood of this, as opposed to vibration within the motor encoder, is high given the consistency of the resulting data. A typical footfall pattern as well as the leg compression during bounding with mechanically blocked wheels are shown in Fig. 6.5a. The footfall clearly shows a bounding gait while the leg length graph illustrates how larger loads are observed in the rear legs (Legs 2 and 4).

Table 6.2 Experimental Results: *PAW* Bounding with *Mechanically Blocked* Wheels

Exp #	Front Leg Touchdown, Liftoff Angles ($\varphi_{ftd}, \varphi_{flo}$) [deg]	Rear Leg Touchdown, Liftoff Angles ($\varphi_{rtd}, \varphi_{rlo}$) [deg]	COM Speed [m/s]	Max Front Comp. (mean) [m]	Max Rear Comp. (mean) [m]	Stride Freq. [Hz]	Phase Diff. (mean) [%]	Front Duty Cycle (mean) [%]	Rear Duty Cycle (mean) [%]
1	(-24, 0)	(-22, 12)	0.81	0.039	0.044	3.14	18	36	41
2	(-20, 4)	(-22, 12)	0.87	0.036	0.040	3.31	19	36	39
3	(-20, 6)	(-22, 14)	0.99	0.034	0.039	3.49	19	40	42
4	(-20, 10)	(-22, 18)	1.18	0.030	0.037	4.21	16	41	46

How do these results compare to those obtained with Scout II? PAW's bounding gait is quite different than Scout II's. PAW's bound is *slightly* slower, has a narrower range of touchdown parameters and has a smaller phase difference between the front and rear legs. In addition, the flight phases demonstrated by the two robots in these experiments are different, as shown in Fig. 6.3. PAW demonstrates what is referred to by biologists, [79], as an "extended" leg flight phase, while in these experiments Scout II demonstrates a "gathered" or "flexed" leg flight phase, in addition to an occasional, short-lived "extended" flight phase. The simulations of PAW discussed in Chapter 4 and in [37] show the same tendency to a single extended flight phase. In the gallop results presented in Chapter 7 one of the two gallops obtained with Scout II demonstrated an extended flight phase. Video footage of experiments on Scout II conducted at McGill University by S. Talebi and M. de Lasa also show Scout II bounding with an extended flight phase. In addition, Talebi showed that by simply varying touchdown angles a pronk – which has a flight phase which is *neither* gathered nor extended – could be achieved on Scout II. Furthermore, results by the Raibert Quadruped, [104], show that a symmetric bound, in which both flight phases

are achieved, is possible. Therefore, with further exploration of the touchdown and liftoff angle parameters it may be possible to duplicate such results on PAW.

6.2.2 PAW Bounding Experiments with Actively Controlled Wheels

Results for bounding experiments with actively controlled wheels are presented in Table 6.3. The plots in Fig. 6.6 were generated with the same set of touchdown and liftoff angles as those in Fig. 6.5 for direct comparison. Measurable wheel rotation is obviously greater (approximately 30° peak-to-peak) in the actively controlled wheels than in the case of blocked wheels. Wheel actuation, as described in Section 6.6.2, probably causes the decrease in forward speed observed in bounding with actively controlled wheels: a maximum speed of 1.00 m/s versus 1.18 m/s with mechanically blocked wheels. A decrease in repeatability is also observed for some leg angle settings, when actively controlled wheels are used; this is discussed in further detail is Section 6.8.3.

Table 6.3 Experimental Results: *PAW* Bounding with *Actively Locked* Wheels

Exp #	Front Leg Touchdown, Liftoff Angles ($\varphi_{ftd}, \varphi_{flo}$) [deg]	Rear Leg Touchdown, Liftoff Angles ($\varphi_{rtd}, \varphi_{rlo}$) [deg]	COM Speed [m/s]	Max Front Comp. (mean) [m]	Max Rear Comp. (mean) [m]	Stride Freq. [Hz]	Phase Diff. (mean) [%]	Front Duty Cycle (mean) [%]	Rear Duty Cycle (mean) [%]
1	(-20, 4)	(-22, 12)	0.75	0.033	0.043	3.35	23.7	40.6	41.8
2	(-20, 6)	(-22, 14)	0.83	0.034	0.044	3.35	20.1	40.4	41.6
3	(-20, 6)	(-22, 16)	0.83	0.035	0.045	3.38	17.0	40.4	41.5
4	(-20, 8)	(-22, 16)	0.91	0.033	0.043	3.52	17.0	40.7	42.4
5	(-20, 10)	(-22, 18)	1.00	0.033	0.042	3.57	18.3	40.9	43.3

It should be emphasized here that to the casual observer there are no immediately apparent differences in the bounding gait using active wheel control with respect to the results obtained with mechanically blocked wheels. The robot bounds in both cases, with visibly separate front and rear leg pair touchdown events, a single ballistic phase in each stride, as well as a common period in which all legs are in stance.

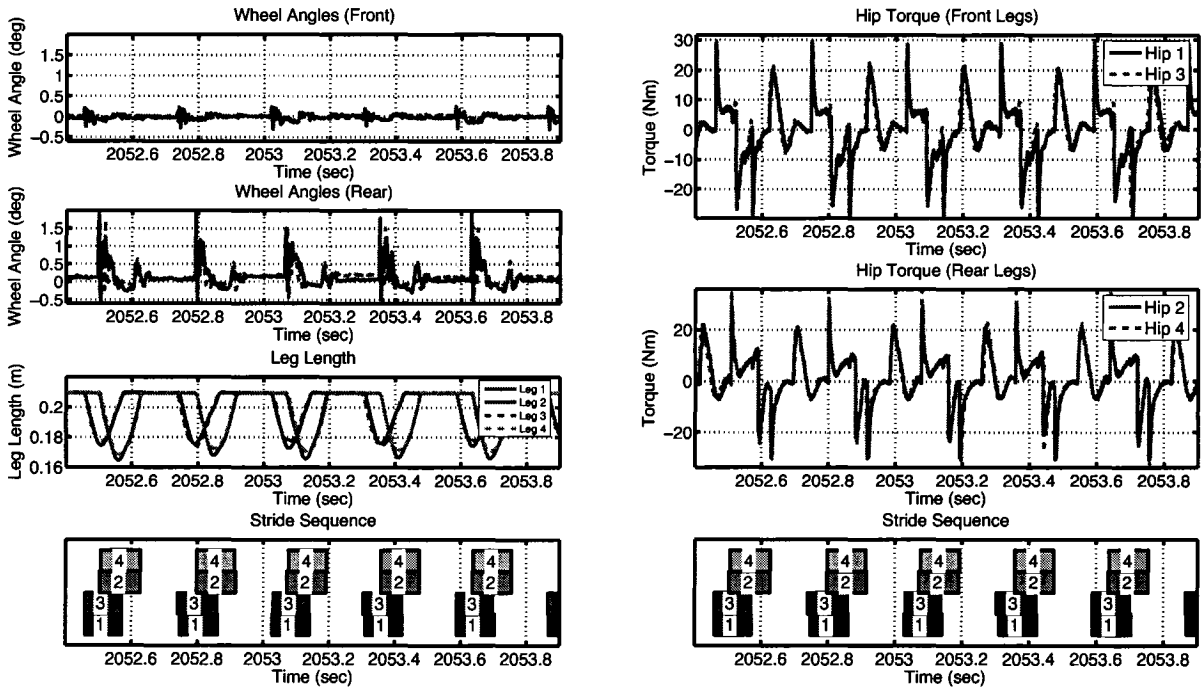

(a) Wheel rotation & leg length

(b) Hip torques

Fig. 6.5 Wheel rotation, leg length and hip torque plots for *PAW* bounding with *mechanically blocked wheels.* Solid blocks represent contact with the ground of a particular leg. Here, legs 1 and 3 are at the front of the robot and touchdown first.

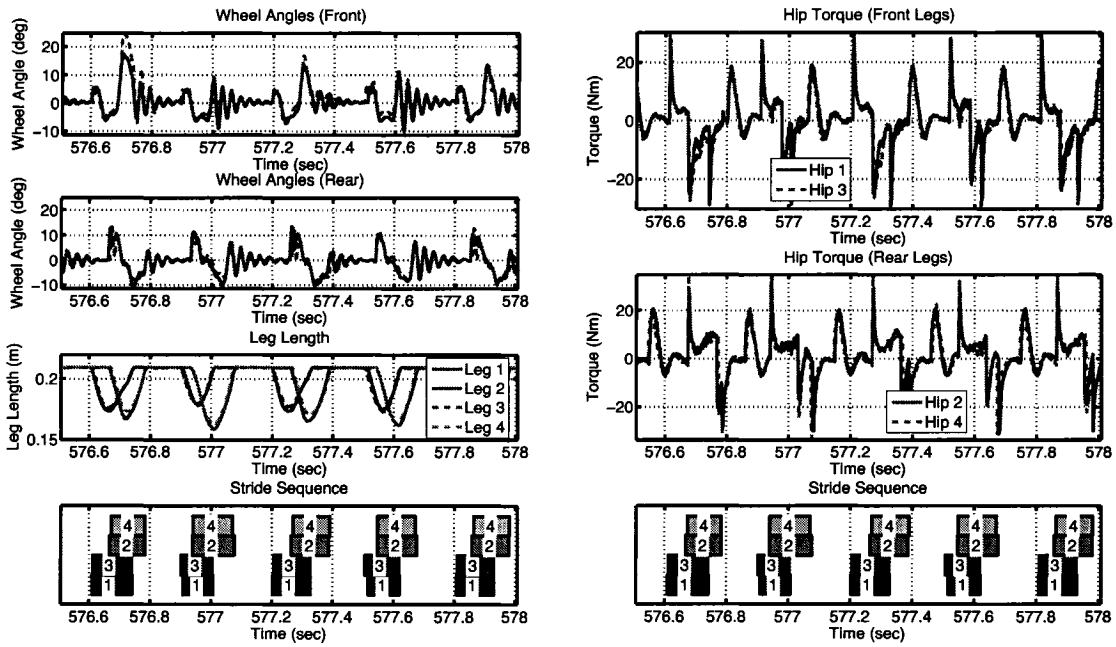

(a) Wheel rotation & leg length

(b) Hip torques

Fig. 6.6 Wheel rotation, leg length and hip torque plots for *PAW* bounding with *actively controlled wheels*. Solid blocks represent leg ground contact.

6.2.3 PAW φ_{lo}-Turning Experiments

While it is possible to achieve turning during the bounding gait using differential torque in the hip motors during stance, as described for the Scout II robot in [103], it is also possible to achieve turning through selection of differential touchdown and liftoff angles. Bounding experiments using variable liftoff angles in lateral leg pairs are discussed in Section 7.1.3 of Chapter 7, with comparisons made to another gait with a significant yaw component, the rotary gallop.

6.3 Selection of Leg Touchdown and Liftoff Angles

This section outlines the strategies used in finding stable bounding gaits on PAW by varying the touchdown and liftoff angles. Here, the strategy of first tuning the touchdown angles to achieve a high-energy but relatively unstable gait is discussed. Then the stability is increased by tuning liftoff angle parameters. Experimental evidence regarding the relationship between liftoff angles and forward speed is also presented.

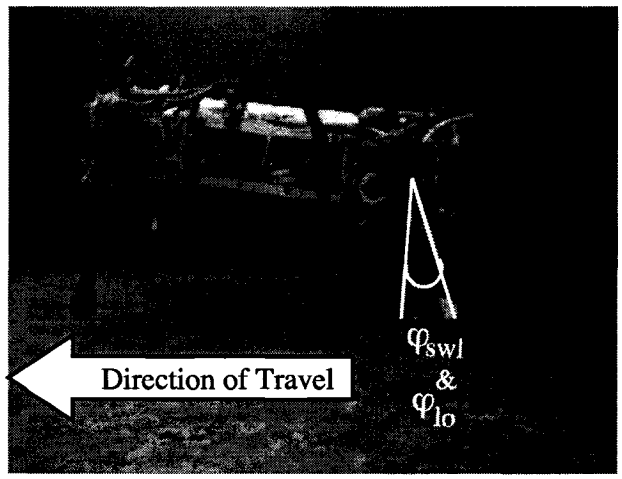

Fig. 6.7 Toe dragging mode of failure on Scout II. In this case it is caused by too great a sweep limit, φ_{swl}, and subsequent liftoff angle, φ_{lo}.

Differently from Scout II, the initial attempts to achieve bounding on PAW by using touchdown angles in the range 14° - 18° resulted in low COM apex height, high frequency bounds which were generally unstable due to toe-stubbing. While toe-stubbing on Scout II sometimes occurred, the nature of the gathered flight phase demonstrated by Scout II, in which rear legs touchdown first, is less susceptible to critical gait failure[2] than toe-stubbing with the front legs after extended flight, since the braking action of the front legs, when stubbed, becomes exaggerated. Subsequently, stable bounding solutions were sought starting at $\varphi_{td} = 30°$, which produces high apex heights and pronk-like gaits, thus avoiding the toe-stubbing instability, but yields rather slow forward motion. The touchdown angles were then gradually decreased to produce better, faster bounding.

The sweep limit angles, φ_{swl}, and the resulting liftoff angles, φ_{lo}, were used on the PAW robot to avoid the two toe-stubbing modes of failure. Increasing of the liftoff angles reduces pitch and, with it, the toe-stubbing and resulting hard braking action of the front legs. Toe-dragging in the rear legs, which slows the robot down, occurs when the liftoff angles are too high, yielding upper bounds on the liftoff angles. The toe-dragging failure mode is what prevents any significant increase in liftoff angle from 0 degrees on Scout II, as shown in Fig. 6.7.

The Scout II robot has a relatively wide range of touchdown angles, φ_{ftd} and φ_{rtd}, in which stable bounding solutions can be found (see Table 6.1). This is in contrast to the

[2]Toe stubbing with the rear legs could also be described as toe-dragging and is shown in Fig. 6.7.

PAW robot which has a narrower band of touchdown angles, varying between approximately -20 and -28 degrees. On the other hand, PAW's range of usable liftoff angles, φ_{flo} and φ_{rlo}, between 0 and +20 degrees, is greater than Scout II's narrow band around 0 degrees. The reason for this difference is probably due to differences in hip separation and/or leg length.

Finding stable bounding regimes is a challenge becaue it involves tuning four parameters in the touchdown-liftoff angle space. One can even add a fifth parameter, the leg sweep speed, in a similar fashion to Talebi's $\dot{\varphi}$-controller [87]. While initially implemented on PAW, this strategy was discarded in favour of allowing the hip motors to achieve their torque limits according to the characteristic torque-speed curve, as previously done for Scout II [18]. The motor saturation is illustrated in the diagonal lines shown in Fig. 6.13, on p. 97. The vertical lines at the extreme limits of the torque values are due to amplifier current-limiting, a safety feature designed to prevent overheating of motor windings.

While it is possible to vary the forward speed of the robot by maintaining the same liftoff angles and only varying the touchdown angles (see Table 6.1 for Scout II and Exps. 1 and 2 of Table 6.2 for PAW), a contrarian hypothesis that *forward speed can be changed uniquely by varying the liftoff angles*, φ_{flo} and φ_{rlo}, was tested.[3] As illustrated in Tables 6.2 and 6.3 and seen in the simulation results of Chapter 4, this hypothesis is, indeed, correct. The effect of varying these control parameters on other aspects of the robot's gait are discussed in the following sections.

6.4 Footfall Pattern, Stride Frequency and Body Pitch

The footfall patterns for PAW's bound with either wheel configuration are remarkably similar, as can be seen in Figs. 6.5 and 6.6. The PAW robot demonstrates a "double-stance" phase [47], shown in the C frames of Fig. 6.3, where both the front leg pair and the rear leg pair are in contact with the ground at the same time. Halfway through the stance phase of the rear legs the front legs liftoff, leading to a relatively long aerial phase, which is often characterized by higher apex heights than the Scout II robot. It should also be noted that Scout II often bounds with a footfall pattern in which there is little to no double stance phase between the front and rear legs, as listed in Table 6.1 and illustrated

[3]Please note that, the liftoff angle, φ_{lo}, and the sweep limit angle, φ_{swl}, nomenclature is for all practical purposes interchangeable. The sweep limit is the angle at which the stance-brake controller attempts to hold the leg, while the liftoff angle is the actual angle at which the leg lifts off the ground. Ideally they are identical.

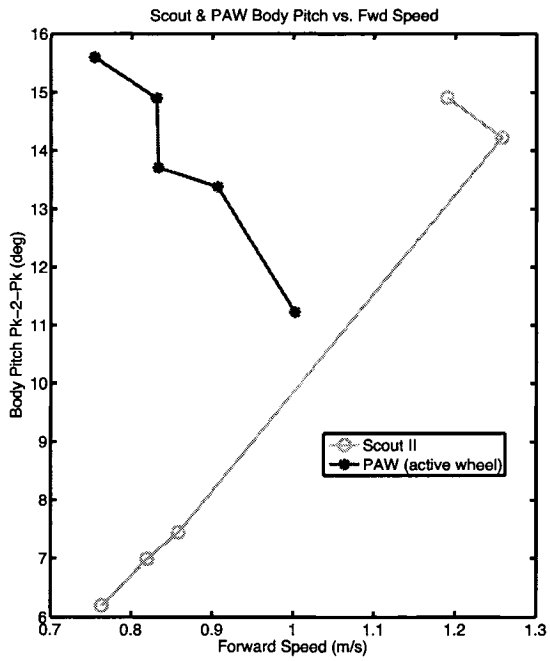

Fig. 6.8 Body pitch amplitude versus forward speed on Scout II and PAW.

in the stride sequences of fast bounding in Fig. 6.2. In other words, while PAW's bound is characterized by a single aerial phase, Scout II can bound at lowest speed with nearly no aerial phase and at higher speeds with two distinct aerial phases.[4]

Differently from Scout II, PAW's bounding stride frequency generally increases with higher forward speed, as shown in Fig. 6.9. This is due in large part to the tendency of PAW to have lower apex heights and body pitch when liftoff angles (and corresponding forward speed) are increased, while Scout II has higher apex heights and body pitch when touchdown angles (and corresponding forward speed) are increased. The pitch values in Fig. 6.8 clearly demonstrate these trends in both Scout II and PAW. Interestingly, at similar speeds PAW's stride frequency is slightly lower in bounding with mechanically blocked wheels than actively controlled wheels (3.14 Hz vs. 3.35 Hz near 0.81 m/s and 3.49 Hz vs. 3.57 Hz at approximately 1.0 m/s). While not directly measured, this probably indicates that PAW bounds lower to the ground when actively controlled wheels are used.

Scout II's duty factor decreases with corresponding increases in forward speed, again because of increased apex height at higher speeds. In contrast, shown in Fig. 6.10, the

[4]Albeit, one flight phase is more significant than the other.

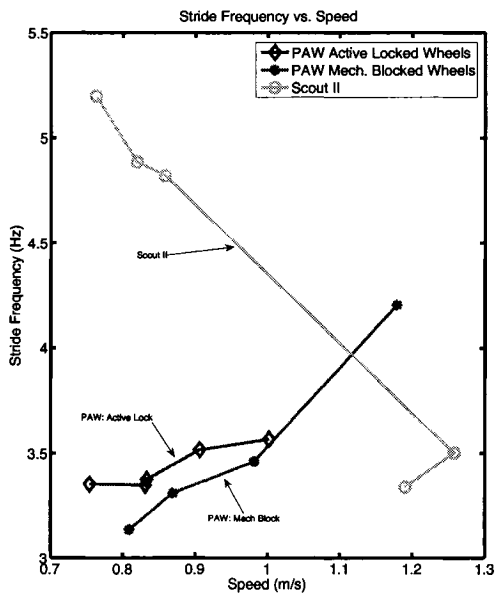

Fig. 6.9 Stride frequency of *PAW*'s bounding gait for both *mechanically blocked* and *actively controlled* wheels and *Scout II*'s bounding gait. See Tables 6.2 - 6.1 for details.

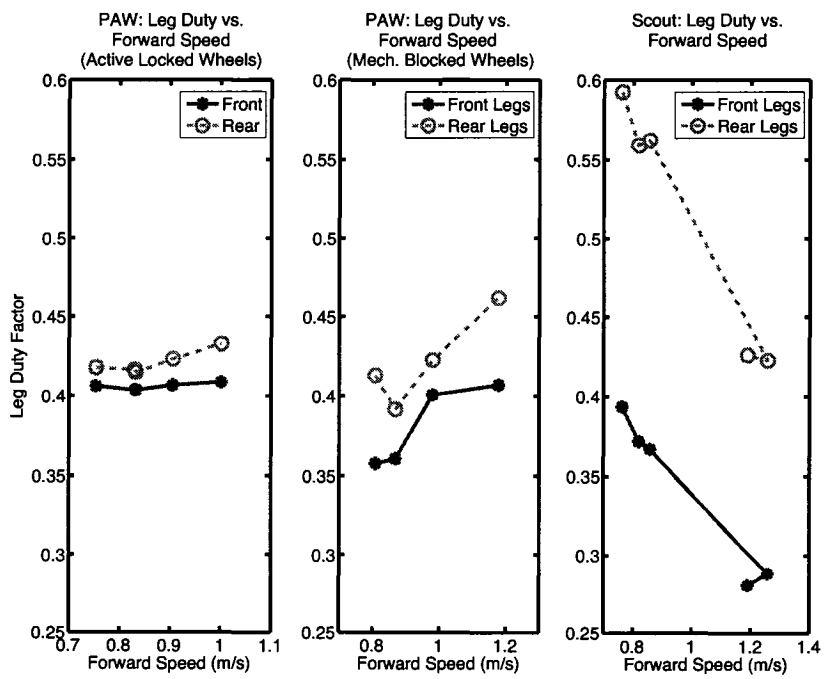

Fig. 6.10 Duty factor of *PAW*'s bounding gait for both *mechanically blocked* and *actively controlled* wheels and *Scout II*'s bounding gait. See Tables 6.2 - 6.1 for details.

duty factor of PAW's legs generally *increases* with an increase in speed. This is important as an indication that as the robot's speed increases, it is spending a greater amount of time in contact with the ground during each stride. This is the desired result given that increasing the liftoff angles, φ_{flo} and φ_{rlo}, are supposed to decrease the apex height of the robot, reducing the amount of time spent in ballistic flight.

From the comparison of the footfall pattern, phase relationship and stride frequency of the two robots' bounding gaits, the following can be stated. First, Scout II's bounding gait is more variable, extending from a near-walk at lowest speed to a full bound at highest speed. PAW's higher apex heights are a significant advantage in broken terrain or if the acrobatic behaviours proposed in [37] are to be attempted. Finally, the opposite trends in duty factor and stride frequency that appear to be based on controller parameters provides an interesting tool in fine-tuning desired duty factor without compromising forward speed.

An additional comparison is worth making with respect to stride frequency and forward speed in animals. In marked contrast with both PAW and Scout II, stride frequency generally does not vary in animals while running [105]. Rather, stride *length* is generally increased at higher speeds. The nature of these two robots, that does not include segmented legs, nor can leg speed be increased during stance due to hip motor saturation, precludes increases in speed due to stride length.

6.5 Leg Compression

This section presents the leg compression results obtained during the bounding trials of PAW and Scout II. Values given are the mean values of the maximum compression of each leg for each stride taken. These mean compression values are related to given forward speeds in Tables 6.1, 6.2 and 6.3. Leg strain is proportional to the leg compression values. Leg compression for Scout II's and PAW's bounding experiments can be seen in Figs. 6.2a., 6.5a. and 6.6a.

Three graphs, showing the mean maximum compression values as a function of forward speed are found in Fig. 6.11, for the two PAW configurations as well as for Scout II. It is immediately apparent from these graphs that the amount of leg compression is different in the front and rear leg pairs. In nearly all cases (except in the slowest bound in Scout II where speed, apex heights and pitching are all reduced) the rear legs compress more than the front legs. As mentioned earlier, this supports the notion, borrowed from biology, [23],

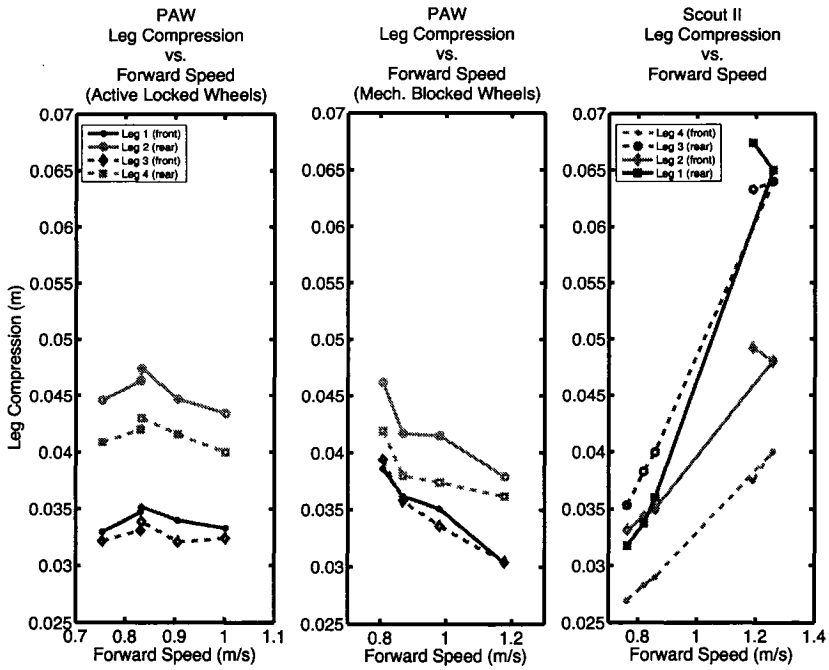

Fig. 6.11 Leg compression for Scout II and PAW during a bound. Mean maximum leg compression for *Scout II*'s bound as well as *PAW* during a bound using either *mechanically blocked* or *actively controlled* wheels. Note how the front legs generally compress less than the rear legs. Also note the reverse leg numbering on Scout II due to it running backwards.

that the rear legs are used primarily for thrust, while front legs are used for the braking action that is necessary for stabilization of the gait.

The Scout II and PAW robots show opposite trends with respect to leg compression and forward speed. As can be seen in results for bounding with mechanically blocked wheels in the middle graph of Fig. 6.11, the basic tendency for PAW's leg compression is to decrease proportionally to the increase in forward speed. This can be explained by the fact that as PAW's speed increases its apex height decreases, resulting in less compression of the legs during stance. Scout II's increased leg compression at higher speeds is, like with stride frequency and duty factor, explained by the higher apex heights it achieves during its ballistic phase.

The use of actively controlled wheels on PAW during the bound complicates this otherwise straight forward relationship between forward speed and leg compression, as shown in the left-most graph of Fig. 6.11. This is worthy of further investigation, especially if one is to come to a deeper understanding of the effect of the wheels on bounding.

6.6 Actuation Details During Bound

While some simulation studies of legged systems use ideal actuation models capable of delivering any desired torque or velocity value, in reality, actuator dynamics play a very important role in the resulting motion of legged systems, as discussed in [18]. In fact, on Scout II and PAW, during the stance-retraction phase of motion, as well as during a large portion of the flight-protraction phase, actuator torque-speed saturation is the dominant characteristic. In addition, it was shown in [18] that without taking into account saturation, the Scout II bounding model does not necessarily converge to stable, cyclic motion using the same controllers as in the experiment. In addition, even if stability was achieved the resulting model was found to be of reduced accuracy. For these reasons this section illustrates the actuator dynamics for bounding on Scout II and PAW.

While actuator saturation seems to have stabilization features, it is not the actuator torques, nor the retraction velocity (such as in the $\dot{\varphi}$-controller for Scout II [87], the bounding controller on RHex [106] or early bounding controllers on PAW) that are the dominant control inputs for the bounding or galloping gaits. Rather, it is the touchdown angles, as discussed in [18], [47] and [59], as well as the the liftoff angles, as presented in this thesis, which dominate control. A theoretical justification for this, in the context of the SLIP model, is presented in [107].

In particular it should be noted that the hip actuators saturate during both the retraction and protraction phases of motion, as shown in the first and third quadrants of the speed-torque curves of Figs. 6.12 and 6.13. While no saturation is found in the braking quadrants of the Scout II speed-torque curves, some occasional saturation during stance-brake does occur on PAW. The wheel actuators, on the PAW robot, do not demonstrate saturation in any driving or braking quadrant of the speed-torque curves, an important feature since saturation would make position control of the wheels harder to accomplish.

6.6.1 Hip Action During Bound

As can be seen in Fig. 6.13 the basic shape of the hip speed-torque curves is the same for both PAW and Scout II. Both robots demonstrate saturation in the stance-retraction and flight-protraction phases (first and third quadrants, respectively). The motor saturation is illustrated in the diagonal lines shown in Fig. 6.13 while the vertical lines are due to amplifier current-limiting, a safety feature designed to prevent motor winding overheating.

While Scout II demonstrates higher torques overall, it should be noted that lower torque is applied during its stance-brake phase. In the two PAW speed-torque curves, one can observe a higher variability in the data points for actively controlled wheel bounding. This occurs in nearly all hip speed-torque plots for actively controlled wheel bounding and seems to correlate to the lessened repeatability of these trials, as discussed in Section 6.8.1.

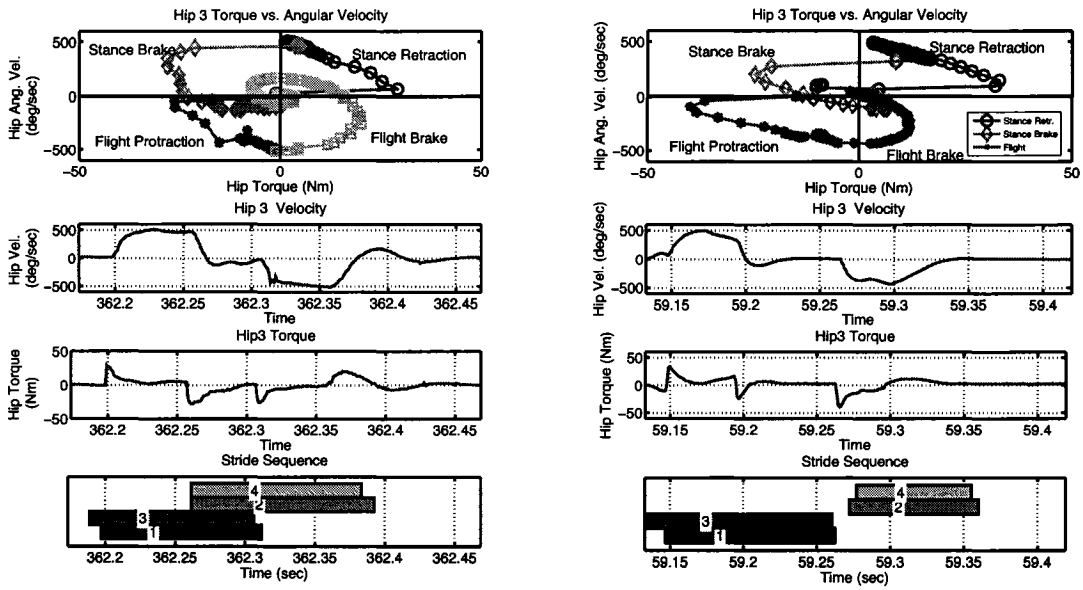

(a) PAW, Active Locked Wheel (b) Scout II

Fig. 6.12 Comparison of hip angular velocity and torque plots during a single stride of a bound gait for PAW's *actively controlled wheels* as well as for Scout II during a fast bound. Note the actuator saturation for both robots in the first and third quadrants.

6.6.2 Wheel Action During Bound

This section discusses the action taken by the wheels during PAW's bounding gait using actively controlled wheels, as per the experiments listed in Table 6.3. Two illustrations of the wheel torque-velocity plots can be found in the top plots of Fig. 6.14, one for a representative front leg (Leg 3) and one for a representative rear leg (Leg 4). Like Fig. 6.13 for the hip speed-torque curves, the wheel speed-torque plots use colour-coordinated curves in order to indicate to the reader the corresponding state of the leg that the wheel is attached to.

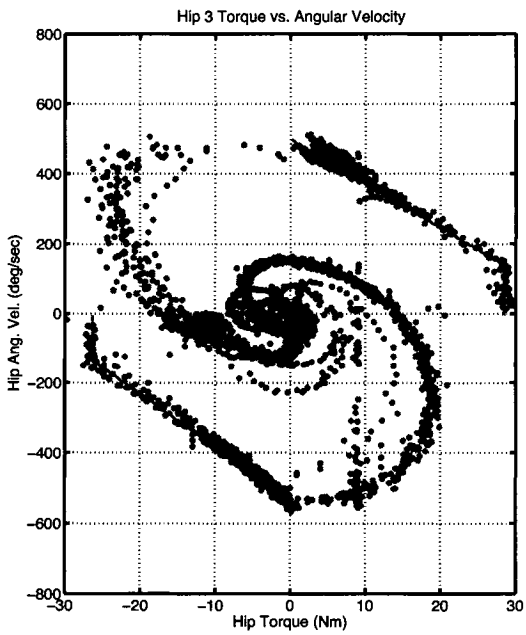

(a) PAW Mech. Blocked Wheel

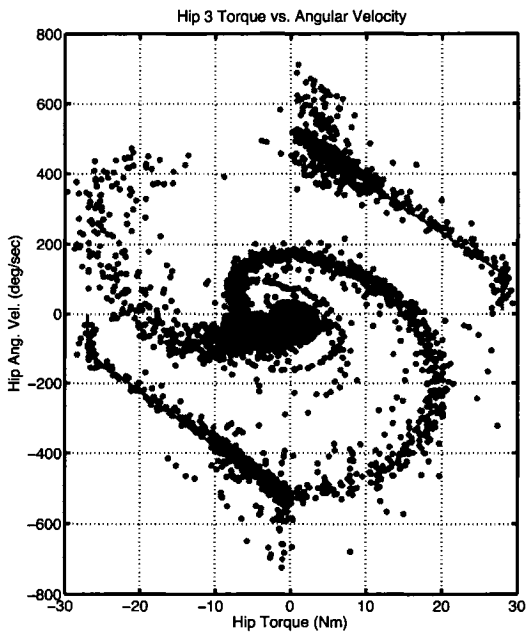

(b) PAW, Active Locked Wheel

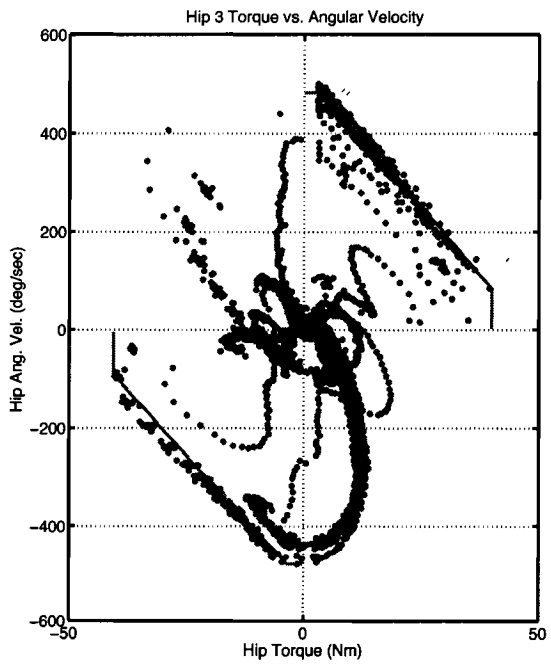

(c) Scout II

Fig. 6.13 Comparison of hip speed-torque plots during the bound gait for PAW's *mechanically blocked wheels* (Exp. 2, Table 6.2) and *actively controlled wheels* (Exp. 2, Table 6.3), as well as for Scout II during a fast bound.

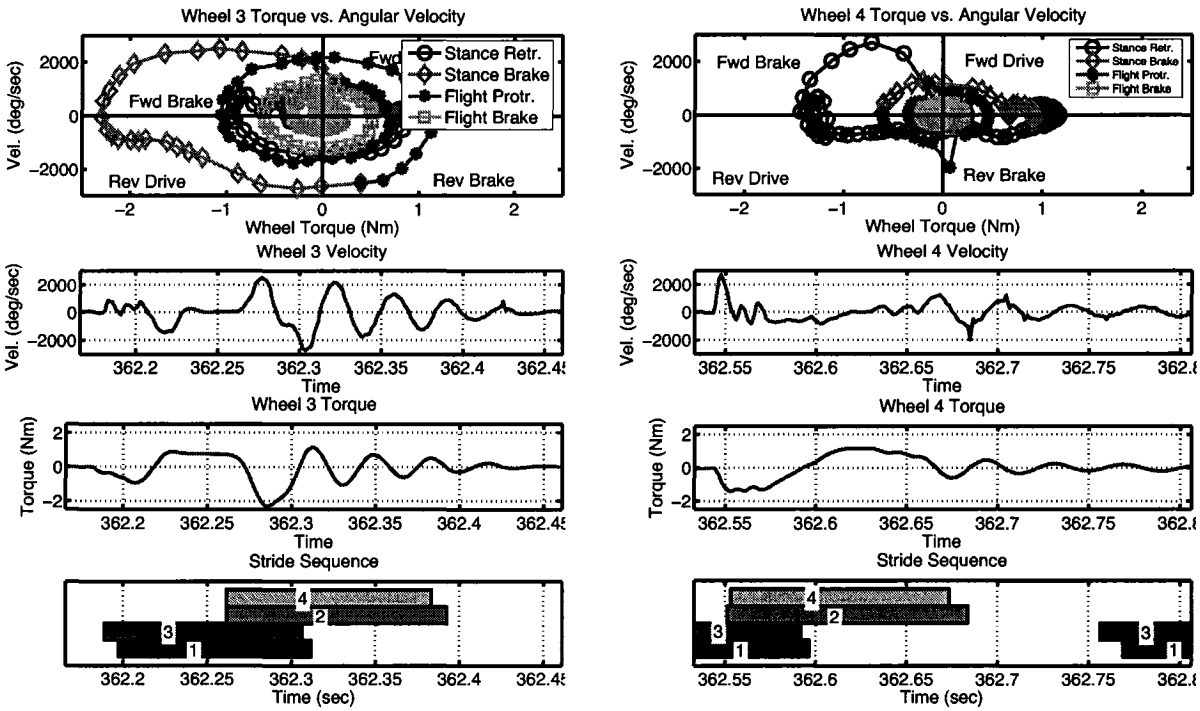

(a) Leg 3 (Front)

(b) Leg 4 (Rear)

Fig. 6.14 Wheel action for one stride of a bound. The Torque vs. Angular Velocity plots illustrate action during the various stages of the leg state during the stride. Note the occasional spike (a single measured point) in wheel velocity due to noise in the motor encoder reading. See text for an explanation of the sequence of wheel events and actions.

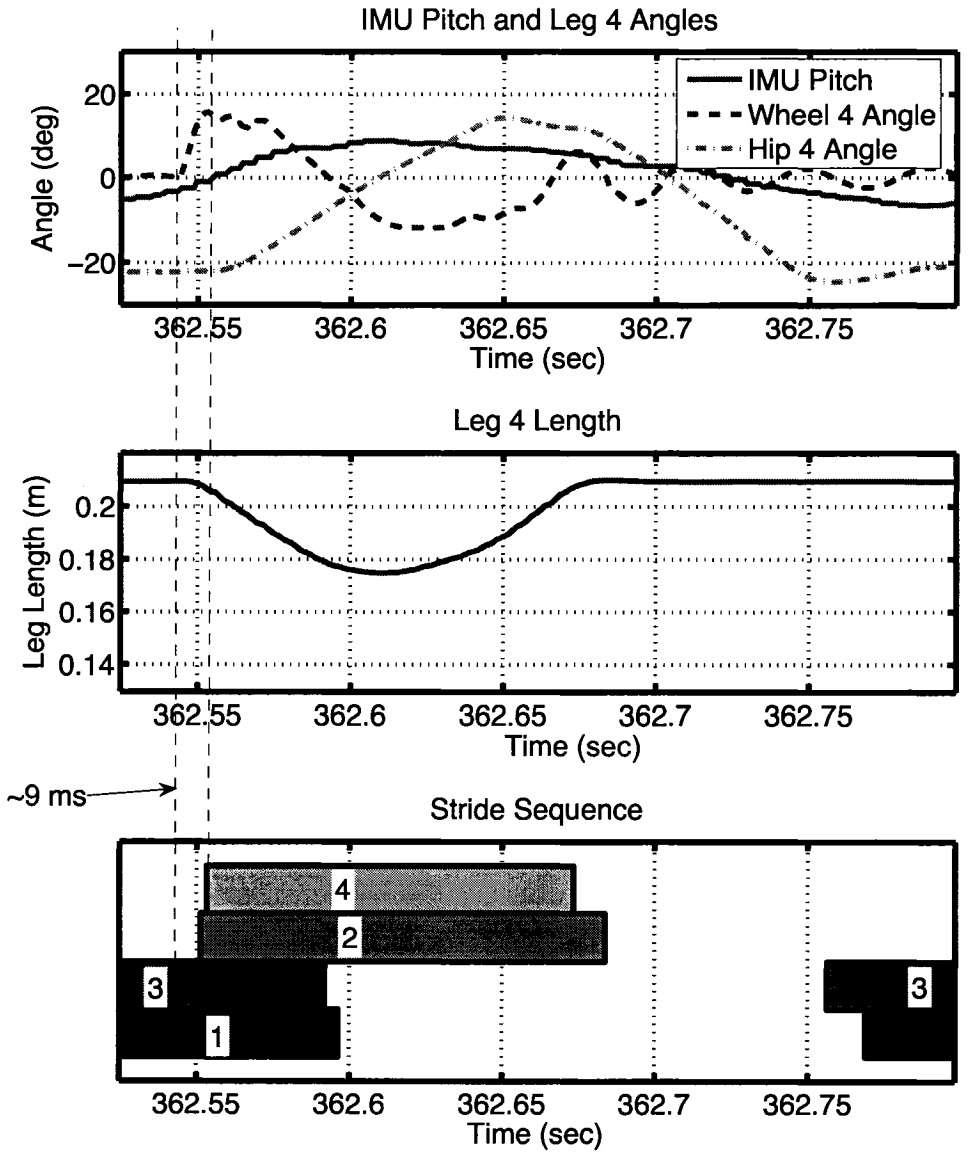

Fig. 6.15 Wheel rotation due to ground contact occurs relatively early compared to leg compression. As shown here, the wheels begin their rotation due to ground contact about 9 milliseconds before leg compression is sufficient to change the leg state.

The actions undertaken by the front and rear wheels differ slightly and will be discussed here. Referring to Fig. 6.14a, note how when the first leg (Leg 3) touches down the leg angle is held fixed with respect to the body, with no retraction occurring, until the second leg (Leg 1) touches down. In that time the wheel switches between the forward-brake and reverse-drive actions, maintaining a low velocity. Once retraction begins, the wheel engages a reverse-brake action and approaches the forward-drive quadrant, where it holds a near constant positive torque with little velocity. When the stance-brake state engages, the wheel shifts into a high-speed, high-torque forward brake phase, followed by reverse driving. As the leg approaches the lift-off condition the decreasing load on the leg seems to allow the wheel to engage in damped oscillation, which it follows through with during the flight phase.[5]

The rear wheel, Fig. 6.14b, begins in the forward-brake quadrant upon touchdown, oscillating between forward-brake and reverse-drive states before proceeding at low speed through the reverse-drive quadrant and into reverse-brake quadrant. As with the front wheel, the rear wheel begins the stance-brake phase oscillating with low speed, between forward-drive and reverse-brake before proceeding into the damped oscillation which led into the flight phase. Just prior to liftoff the rear leg's wheel oscillates, indicating that the load on the leg has decreased appreciably.

Why are these sequences of wheel actuation of any interest to the reader? Because, as evidenced by the specific resistance plot of Fig. 6.16 the use of wheels currently has a *detrimental effect* on the energy efficiency of the bounding gait. This runs counter to the assumption that the wheels could be used to inject energy into the robot to provide an increase in performance. In contrast to the hip motors, the wheel motors are not driven to saturation during the legs' stance phase, opening up the possibility of using more complex control schemes to improve bounding performance. Since the currently implemented, and admittedly simple, wheel controller does a relatively poor job in terms of energetics, what could possibly lead to an improvement? A first suggestion would be a state-based controller which replaces the front wheels' reverse-driving action by forward-driving at the end of the leg's stance-brake phase. This would complement the forward motion of the robot. Similarly, the rear wheels, which are driving in the forward direction for much of the rear

[5]Note that in Fig. 6.14 a few spikes can seen in the velocity curves. These spikes last one cycle of the control code (approximately 1 ms) and are representative of noise from the wheel motor encoder (they can also be seen in the wheel angle curves).

legs' stance-brake phase, could be driven harder and faster in the forward-drive quadrant prior to lift-off.

Another aspect of wheel rotation which is of interest is in using this data for ground detection. By using the actuator as a sensor it may be possible to detect ground contact faster than through the use of the leg length potentiometer. By referring to Fig. 6.15 one can see that wheel rotation is visible about three milliseconds before any significant leg compression is detected and *nine* milliseconds before the compression is sufficient to detect the change in leg state. This can be particularly important if harder leg springs are used in the future, making it impossible for the potentiometers to move beyond the *signal noise floor* during low apex-height bound strides.

6.7 Energetics: Power and Specific Resistance

The basic trend for energy efficiency onboard Scout II during bounding and PAW in both bounding and rolling is that the robots become more efficient as they speed up. This is readily apparent in the results for all bounding cases and for rolling, as can be seen in Table 6.4 and Fig. 6.16.

Bounding with mechanically blocked wheels is more efficient than bounding with actively controlled wheels. This is to be expected since by not driving the wheels during the stance phase the robot saves power. In addition, the use of the wheels slows the robot down given the same touchdown and liftoff angles, as indicated in Tables 6.2 and 6.3. Therefore, unless a mode of wheel control is found with increased efficiency during actively controlled wheel bounding it may be advisable to devise a mechanism to lock the wheels during legged modes of locomotion.

6.8 Measuring Gait Success

In this section the qualitative and quantifiable success of experimental gait trials is discussed, based on whether the gait is stable, how stable it is and how fast it achieves stability. To begin with, the pitch phase plots are examined to get a qualitative, visual impression of how stable a particular gait was. The first quantifiable measure of success presented is *repeatability* in achieving a bounded limit cycle over a given number of trials. Then, for gaits which achieve a bounded limit cycle, the quantization of the gait's stabil-

Table 6.4 Scout II & PAW Specific Resistance (Bounding and Rolling). *Italicized values are for single trials.* See graphical representation in Fig. 6.16.

Robot	Behaviour	Exp.	Speed (m/s)	Power (Watts)	Spec. Resistance
PAW	Bounding (active wheel control)	1	0.75	518	3.42
		2	0.83	493	2.96
		3	0.83	450	2.69
		4	0.91	488	2.68
		5	1.00	474	2.35
	Bounding (mech. blocked wheel)	1	0.81	328	2.01
		2	0.87	371	2.12
		3	0.98	396	2.01
		4	1.18	358	1.51
	Rolling	1	1.4	51	0.18
		2	2.0	56	0.14
Scout II	Bounding	*1*	*0.76*	*464*	*2.51*
		2	0.86	462	2.22
		3	1.26	431	1.41
		4	*1.19*	*428*	*1.48*

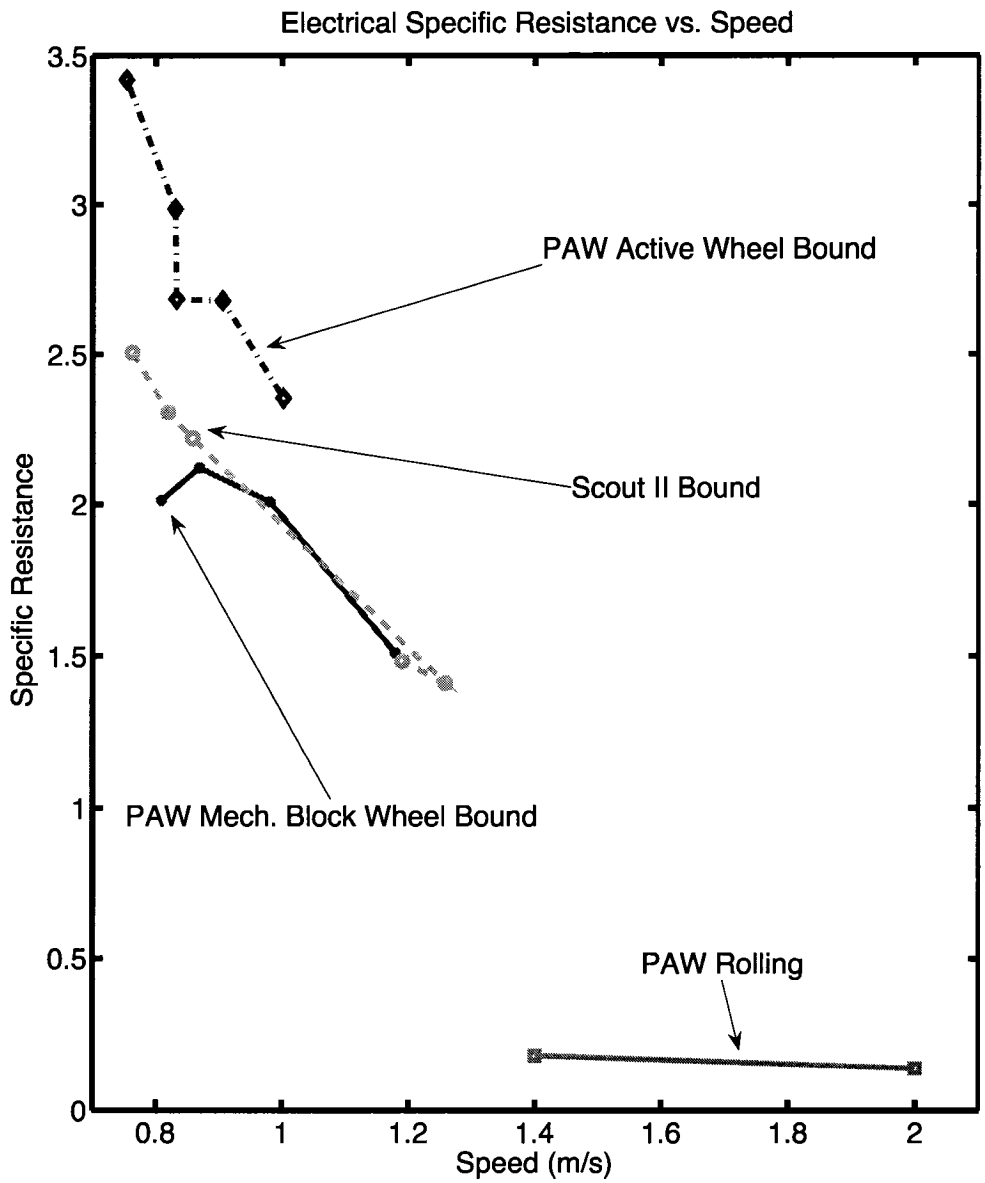

Fig. 6.16 Specific resistance of *Scout II* bounding as well as *PAW* while bounding with *actively controlled* wheels and *mechanically blocked* wheels. PAW's rolling specific resistance is also provided.

ity is discussed from the perspective of *rate of convergence* as well as the *variability* of a particular performance index via the measurement of its standard deviation.

As can be seen in Fig. 6.18a, the pitch of the robot varies widely at first and eventually settles to a bounded, cyclical pattern. The pitch information can also be represented in the pitch phase form, as shown in Fig. 6.18b, and is discussed below.

Table 6.5 *Scout II* stability for bound gait. Exps. 1 and 4 are not included as they only encompass a single trial each.

Exp #	Front Leg Touchdown, Liftoff Angles ($\varphi_{ftd}, \varphi_{flo}$) [deg]	Rear Leg Touchdown, Liftoff Angles ($\varphi_{rtd}, \varphi_{rlo}$) [deg]	COM Speed [m/s]	Stride Freq. (mean) [Hz]	Stride Freq. (std. dev) [%]	Strides to Converge.	Repeat.
2	(-16, 0)	(-14, 0)	0.86	4.82	2.5	5	10 / 10
3	(-21, 0)	(-19, 0)	1.26	3.50	1.8	7	10 / 10

Table 6.6 *PAW* stability for bound gait with mechanically blocked wheels.

Exp #	Front Leg Touchdown, Liftoff Angles ($\varphi_{ftd}, \varphi_{flo}$) [deg]	Rear Leg Touchdown, Liftoff Angles ($\varphi_{rtd}, \varphi_{rlo}$) [deg]	COM Speed [m/s]	Stride Freq. (mean) [Hz]	Stride Freq. (std. dev) [%]	Strides to Converge.	Repeat.
1	(-24, 0)	(-22, 12)	0.81	3.14	3.8	5.2	10 / 10
2	(-20, 4)	(-22, 12)	0.87	3.31	4.1	5.6	10 / 10
3	(-20, 6)	(-22, 14)	0.99	3.49	3.9	3.8	10 / 10
4	(-20, 10)	(-22, 18)	1.18	4.21	5.4	8.8	10 / 11

6.8.1 Trial-to-Trial Repeatability

Not all of PAW's bounding experiments resulted in 100% repeatable results. While all of Scout II's bounding trials, as well as nearly all of PAW's trials conducted using mechanically

Table 6.7 *PAW* stability for bound gait with actively controlled wheels.

Exp #	Front Leg Touchdown, Liftoff Angles ($\varphi_{ftd}, \varphi_{flo}$) [deg]	Rear Leg Touchdown, Liftoff Angles ($\varphi_{rtd}, \varphi_{rlo}$) [deg]	COM Speed [m/s]	Stride Freq. (mean) [Hz]	Stride Freq. (std. dev) [%]	Strides to Converge.	Repeat.
1	(-20, 4)	(-22, 12)	0.75	3.35	8.5	4.9	12 / 17
2	(-20, 6)	(-22 , 14)	0.83	3.35	13.6	6.6	11 / 11
3	(-20,6)	(-22, 16)	0.83	3.38	17.7	6.6	13 / 15
4	(-20,8)	(-22, 16)	0.91	3.52	12.9	6.5	12 / 12
5	(-20,10)	(-22, 18)	1.00	3.57	13.4	5.8	12 / 16

blocked wheels were successful, as shown in Tables 6.5 and 6.6, yielding cyclic bounding gaits with no toe stubbing or other non-trivial modes of failure, a significant number of trials conducted for PAW's actively controlled bounding experiments ended in critical failures which forced the termination of the runs. It does not seem to be coincidental that the least repeatable runs, as listed in Table 6.7, result in some of most divergent orbits in the pitch phase plots, such as Fig. 6.19b. It is also interesting to note how the decrease in repeatability is most apparent at both the slowest (Exp. 1 in Table 6.7) and fastest (Exp 4 in Table 6.6 and Exp 5 in Table 6.7) settings. This is probably due to two factors. First, at the slowest speed the robot's liftoff angles are forcing it into higher ballistic phases, with a proportional decrease in stance time. If one considers that the stance phase is responsible for stabilizing the motion of the robot, this effectively means that the robot is spending more time in a mode in which it is vulnerable to destabilization. Second, as the forward speed of the robot is increased the apex heights it reaches during the ballistic phases of motion are decreased, making it stay closer to the ground. This increases its vulnerability to toe-stubbing when the legs are protracted, which in turn increases the chances of critical failure. This mode of failure is common to both Scout II and PAW, whether liftoff or touchdown angles are adjusted and regardless of whether actively controlled wheels or fixed toes are used. PAW is more vulnerable, though, because of its use of the extended flight phase.

What are the reasons for the higher number of failures in bounding with actively con-

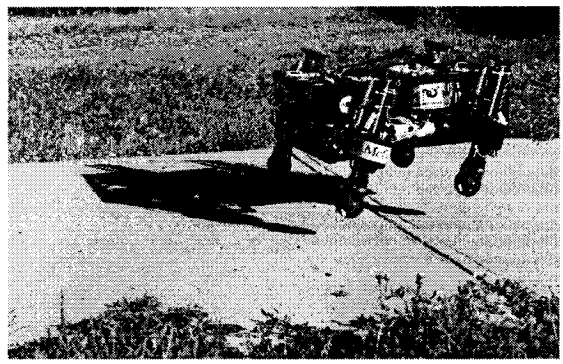

Fig. 6.17 The PAW robot bounding on concrete with active wheel control. [Photo courtesy of DRDC–Suffield]

trolled wheels versus bounding with mechanically blocked wheels? The most obvious culprit is the wheel control and the resulting rotation which occurs during the stance phase of motion. The use of wheels has a negative effect on hip actuator control, as pointed out in Section 6.6.1, where the increased variability of data points in the hip speed-torque plots is clear. The likelihood that the hip actuation variability affects gait stability is high. While early bounding results, such as the bounding on concrete shown at DRDC–Suffield in Fig. 6.17, were achieved with wheel rotations in the neighbourhood of 10° peak-to-peak, the control gains had to be reduced due to lower frequency control loops once the IMU was introduced onboard. The higher sampling periods are due to issues related to program task threading and to the increased processing load on the CPU when communicating with the IMU. The lowered gains effectively increase the peak-to-peak wheel rotations, making the the fixed-toe approximation less valid and, most likely, makes the robot more susceptible to (or are responsible for) perturbations during the bound.

6.8.2 Stability Overview: Pitch Phase Plots

Here we take the notion of stability to mean, within the context of dynamically stable legged locomotion, the "repeatability of a gait pattern in the sense of orbital stability", [108]. This can also be referred to as "body path stability." In practice, this means that as the robot traverses a particular path its motion must be cyclical, with certain bounded variables.

An example of the evolution of PAW's pitch angle θ, one of the key state variables in the bound, over time can be found in Fig. 6.18a. As can be seen, the pitch angle varies

considerably, at first because of the kick-start (from 623 to 624 seconds) and then as the robot settles into a cyclic bounding motion (from 625.5 to 627 seconds). The orbital nature of the motion, as required by the definition of stability given earlier, is evident in the pitch phase plot of Fig. 6.18b. The pitch phase plot illustrates a concentration of orbits which correspond to the stable bounding motion from 625.5 to 627 seconds.

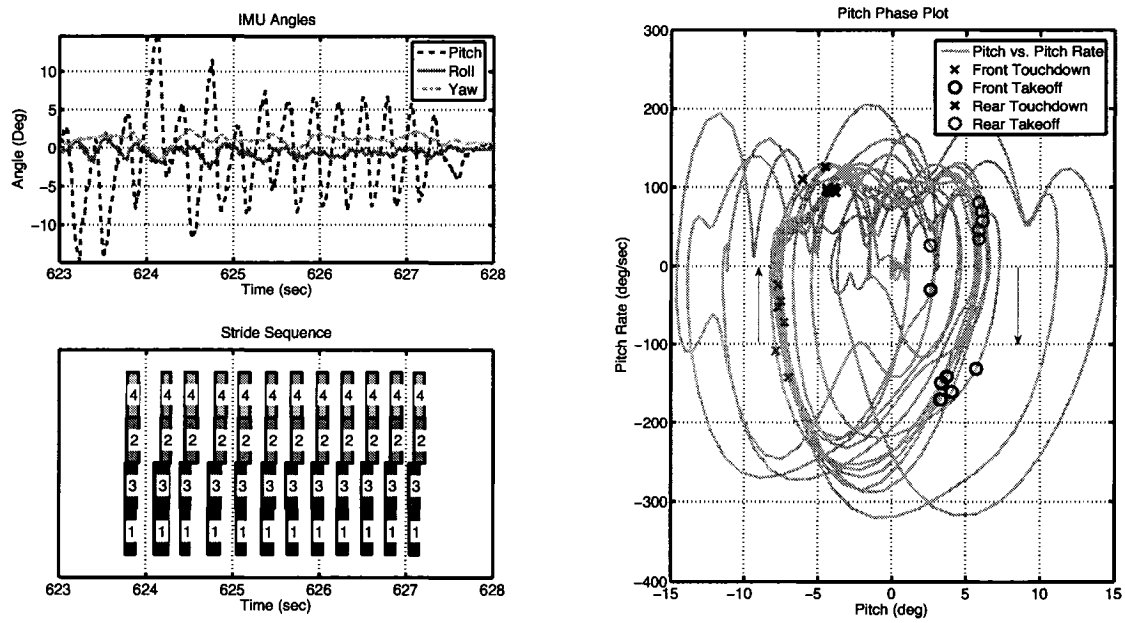

(a) IMU Angles vs. Time

(b) Pitch Phase

Fig. 6.18 Example PAW IMU Angles vs. Time & Pitch Phase Plot corresponding to Experiment 4 for bounding with actively controlled wheels as per Table 6.3. Events such as leg touchdown and liftoff as shown. Time evolution of the data is clockwise.

The progression is clockwise for all graphs in Fig. 6.19. PAW's flight phase is in the upper portion of Fig. 6.19a. while Scout II's is in the lower portion of Fig. 6.19d. This is due to Scout II's gathered flight phase versus PAW's extended flight phase, as discussed in Section 6.2.1, resulting in opposite pitching direction during stance and in the significant touchdown and liftoff events occurring at different points around the pitch phase curves for both robots.

With the confirmation that, from an orbital stability perspective the gait displays repeatability, one can now look at how this repeatability can be quantified. One method

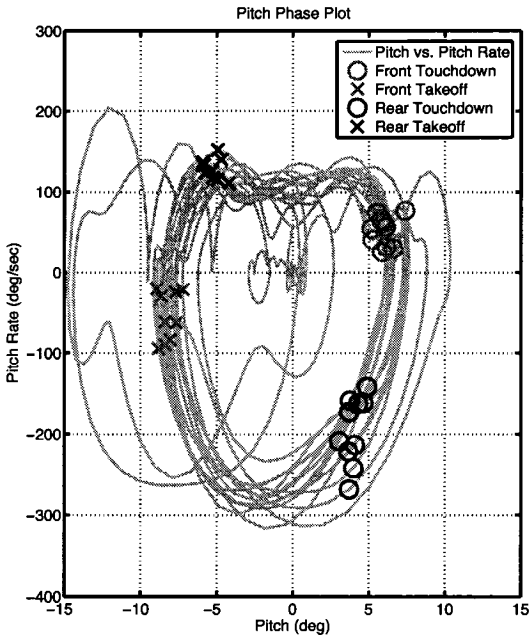

(a) PAW Active Wheel Bound Exp. 2

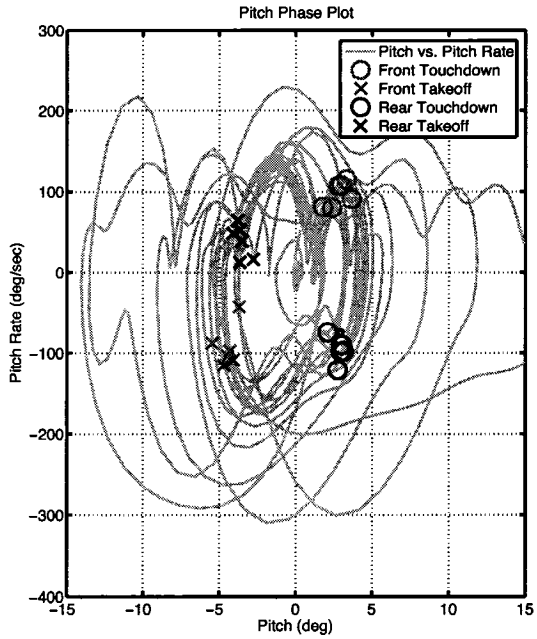

(b) PAW Active Wheel Bound Exp. 5

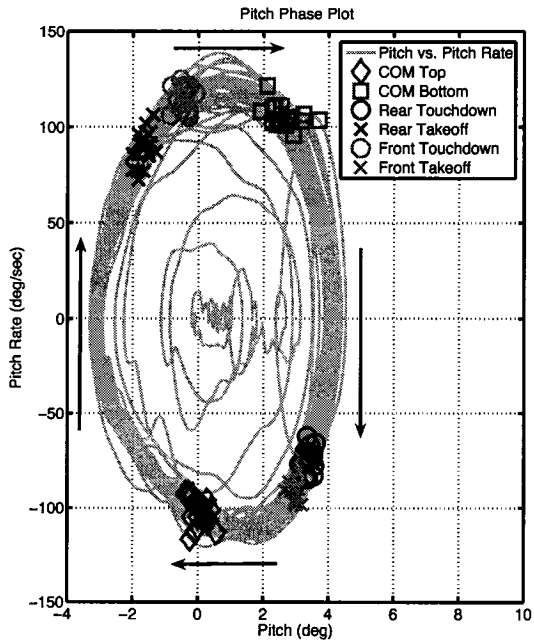

(c) Scout II Bound Exp. 3

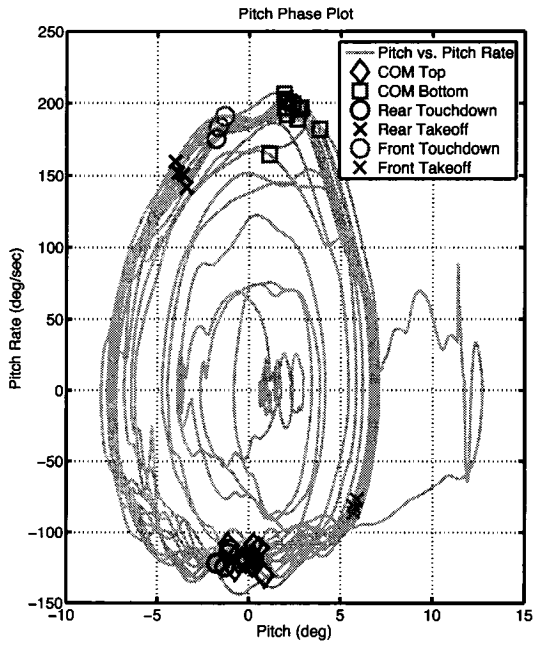

(d) Scout II Bound Exp. 4

Fig. 6.19 The pitch phase plots of the two robots during bounding at various settings of touchdown and liftoff angles, demonstrating stable limit cycles. Events such as touchdown and liftoff of front and rear legs are shown. See Tables 6.1 and 6.3 for setting details.

for quantifying the stride-to-stride repeatability would be to examine the variability of certain fixed-points, such as those for front leg touchdown, on the pitch phase plots. Unfortunately, given that pitch phase plots are not available for all bounding or galloping results, an alternate performance index, the stride frequency, common to all experiments, was examined.

6.8.3 Quantifying Stability with Convergence Rate and Standard Deviation

The stride frequency easily lends itself to quantization from robot data. Changes in the stride frequency, such as during convergence to stable motion, have strong audible components that are immediately recognizable to the trained ear[6], making evaluation of gait success relatively easy to the robot operator. Using the stride frequency values recorded by the robot one can measure both the rate of convergence as the number of strides to converge, and the variability of the gait as the standard deviation of the stride frequency during steady-state motion. These two values quantify the degree of stability of the system, with faster convergence rates and lower standard deviations being more desirable. These values are listed in Table 6.5 for Scout II and Table 6.6 and 6.7 for PAW. While the average number of strides required for convergence is only slightly lower with mechanically blocked wheels on PAW, the standard deviation for actively controlled wheels is significantly higher. Scout II's standard deviation is lower than both sets of PAW results, indicating that its bounding gait is more stable.

6.9 Summary

The hypothesis that the *liftoff angle parameters could be used to regulate forward speed* was tested in this chapter. While it was not possible to directly test the hypothesis on Scout II due to the foot-dragging that results from low apex heights during bounding, the hypothesis was confirmed on the PAW robot. It is felt that this presents a complementary, "fine-tuning" approach to the traditional method of forward speed adjustment using touchdown angles.

The experiments performed on PAW *with and without wheels* yield some interesting conclusions. First, the basic bounding gaits with and without wheels are similar enough

[6]In the same way, the robot operator can hear changes in leg phase differences such as those between one-, two- and four-beat gaits.

that the casual observer does not notice major differences. Upon closer inspection it was found that the bounding with actively controlled wheels is less efficient and exhibits relatively constant leg compression and duty factor values. Most important, not only is the reliability reduced, as shown in Tables 6.6 and 6.7, but forward speed is reduced by about 15% due to wheel usage. Countering these negative aspects, wheel rotation sensing, shown to be faster in detection of leg contact with the ground than the leg length potentiometer, may prove to be an asset in ground detection, especially if harder leg springs are used in the future. It is also thought that with higher frequency control loops, and therefore higher control gains and better wheel control, the negative aspects can be improved upon.

Experimental *leg compression* data for bounding on both Scout II and PAW has been presented here for the first time. While both robots have distinctive bounding gaits, as discussed earlier, they both demonstrate larger leg compression in the rear legs than in the front legs at nearly all speeds. This is important as it reinforces the notion borrowed from biology that the rear legs are primarily used for thrust, while the front legs aid in stabilization.

Finally, measures for gait success were presented in Section 6.8 and the bounding gaits for both robots are shown to have good rates of convergence, stable limit cycles and very good repeatability.

Chapter 7

Galloping: The First Implementation

This chapter presents the first gallop gaits on engineered, non-simulated systems. This is significant for two reasons. First, all previously-proposed 3D gallop controllers have required a minimum of eight actuated degrees of freedom. Here, it is shown that underactuated galloping can be achieved with leg compliance and only four hip motors. Second, until now and without exception, no individual or group has achieved galloping on a real robot. The rotary gallop gait variant is demonstrated here on not one, but *two* robots.

In Section 7.1.1, the control strategy for underactuated galloping is presented. The controller, which is derived from the φ-bound controller, requires no controlled coupling between front and rear legs in Scout II and no coupling between any leg in PAW. The basic experimental results obtained on Scout II and PAW, which result in a significant yaw component, are given and contrasted with φ_{lo}-turn controller trials. The φ_{lo}-turn controller uses differential liftoff angles in lateral leg pairs to achieve yaw, as opposed to the gallop controller which uses differential touchdown angles. While it is easier to maintain higher forward speeds with the φ_{lo}-turn controller the range of yaw rates is greater with the gallop controller. The relationship between the leg compression and the selection of "leading leg", and the direction of turning is discussed in Section 7.2 for both the φ_{lo}-turn and the rotary gallop. Energetics are presented in Section 7.3. Finally, stability of the galloping and φ_{lo}-turn gaits is examined in Section 7.4. These gaits are found to have good rates of convergence, good repeatability and low stride frequency standard deviation.

7.1 Experimental Setup and Baseline Results

This section describes the galloping trials performed on both Scout II and PAW as extensions of the previously described bounding results. Still frames from video footage of Scout II and PAW galloping can be seen in Fig. 7.1. A contrast between the rotary gallop and turning using the φ_{lo}-turn controller with differential sweep-limit and liftoff angles, φ_{swl} and φ_{lo}, is also presented here.

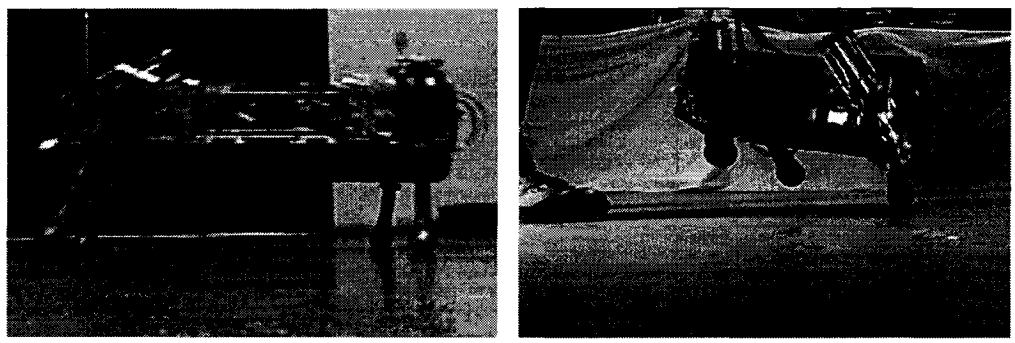

(a) Scout II (b) PAW

Fig. 7.1 While Scout II demonstrates a faster gallop, with better phase differentiation, it travels very low to the ground. PAW achieves a slower gallop but with greater apex heights. However, its short legs lead to limited phase differentiation even with large differences in touchdown angles.

The main distinguishing factor between gaits in different experiments is the *phase difference* between legs. The phase difference is a temporal measure between ground contacts of each of the four legs and is expressed as a percentage of a given stride period. The phase differences for each experiment are listed in Tables 7.1 through 7.3. Two-beat gaits such as the bound are defined by a single phase difference value between the front and rear legs. Here, the gallop is a four-beat gait which necessitates listing three values plus the trivial 0 value for the synchronization or reference leg, Leg 3. If one examines the phase differences listed in Experiment 2 of Table 7.1, Leg 3 is shown to touchdown first (0%), followed by Leg 1 (7.0%), Leg 2 (40.8%) and then Leg 4 (50.8%). Phase differences between adjacent legs of less than 4% are considered to represent identical touchdown times. In addition to the four-beat gallop, three-beat results are also presented. These include the *half-bound*, in which either the front or rear lateral legs (but not both pairs) touch down simultaneously,

or the *canter*, in which one rear leg and one front leg touchdown at the same time.

7.1.1 Scout II Galloping Experiments

Scout II is the first quadrupedal robot made to run in a gallop gait. An overview of the experimental development of the rotary gallop gait, one of three possible four-beat variants, is given here. The goal of these trials was to demonstrate that at least one gallop gait could be achieved on an underactuated robot with passively compliant legs. The first experiment, Exp. 1 of Table 7.1, demonstrates that the rotary gallop gait is possible through the modification of the Scout II φ-bound controller, presented in the previous chapter. Thus, as is the case with the φ-bound controller, it can be stated explicitly here that galloping can be achieved without sensing or tracking of robot orientation in the global reference frame. This agrees with the conclusions made in [23] regarding horses not requiring vestibular sensing and knowledge of spatial orientation for gallop gait control.

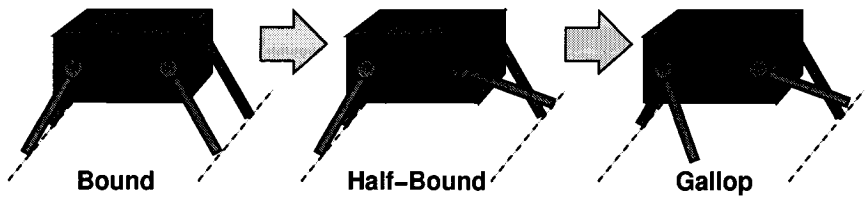

Fig. 7.2 Bound to Gallop via asymmetric touchdown angles.

As was discussed in Chapter 6, it is the touchdown and liftoff angles that serve as the dominant control inputs for the bounding controller. The following strategy for setting the touchdown angles was adopted for the development of gallop gaits. Within one lateral leg pair one chooses the touchdown angles of the first leg to be similar or identical to a successful bounding touchdown angle. The second leg's touchdown angle is set so that it is positioned *higher* than the first leg, as shown in Fig. 7.2. In this way the robot must roll to cause the second leg to contact the ground. In a similar fashion, the third leg (directly behind the second leg) is made to have a smaller touchdown angle than the fourth, so that it contacts the ground ahead of the fourth leg. This rolling motion, while visible in video footage but not measured on Scout II, is readily apparent in the inertial measurements taken onboard PAW, shown in Fig. 7.8c on page 122.

Not only must touchdown angles be asymmetric, but another change with respect to the φ-bound controller must be made. The enforcement of virtual leg control, which only allows

retraction of both legs in a pair to occur when both are in the same state, is dropped in the case of the gallop. The PD controller, Eq. (3.13) on p. 44, which is used to synchronize leg retraction during the bound on Scout II is adjusted during the gallop to take into consideration the phase difference ϵ between legs in a lateral leg pair. In other words, while control of lateral leg pairs is tightly coupled in Scout II's bound, the coupling is relaxed during the gallop. As with the φ-bound controller, there is *no* controlled coupling between the front and rear legs. This is especially significant since it is generally assumed, as in [23], that galloping requires coupled control of all four legs.

Liftoff angles are not varied in either the Scout II or PAW gallop experiments presented in Tables 7.1 and 7.2. The effect of liftoff angles is examined, however, in the φ_{lo}-turning work described in Section 7.1.3.

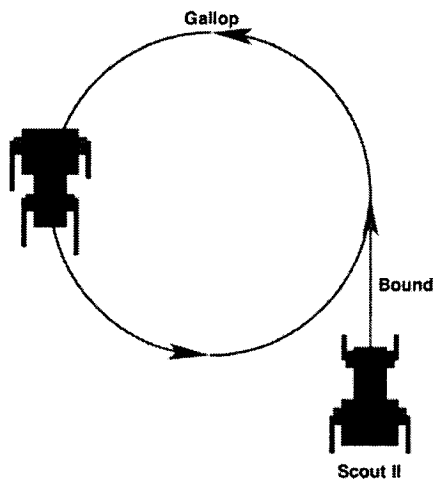

Fig. 7.3 Top view of bound to gallop sequence on Scout II.

Experiments 1 and 2 were conducted with different springs, 3520 N/m and 4300 N/m, respectively, the latter chosen to increase the apex height of the gallop during flight.[1] With these stiffer springs it became possible to increase the maximum speed of the robot from 1.25 m/s bounding to a mean of 1.29 m/s in gallop, with some results at up to 1.4 m/s. In the second gallop experiment a bound-gallop transition was introduced, as shown in Fig. 7.3. This allows the robot to converge first to a stable limit cycle after the initial kick-jump, in a bid to improve repeatability. In the first experiment the robot was made to yaw clockwise in configuration (a) of Fig. 7.4, while a counter-clockwise yaw in configuration

[1]Note that Exp. 1 has an extended flight phase, while Exp. 2 has a gathered flight phase.

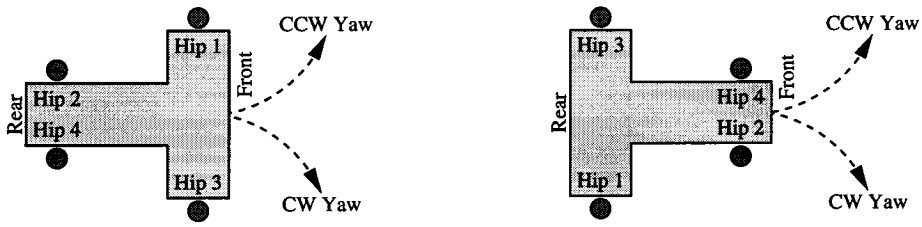

(a) Wide End in Front (b) Narrow End in Front

Fig. 7.4 Direction of yaw and alignment of robot. All experiments on PAW and Scout II were conducted in configuration (a), except for Exp. 2 of Table 7.1 in which configuration (b) was used.

(b) was used for the second experiment. Basic results, showing stride sequences, applied hip torques and leg compression are visible in Fig. 7.5.

Further development of the rotary gallop gait was performed on the PAW robot, described in the next section.

Table 7.1 Experimental Results: *Scout II* Rotary Gallop. Legs 1 and 3 are in front for Exp. 1 and in the rear for Exp. 2, as shown in Fig. 7.4.

Exp #	Front Leg Touchdown, Liftoff Angles ($\varphi_{ftd}, \varphi_{flo}$) [deg]	Rear Leg Touchdown, Liftoff Angles ($\varphi_{rtd}, \varphi_{rlo}$) [deg]	COM Speed [m/s]	Yaw Rate [deg/sec]	Max Comp. (mean) (Leg 1, Leg 3) [m]	Max Comp. (mean) (Leg 2, Leg 4) [m]	Stride Freq. [Hz]	Phase Diff. (mean) (1, 3, 2, 4) [%]	Duty Cycle (mean) (1, 3) [%]	Duty Cycle (mean) (2, 4) [%]
1 CW Gallop	(-17, 0) (-32, 0)	(-32, 0) (-17, 0)	<1	n/a	(0.034, 0.023)	(0.042, 0.075)	2.89	(-7.9, 0 19.4, 7.4)	(40.4, 23.7)	(44.8, 46.4)
2 CCW Gallop	(-21, 0) (-19, 0)	(-19, 0) (-17, 0)	1.3	57	(0.061, 0.044)	(0.049, 0.036)	3.86	(7.0, 0, 40.8, 50.8)	(40.9, 37.6)	(33.0, 24.3)

7.1.2 PAW Galloping Experiments

The PAW gallop controller and experiments were developed in a similar manner to those for Scout II. Notable differences include lack of synchronization between lateral legs during

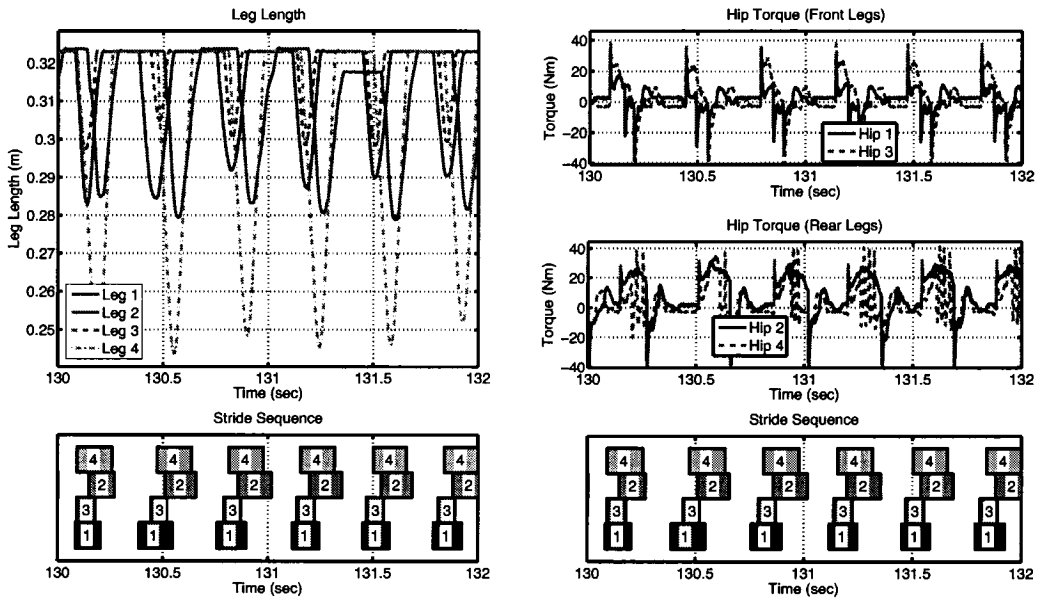

(a) Leg length

(b) Hip torques

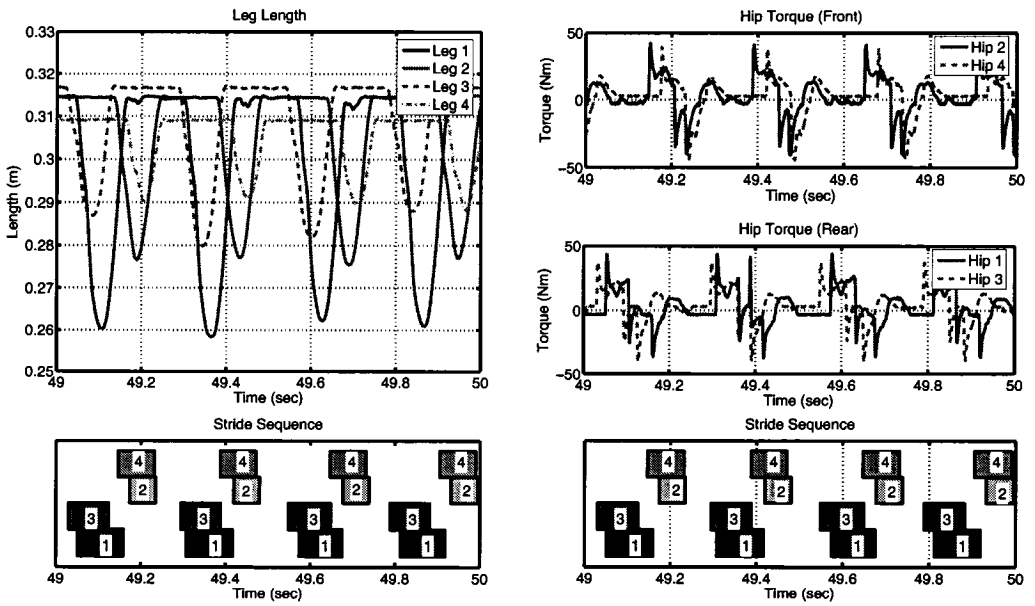

(c) Leg length

(d) Hip torques

Fig. 7.5 Leg lengths and hip torques for Scout II galloping in clockwise (a,b) and counter-clockwise (c,d) directions, corresponding to Exps. 1 and 2 of Table 7.1, respectively.

sweep and an automated transition from bound to gallop (set to five strides in PAW), whereas the transition was commanded by the operator in Scout II. PAW's wheels were mechanically blocked throughout these trials.

While a half-bound was achieved on Scout II [28], it is not discussed in any detail here as the trials which led to it were limited. The gallop controller on PAW led to a half-bound (Exp. 6, Table 7.2) and a canter (Exp. 1, Table 7.2) in addition to the rotary gallop (Exps. 2 - 5, Table 7.2).

The reader's attention is drawn to how the strategy of developing phase differences through asymmetric touchdown angles in lateral leg pairs has a direct effect on forward speed. By increasing the touchdown asymmetry one increases the phase difference, but this, in general, leads to lower stride frequency and forward speed due to higher resulting pitch values and apex heights during flight, as can be seen in photo of PAW in Fig. 7.1b. Because PAW's legs are significantly shorter that Scout II's, the difference in touchdown angles in the lateral legs pairs needs to be even greater on PAW in order to achieve similar phase differences. This, in turn leads to PAW's gallop being significantly slower than Scout II's for the same phase differences.

In addition to the information given in Table 7.2, leg compression, applied hip torque and stride sequence data for Experiment 4 of Table 7.2, are illustrated in Fig. 7.6a and b.

7.1.3 PAW φ_{lo}-Turn Experiments

The concept behind this controller is analogous to using long paddle strokes in a kayak or canoe. If one uses longer strokes on one side of the boat than on the other a moment will be created which will yaw the boat away from these longer strokes. By forcing the sweep limit further back on one side of the robot, the resulting liftoff angle will let the legs extend at the end of stance so that the robot will yaw towards the opposite side.

The φ_{lo}-turn experiments were conducted in a similar fashion to the bounding experiments reported in Chapter 6. After the open-loop jump a single bound stride was taken, after which the φ_{lo}-turn controller was engaged. At this point the robot began to yaw either clockwise or counter-clockwise depending on the controller settings.

A summary of the φ_{lo}-turn controller experiments is found in Table 7.3, while illustrations of applied hip torques, leg compression and the stride sequence are shown in Fig. 7.6c and d. As with the PAW gallop trials, the wheels were mechanically blocked throughout

Table 7.2 Experimental Results: *PAW* Rotary Gallop (4-beat), Canter and Half-Bound (3-beat). Legs 1 and 3 are in front, 2 and 4 in back. Yaw rate in Experiments 4 to 6 was measured by IMU.

Exp #	Front Leg Touchdown, Liftoff Angles ($\varphi_{ftd}, \varphi_{flo}$) [deg]	Rear Leg Touchdown Liftoff Angles ($\varphi_{rtd}, \varphi_{rlo}$) [deg]	Fwd. COM Speed [m/s]	Yaw Rate [deg/sec]	Max Front Comp. (1, 3) [m]	Max Rear Comp. (2, 4) [m]	Stride Freq. (mean) [Hz]	Phase Diff. (mean) (1,2, 3,4) [%]	Duty Cycle (mean) (1, 3) [%]	Duty Cycle (mean) (2, 4) [%]
1 CW Canter	(-17, 4) (-37, 4)	(-37, 12) (-17, 12)	0.5	-50	(0.034, 0.030)	(0.029, 0.069)	2.60	(-18.8,13.8, 0, 2.6)	(39.7, 19.6)	(28.9, 39.8)
2 CCW Gallop	(-35, 4) (-18, 4)	(-18, 12) (-35, 12)	0.6	30	(0.034, 0.033)	(0.064, 0.034)	2.68	(10.7, 16.9, 0, 26.7)	(22.6, 38.2)	(40.3, 32.0)
3 CCW Gallop	(-35, 4) (-18, 4)	(-18, 12) (-30, 12)	0.6	30	(0.032, 0.032)	(0.065, 0.030)	2.69	(14.1, 18.6, 0, 29.7)	(21.1, 40.2)	(40.6, 30.6)
4 CCW Gallop	(-33, 4) (-18, 4)	(-18, 12) (-25, 12)	0.9	12	(0.037, 0.035)	(0.048, 0.041)	3.04	(5.1, 15.4 0, 20.7)	(30.8, 37.2)	(41.8, 37.5)
5 CCW Gallop	(-29, 4) (-18, 4)	(-18, 12) (-25, 12)	0.9	7	(0.035, (0.033)	(0.043, 0.035)	3.28	(4.7, 19.4 0, 25.6)	(33.0, 39.6)	(44.2, 38.1)
6 CCW Half-Bound	(-25, 4) (-18, 4)	(-18, 12) (-25, 12)	1.0	2	(0.037, 0.034)	(0.044, 0.036)	3.20	(2.8, 17.9, 0, 23.0)	(34.1, 38.6)	(44.1, 37.4)

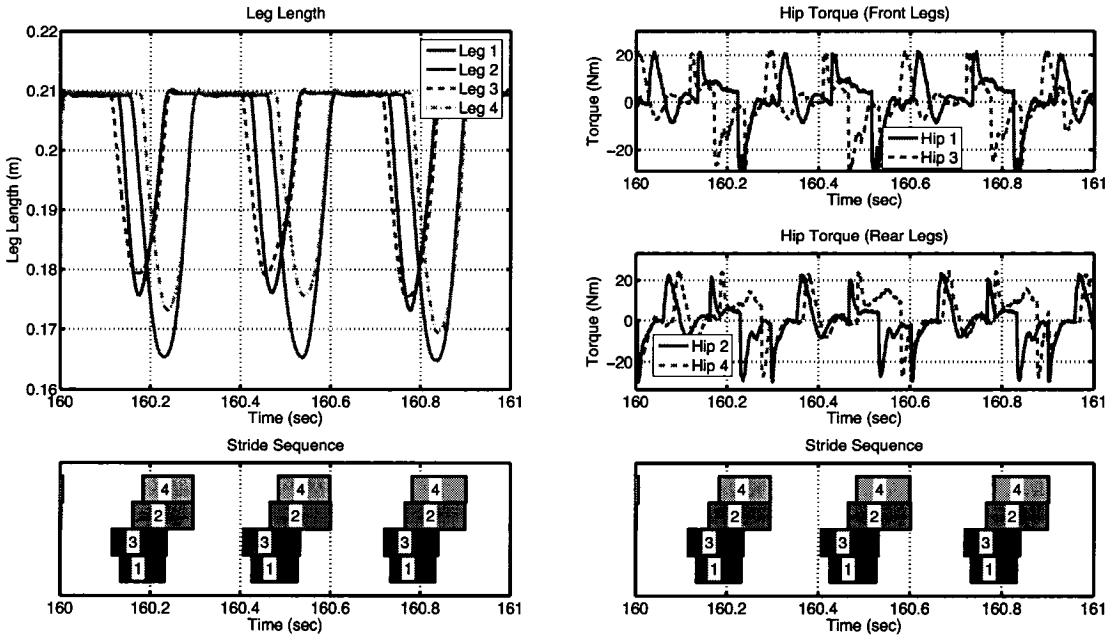

(a) Leg length (b) Hip torques

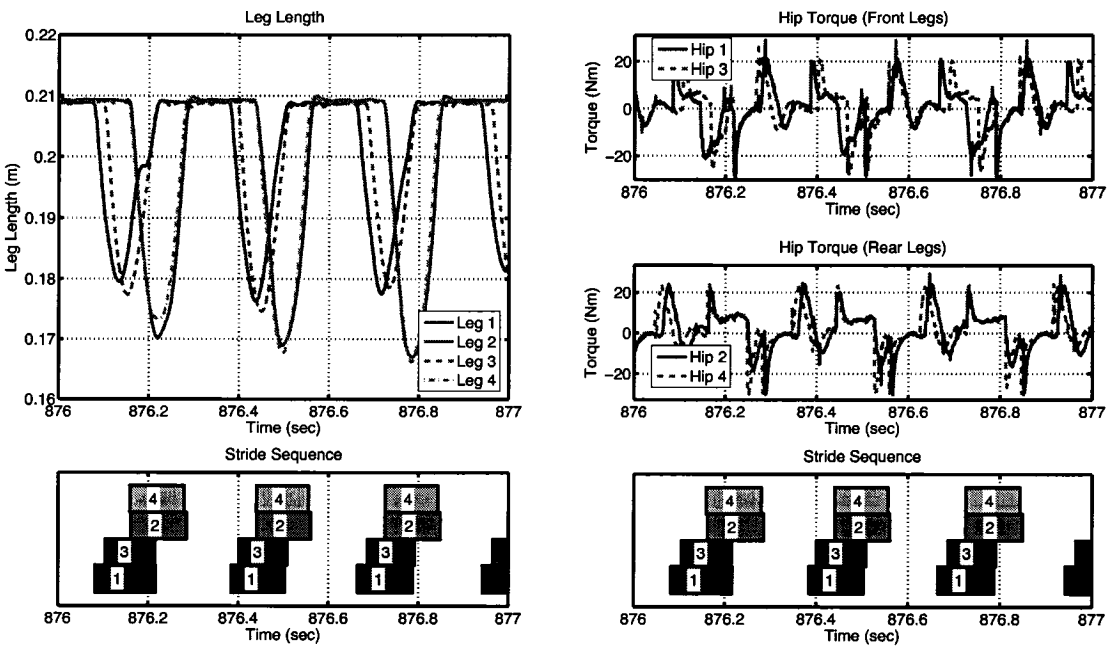

(c) Leg length (d) Hip torques

Fig. 7.6 Leg lengths and hip torques for PAW galloping in the counter-clockwise (a and b, Table 7.2, Exp. 4) and φ_{lo}-turn in the clockwise (Table 7.3, Exp. 1) directions, c and d. Note the half-bound stride pattern of the φ_{lo}-turn.

(a) In Flight (begin)

(b) Leg 3 Touchdown

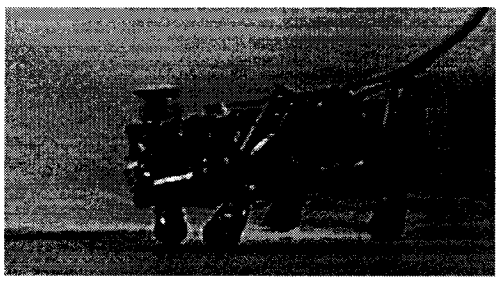

(c) Leg 1 Touchdown

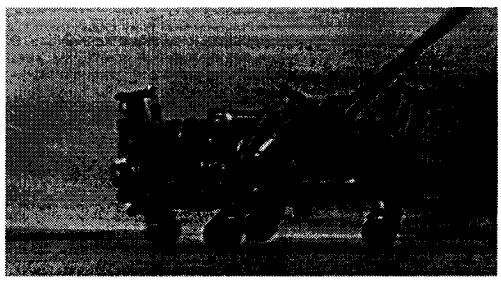

(d) Leg 2 Touchdown

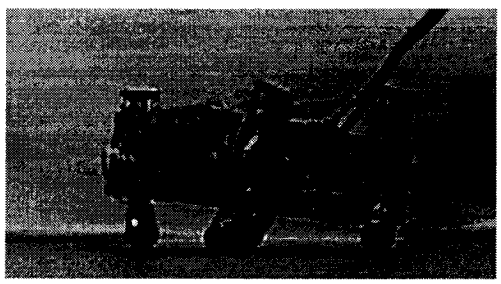

(e) Leg 4 Touchdown

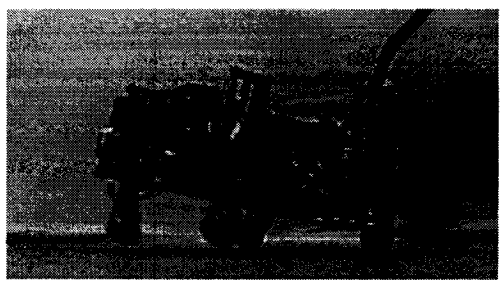

(f) Front Leg Liftoff

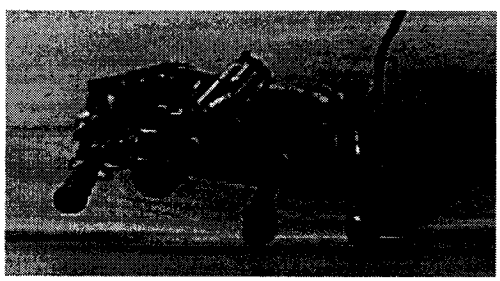

(g) Rear Leg Liftoff

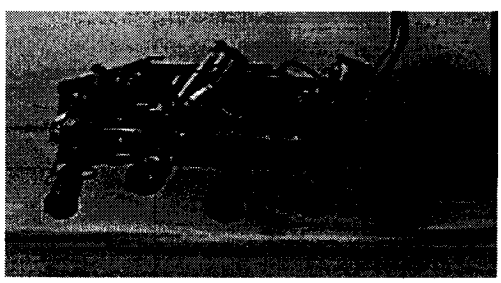

(h) In Flight (end)

Fig. 7.7 Still frame images from PAW galloping experiments (Exp. 2, Table 7.2). Note the large apex height and toe clearance.

the experiments.

These results demonstrate the possibility of achieving yaw control using longitudinal leg pair sweep limits and related liftoff angles. While it is apparent that changing the liftoff angles in longitudinal leg pairs does have a significant – though asymmetric, in PAW's case – change on yaw rate, the change does not greatly affect forward speed. The measured forward speeds, 1.0 to 1.1 m/s, while slower, are still close to the maximum forward speed achieved during bounding, 1.2 m/s. The fact that this controller, unlike what occurs with the rotary gallop, does not suffer a significant reduction in forward speed during yaw is a distinct advantage. Unfortunately, it does not offer the range of yaw rates that have been demonstrated with the rotary gallop because of the limited range of liftoff angles which result in stable motion.

Table 7.3 Experimental Results: *PAW* φ_{lo}-Turn

Exp #	Front Leg Touchdown, Liftoff Angles ($\varphi_{ftd}, \varphi_{flo}$) [deg]	Rear Leg Touchdown, Liftoff Angles ($\varphi_{rtd}, \varphi_{rlo}$) [deg]	COM Speed [m/s]	Yaw Rate [deg/sec]	Max Front Comp. (mean) [m]	Max Rear Comp. (mean) [m]	Stride Freq. (mean) [Hz]	Phase Diff. (mean) (1, 2, 3, 4) [%]	Duty Cycle (mean) (1, 3) [%]	Duty Cycle (mean) (2, 4) [%]
1 CW Half-bound	(-20, 10) (-20, 6)	(-22, 18) (-22, 14)	1.1	-11.4	(0.032, 0.033)	(0.041, 0.038)	3.55	(-4.4, 14.2, 0, 16.0)	(40.2, 38.2)	(44.9, 40.3)
2 CCW Bound	(-20, 6) (-20, 10)	(-22, 14) (-22, 18)	1.0	6.2	(0.034, 0.033)	(0.041, 0.038)	3.73	(1.8, 17.7, 0, 18.9)	(39.1, 41.0)	(43.4, 41.2)
3 CCW Gallop	(-20, 6) (-20, 14)	(-22, 14) (-22, 22)	1.1	8.1	(0.030, 0.029)	(0.037, 0.037)	4.12	(5.3, 23.6, 0, 28.5)	(37.6, 41.4)	(49.0, 45.6)

7.2 Lead Leg and Asymmetric Leg Compression

In this section the role of the lead leg is examined for the gallop and φ_{lo}-turn gaits with the aid of inertial measurement and footfall data, displayed in Fig. 7.8. The leg compression values are also examined and related to the leg sequence.

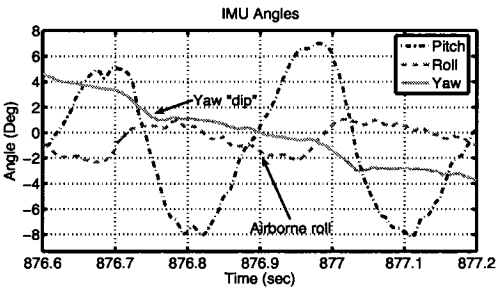

(a) φ_{lo}-turn CW

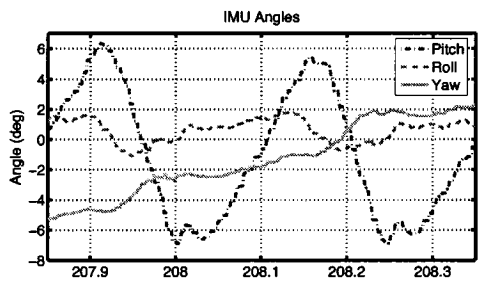

(b) φ_{lo}-turn CCW

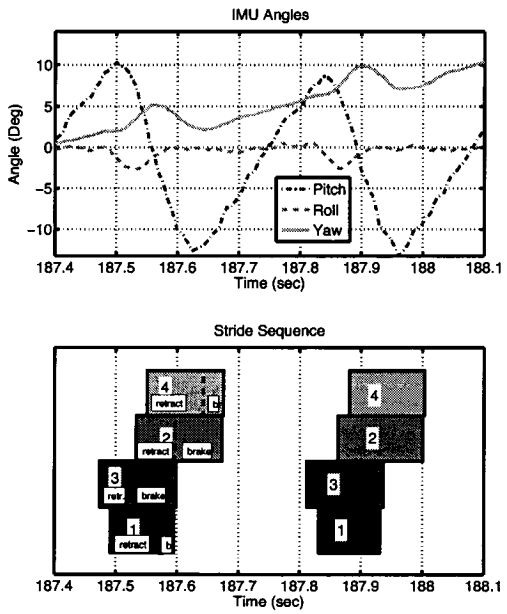

(c) Rotary Gallop CCW

Fig. 7.8 IMU data for the φ_{lo}-turn in clockwise (a, Exp. 1, Table 7.3), counterclockwise (b, Exp. 3, Table 7.3) and gallop (c, Exp. 2, Table 7.2) IMU data. Note the pronounced yaw and roll components that are not as important in the bounding IMU plots, shown in Fig. 6.18 on p. 107.

7.2.1 Lead Leg's Role in Turning

The front *lead* leg (or simply, the lead leg) is the second leg in the front pair to touchdown. It is termed "lead" because it is physically in front of the other leg during stance; this is the *opposite* of a temporal "lead". As observed in cheetahs and horses, the lead leg is a predictor of the direction of yaw [79], and is the forefoot on the inside of a given turn. On PAW and Scout II this means that if the wide end is considered to be the front, see Fig. 7.4a, and the robot is yawing counter-clockwise, then Leg 1 is the *lead* lag, while Leg 3 is the *lag* leg. This relationship has been found to hold on both robots, in both clockwise and counter-clockwise turning, regardless of whether the wide or narrow end of the robot is in front.

While it would be straightforward to assume that the robot uses the lead leg to pivot on in order to yaw, analysis of the IMU data from PAW[2] reveals that this relationship is somewhat more complex. The reader is presented here with a detailed explanation of IMU data throughout rotary gallop and φ_{lo}-turning experiments. In the case of the φ_{lo}-turn we examine a *clockwise* turn, in Fig. 7.8a. In the rotary gallop case we examine the motion of the robot during a *counter-clockwise* turn, illustrated in Fig. 7.8c.

In the rotary gallop case the counter-clockwise (positive slope) yaw begins during the stance-retraction phase of the front legs but is tempered by the earlier braking in the *lag* leg, Leg 3, as it reaches the sweep limit angle before the *lead* leg, Leg 1, does. This causes the robot to pivot about the *lag* leg in the clockwise direction. When the *rear* lag leg, Leg 2, brakes at its sweep limit angle, φ_{swl}, the robot slows its clockwise yaw and eventually resumes counter-clockwise yaw, which it maintains during flight. Therefore, rather than pivoting about the front *lead* leg, Leg 1, the pivoting in the main direction of yaw is done about Leg 2, *directly behind the lead leg.*

In φ_{lo}-turning the yaw component of motion is generated differently than in the rotary gallop case. While the front lag leg, with its larger sweep limit and liftoff angle, forces the robot to yaw about the lead leg, this motion is tempered by the touchdown of the rear legs. Another interesting remark can be made with respect to the leg phase difference due to the rolling action of the robot. While an explicit phase difference is not set up in the robot as it is with the touchdown angles in the rotary gallop (the desired touchdown angles φ_{td} are

[2]Inertial data is not available from Scout II, but the conclusions drawn from PAW are applicable since overall motion on both robots is consistent.

identical in each of the lateral leg pairs), the rolling action of the robot during flight causes one front leg to be chosen as lead and the other as lag. The results for turning clockwise in Fig. 7.8a can be contrasted with opposite results for turning counter-clockwise, shown in Fig. 7.8b.

In summary, while both Scout II and PAW demonstrate the same lead-leg vs. yaw relationship observed in biology, the inertial measurements reveal that the lead leg is not necessarily used as a pivot point for yaw. Further study, using a robot with knees, in which a sweep limit is not used to effect changes in liftoff angles to achieve toe clearance during protraction, should be conducted to see if the same relationship can be observed.

7.2.2 Leg Compression

The rotary gallop data, in Tables 7.1 and 7.2 and Figs. 7.5 and 7.6a, for both Scout II and PAW reveals an interesting result when it comes to examination of the compression of the legs. In both cases the leg directly behind the front lead leg compresses more than any other. In addition, in the more extensive PAW data, there is a correlation between the difference in compression between this rear leg and the front lead leg and the yaw rate, as shown in Fig. 7.9.

7.3 Energetics

As with the bounding and rolling results the reader's attention is now drawn to the energy consumption of the two robots during various gaits. In this section we examine the specific resistance, as noted earlier on page 71, one of the standard methods of measuring energy efficiency of a running robot, for galloping and the other gaits described in this chapter. These specific resistance values are plotted in Fig. 7.10. As can be seen, Scout II may gallop slightly faster than it bounds, but it does so less efficiently at this highest speed. At Scout II's slowest gallop setting it is actually more efficient.

The PAW robot's gallop controller results in the slowest gaits demonstrated on the robot to date, excluding trivial rolling behaviours. The reason that these gallops are so slow is that much of the stride is spent in ballistic flight, with the COM reaching heights of 0.22 to 0.25 m (30% - 50% greater than COM while standing) and toe clearance of over one wheel diameter (0.066 m). These large apex heights produce large pitch values which, in turn, aid in achieving necessary footfall phases for galloping. As these phase differences become

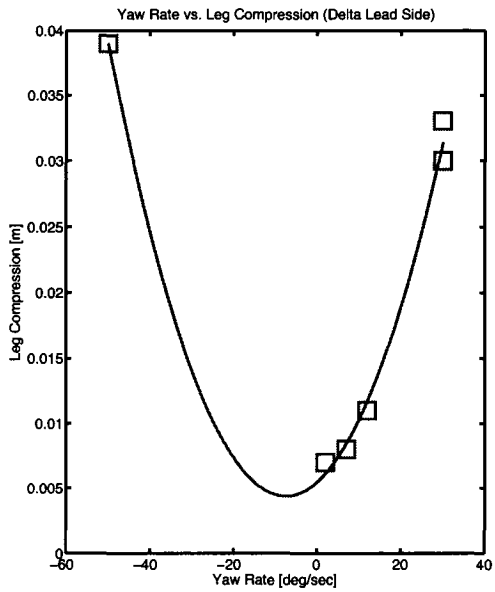

Fig. 7.9 The PAW yaw and leg compression data reveals a correlation between yaw rate and the difference in leg compression between the front lead leg and the leg directly behind it. The greater the yaw, the greater the difference in leg compression.

smaller, the robot speeds up, travels closer to the ground and achieves more efficient motion. The reduced phase differences also reduces the yaw rate, straightening out the robot. All this comes at the expense of the footfall phase difference which separates the gallop from other gaits. At slower rates, PAW's gallop is, through extrapolation of the trends in Fig. 7.10, only marginally less efficient than PAW's bounding gait. At the faster rates with reduced phase differences (Exps. 4, 5 and 6 of Table 7.2) the asymmetric gait (either a gallop or a half-bound) is equally or more efficient than the symmetric bound.

Thus, while Scout II's gallop may become less efficient at higher speed, PAW's seems to be more efficient than the equivalent bound. Whether the source of this difference is body morphology or controller parameters is not known. Further study to determine the nature of this difference is worth pursuing.

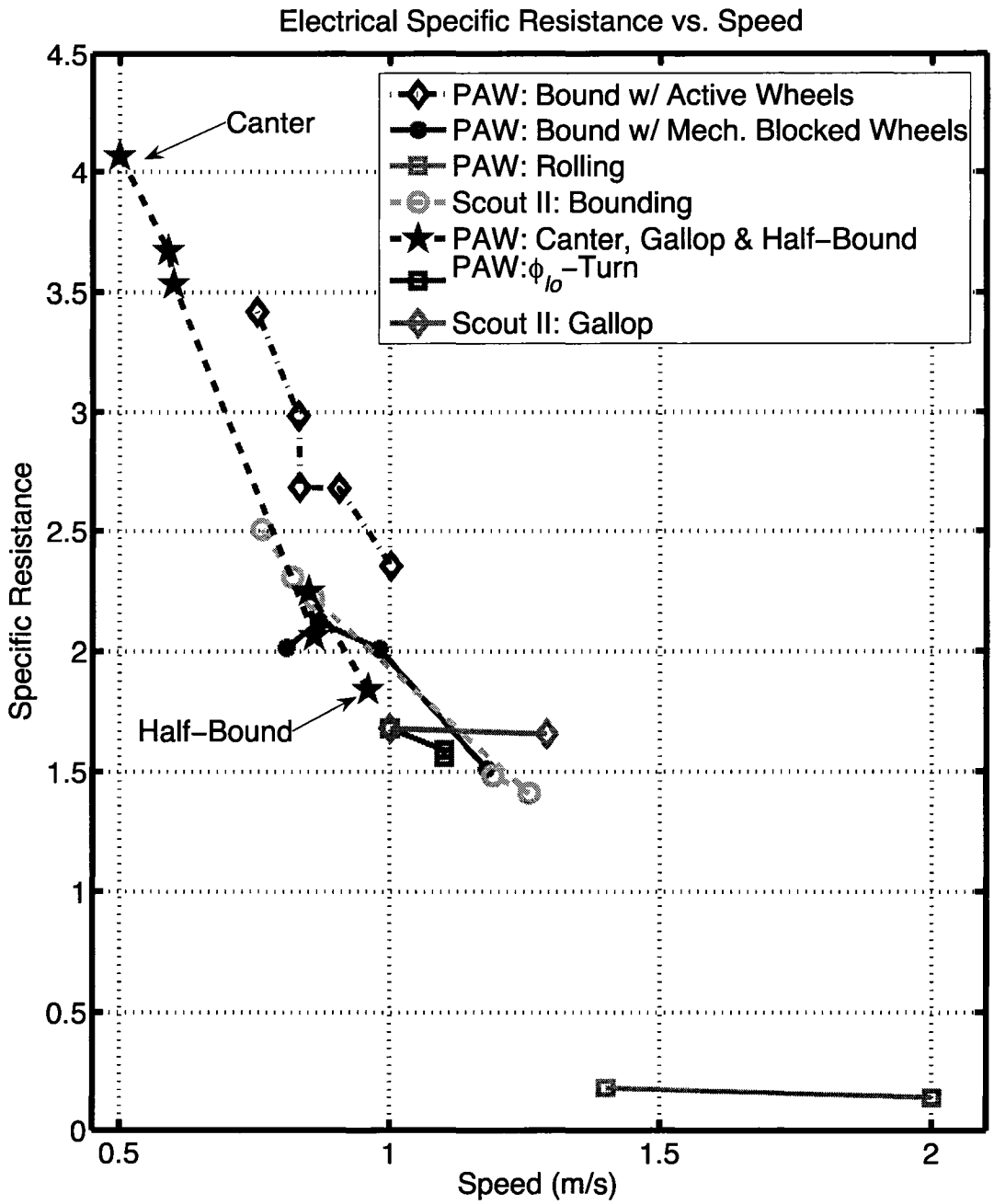

Fig. 7.10 The specific resistance values for Scout II and PAW when galloping and engaging in the φ_{lo}-turn, as compared to the other gaits that they have been shown to use.

7.4 Measuring Gait Success

Quantifying the stability of legged locomotion systems is important in the evaluation and comparison of these systems, as discussed in [50]. In this section the success of experimental gait trials is discussed, based on how stable the gait is and how rapidly the gait achieves stability. This is similar to the gait success discussion for bounding in the previous chapter. The first quantifiable measure of success presented is repeatability in achieving a bounded limit cycle over a given number of trials. Then, for gaits which achieve a bounded limit cycle, the measurement of the gait's stability is discussed from the perspective of rate of convergence as well as the variability of a particular variable (performance index or state variable) via the measurement of its standard deviation.

As with the bounding results, the pitch of the robots varies widely at first and eventually settles to a bounded, cyclical pattern. Some of the trials presented here, such as Experiments 4 - 6 in Table 7.5 and Experiments 1 - 3 in Table 7.6 for PAW, as well as Experiment 2 in Table 7.4 for Scout II engage a bounding gait prior to a gallop. These initial bounding strides have an effect on repeatability, as discussed below.

Table 7.4 Experimental Results: *Scout II* Stability for Rotary Gallop.

Exp #	Front Leg Touchdown, Liftoff Angles ($\varphi_{ftd}, \varphi_{flo}$) [deg]	Rear Leg Touchdown, Liftoff Angles ($\varphi_{rtd}, \varphi_{rlo}$) [deg]	COM Speed [m/s]	Stride Freq. (mean) [Hz]	Stride Freq. (std. dev) [%]	Strides to Steady-State Converge. (mean) [#]	Trial Repeat.
1 CW	(-17, 0) (-32, 0)	(-32, 0) (-17, 0)	< 1	2.89	4	1.0 (no bound)	1 / 1
2 CCW	(-17, 0) (-19, 0)	(-19, 0) (-17, 0)	1.3	3.86	5	10.7 (incl. 7.4 bounds)	10 / 10

7.4.1 Trial-to-trial Repeatability

As with bounding, not all gallop and φ_{lo}-turn experimental trials were found to be 100% repeatable. This is based on several factors. Software or electronic errors leading to trial failure are not included in repeatability measures as they occur independently of gait parameters or dynamics. Critical failures due to events such as toe-stubbing are counted,

Table 7.5 Experimental Results: *PAW* Stability for Rotary Gallop, Half-Bound and Canter.

Exp #	Front Leg Touchdown, Liftoff Angles ($\varphi_{ftd}, \varphi_{flo}$) [deg]	Rear Leg Touchdown, Liftoff Angles ($\varphi_{rtd}, \varphi_{rlo}$) [deg]	COM Speed [m/s]	Stride Freq. (mean) [Hz]	Stride Freq. (std. dev) [%]	Strides to Steady-State Converge. (mean) [#]	Trial Repeat.
1 CW Canter	(-17, 4) (-37, 4)	(-37, 12) (-17, 12)	0.5	2.60	7	3.0	1 / 1
2 CCW Gallop	(-35,4) (-18,4)	(-18,12) (-35,12)	0.6	2.86	3	5.5	6 / 6
3 CCW Gallop	(-35, 4) (-18, 4)	(-18, 12) (-30, 12)	0.6	2.69	2	2.7	3 / 3
4 CCW Gallop	(-33, 4) (-18, 4)	(-18, 12) (-25, 12)	0.9	3.04	4	8.0	16 / 18
5 CCW Gallop	(-29, 4) (-18, 4)	(-18, 12) (-25, 12)	0.9	3.28	3	4.3	11 / 11
6 CCW Half-bound	(-25, 4) (-18, 4)	(-18, 12) (-25, 12)	1.0	3.20	4	5.1	11 / 12

Table 7.6 Experimental Results: *PAW* Stability for φ_{lo}-Turn.

Exp #	Front Leg Touchdown, Liftoff Angles ($\varphi_{ftd}, \varphi_{flo}$) [deg]	Rear Leg Touchdown, Liftoff Angles ($\varphi_{rtd}, \varphi_{rlo}$) [deg]	COM Speed [m/s]	Stride Freq. (mean) [Hz]	Stride Freq. (std. dev) [%]	Strides to Steady-State Converge. (mean) [#]	Trial Repeat.
1 CW Half-Bound	(-20, 10) (-20, 6)	(-22, 18) (-22, 14)	1.1	3.55	6	5.1	10 / 11
2 CCW Bound	(-20, 6) (-20, 10)	(-22, 14) (-22, 18)	1.0	3.73	9	2.0	4 / 5
3 CCW Gallop	(-20, 6) (-20, 14)	(-22, 14) (-22, 22)	1.1	4.12	5	5.0	10 / 11

however, as they are generally due to gait parameters and dynamics. The trial-to-trial repeatability results for both galloping (Scout II and PAW) and φ_{lo}-turn (PAW only) are similar to the results obtained for bounding with fixed toes or mechanically blocked wheels in the previous chapter. While excellent repeatability was obtained for PAW gallop experiments 1 - 3, Table 7.5, even with no bounding acceleration phase, a bound acceleration phase similar to that used on Scout II was used for PAW gallop experiments 4 - 6 and all φ_{lo}-turn experiments.[3] The acceleration phase was not necessary in PAW gallop experiments 1 - 3 because the gait parameters were so extreme that it was very difficult for the robot not to stabilize on a limit cycle. In the other cases, where the touchdown angles were less extreme, it was far easier for the robot to be "attracted" to other limit cycles such as bounding or half-bound after the initial open-loop jump-kick. In addition, because the robot travelled closer to the ground, it was more vulnerable to toe stubbing. By introducing the bounding acceleration phase, variability in initial conditions was decreased as the robot was allowed to converge first on a bounding limit cycle prior to engaging in a gallop or φ_{lo}-turn.

[3]A discussion of the bound acceleration is found in Section 7.1.1, with an illustration in Fig. 7.3.

7.4.2 Quantifying Stability with Convergence Rate and Standard Deviation

As with the bounding results, the rates of convergence, measured in average strides taken to achieving a steady-state gait, are given in Tables 7.4 to 7.6. These values are based on examination of the time it took for the stride frequency to settle to steady state, as well as examination of the settling of other variables such as leg length. The rate of convergence for these trials is similar to the results obtained for Scout II bounding and PAW bounding with mechanically blocked wheels. The standard deviation, calculated on the aggregate values using Microsoft Excel's *stdev()* function, was also found to be similar to the previous bounding results, shown in Tables 6.5 and 6.6.

7.5 Summary

In this chapter Scout II and PAW are shown to be the *first robots* to demonstrate any gallop gait. Unlike other current robotic projects such as KOLT, [109], or past quadruped simulations, e.g. [23], this has been accomplished using underactuated robots, with either lateral leg pair coupling or no coupling whatsoever, and without the need for inertial measurements such as pitch, yaw or roll.

While the yaw of the rotary gallop is generated by varying the touchdown angles, the yaw of the φ_{lo}-turn is generated by controlling the liftoff angles. The φ_{lo}-turn controller is able to maintain relatively high speed during yaw, unlike the gallop controller. However, the range of yaw rates is far greater with the gallop controller. As with observations made in nature by Hildebrand, [79], the lead leg was found here to consistently coincide with the direction of yaw in the rotary gallop. In addition, it was found that the leg directly behind the lead leg consistently compressed more than any other leg. Given that the rear legs tend to compress more than front legs during straight line motion and that this tendency is even more apparent during the yaw manoeuvres it is a recommended that this be considered in future leg designs.

As with bounding, the gallop gaits which achieve large ballistic phases are shown to be less efficient. It is especially evident on PAW that as the difference in touchdown angles is increased to achieve the gallop, the yaw rate and apex heights are increased and the forward velocity is decreased. The use of knees to achieve the phase differences required would alleviate this issue.

The quantifiable measures of stability, rate of convergence and standard deviation of the stride frequency, are shown here to be equivalent to the results obtained earlier with Scout II and PAW bounding gaits. The use of a bounding acceleration phase was tested and shown to improve repeatability of the gallop gait, especially when leg phase differences were more moderate.

Chapter 8

Conclusions and Future Work

This chapter summarizes work conducted on two underactuated quadrupedal robots equipped with compliant legs, Scout II and PAW. The main contributions are given here within the context of conclusions drawn from the individual chapters of this thesis.

While running gaits are widely used in nature, they are rarely seen in robots. The bounding gait has been demonstrated previously on only a select number of robots, while the gallop has *only* been demonstrated on *two* robots, Scout II and PAW, employed in this research. Until now, and apart from biological studies, the gallop gait has only ever been studied in simulation, with most simulations examining the gait in planar fashion. Here, the gallop gait has been studied, with particular focus paid to three-dimensional motion. The PAW robot can also be configured to use actuated wheels at the distal ends of its compliant legs in both bounding and wheeled modes of locomotion. This is the first robot capable of both hybrid wheeled-leg behaviours and dynamically stable running, making it suitable as a platform for exploring unique combinations of these novel modes of locomotion.

This thesis has shown that dynamically stable gaits such as bounding are possible using actively controlled wheels at the distal ends of the legs. These results have been contrasted with baseline trials on two robots using traditional fixed toes. These bounding trials have also provided baseline results for the development and testing of the rotary gallop gait on both PAW and Scout II.

Below, individual contributions are addressed in greater detail.

8.1 Rolling Behaviours

Three rolling mode controllers have been introduced in this thesis which take advantage of the hybrid nature of the PAW platform. The inclined turning method illustrates how to improve turning over simple skid-steering by repositioning the wheels and lowering the centre of mass. This was shown to immediately reduce shear forces and resulting wear on the tires and, due to the lowering of the center of mass, it is expected to have a beneficial effect in reducing the possibility of roll-over during high-speed turning. An improvement to braking has been proposed by placing the wheeled-legs in a sprawled position prior to braking and using the wheel motors to dissipate energy. The third behaviour takes advantage of an inertial measurement unit and the ability to reposition the wheels in order to maintain pitch while ascending and descending slopes.

8.2 Bounding Gait

The work in this thesis conclusively demonstrates that dynamic gaits such as the bound are possible in systems that are not strictly legged. Of particular importance is the fact that a stable, albeit less efficient and repeatable, bounding gait is possible given that the wheels, while actively controlled and not mechanically blocked, rotate a non-negligible amount during the stance phase. This is the first time that such experimental results have been presented in the literature to date.

It is shown here that, in addition to the traditional φ-controller in which touchdown angles uniquely regulate forward speed during the bound, the liftoff angle, φ_{lo}, can be used to adjust forward speed. Because of the smaller variations possible in the φ_{lo} variables and the opposite effect it plays on many gait variables, it is seen as a complementary, fine-tuning control parameter.

Through work on a three-dimensional simulated model of the PAW robot, asymmetrical mass distribution in both Scout II and PAW have been found to be the cause of a slight yaw component visible during bounding of the simulated and real platforms.

8.3 Galloping Gait

This thesis presents the first gallop gaits implemented on non-simulated, engineered systems. Furthermore, it is also significant that all previously-proposed 3D gallop controllers have required a minimum of eight actuated degrees of freedom. The work on Scout II and PAW galloping shows that underactuated galloping can be achieved with leg compliance and only four hip actuators. The rotary gallop gait variant has been demonstrated here on not one, but *two* robots.

The gallop controllers described in this thesis alternately use separate controllers for the front and rear hip pairs (Scout II), as well as four separate controllers for all four individual legs (PAW). In addition, the mechanical design rigidly couples the hips together. This is in stark contrast to Herr's work, whose gallop controller presented in [23] required coupled control of all four legs or Ringrose's gallop controller, presented in [49], which used revolute joints to couple the two hip pairs to the rigid spine of his model.

Although it is possible to achieve a stable rotary gallop gait from a standstill as shown by the author in [28], the most repeatable galloping results have been achieved by transitioning from another gait. In the particular case of Scout II and PAW this has meant starting with a bound and transitioning to a rotary gallop by adding asymmetry to the leg touchdown angles.

One of the most striking results of Scout II's rotary gallop is that the overall result of the gait, which has important pitch and roll characteristics, is to force the robot to yaw. Not only can the robot now yaw by varying hip torque during the stance phase of the bound, [103], but it can also yaw through selection of the touchdown order of its legs during the rotary gallop, as well as by selection of liftoff angles in the φ_{lo}-turn controller. It was found that while the φ_{lo}-turn controller maintained higher forward speed during the yaw than the gallop controller, its yaw rates were more limited.

The relationship found in biology between yaw direction and the "leading" leg is found to also occur in the robots used here. In addition, it was found that the leg directly behind the lead leg consistently compressed more than any other leg. Given that the rear legs tend to compress more than front legs during straight line bounding motion and that this tendency is more apparent during yaw maneuvers it is a recommended that this be considered in future leg designs.

Finally, both the bounding and galloping gaits on Scout II and PAW have been demon-

strated using a minimalist approach, in terms of sensing and actuation, and have resulted in surprisingly stable and repeatable experimental results. The results agree with previously presented simulation work such as that by Herr, [23], in which it has been stated that little sensing and, just as important, no requirement for explicit postural stabilization during the gallop (or the bound, for that matter) is required.

8.4 Recommendations and Future Work

The following is a series of recommendations for work related either specifically to the Scout II and PAW robots or to legged or hybrid wheeled-leg systems, based on the author's experiences in the course of completing the research contained in this thesis.

Regarding the PAW platform's hybrid rolling behaviours, the following recommendations for future work can be made. First, the author believes that PAW can be made more energy-efficient during general rolling. To achieve this, unnecessary electronics hardware would have to be removed and the gains on the wheel and hip motors would need to be reduced in order to reduce the likelihood of current spikes. Second, a more accurate model introduced in Section 5.1.1 and improved coordination between the hip and wheel actuators may improve the accuracy of turning. Third, better, more precise turning may be obtained by using the IMU to obtain a better estimate of the radius of curvature. This may also be helpful in detecting possible roll-over conditions in high-speed turns. Likewise, slope ascent and descent control can be modified to compensate for roll components.

While the bounding gaits performed on both Scout II and PAW demonstrated impressive results, especially considering the underactuated and minimally sensing nature of these robots, there is room for improvement and further exploration. While it has been shown here that bounding can be conducted with actuated wheels, the performance is not as good as with fixed toes. Further study should be conducted to improve the effectiveness of the active wheel control in PAW's bounding gait. As suggested in Section 6.6.2, a study of the usage of PAW's wheels in the detection of leg touchdown for bounding and galloping could prove to be fruitful. As well, further exploration of the leg angle parameter space should be conducted to examine other versions of the bounding gait as well as the pronk. It would be particularly interesting to explore the possible correlation between flight phase type (i.e., extended, gathered) and leg touchdown angles. With some improvements to the current PAW simulation, in line with the model of Scout II used in [18], the above studies could be

explored in simulation prior to execution on the robot. As well, the simulation environment would be ideal to explore the effect of changes that leg length and hip spacing, among other parameters, would have on development of future bounding and galloping gaits.

While the rotary gallop has been shown on both Scout II and PAW, a consistent, repeatable *transverse* gallop has eluded the author. Can this gait be achieved in an underactuated system like Scout II or PAW? A repeatable straight-line gallop with these two platforms has also been difficult to achieve and is a good candidate for further research.

Lastly, a number of acrobatic behaviours were proposed for the PAW platform in [37]. Many of these, such as inverted pendulum rolling and jumping onto obstacles could be attempted on the actual robot.

Appendix A

Glossary

Active Balancing also referred to as *Active Stabilization.* "High-bandwidth" method of control used by Raibert [17] in the 1980's for locomotion which requires that components such as pitch, yaw and roll must be actively controlled in order to ensure that the robot does not fall over, as opposed to "low-bandwidth" self-stabilizing methods by Ringrose [49], Herr [83] and others.

Artiodactyl "An order of the *Ungulata* or hoofed mammals, comprising all those in which the number of the toes is even.... This division includes all the hoofed animals used for human food, and domesticated from time immemorial." [Webster's New Twentieth Century Dictionary of the English Language, Unabridged, 1965]

Balance 1. "Balance maintenance is a central concern for all legged creatures. Balance is largely synonymous with tip-over stability, dynamic stability, and postural stability and it refers to the preservation of *overall rotational stability.*" [108] 2. "there is no mathematically precise definition of balance." [27, p. 4] 3. "Precise and universally accepted definitions of stability that is applicable to the gait and posture of biped robots remain elusive." [108]

Biomimesis, also known as *biomimetics.* To mimic life, to imitate biological systems, [110].

Biomimesis, Functional, also known as *functional morphology.* Capturing the fundamental function of an organism without copying its morphology, [111].

Biomimesis, Morphological, also known as *morphological biomimetics.* Also refer to *Morphology* and *Functional Morphology.* As opposed to the *functional* approach, this design methodology involves copying many of the morphological details regardless of whether there are any task-oriented functional advantages.

Body Path Stability 1. The measure of how closely the robot follows a given trajectory along the ground while also maintaining a gait which is cyclical, with certain bounded variables (performance indices or state variables). 2. "Body stability, body path stability and stationary gait stability ... are among the most pragmatic stability definitions but they refer to the repeatability of a gait pattern in the sense of orbital stability." [108] 3. "... guarantees that the biped robot body returns to its original average velocity after a perturbation." [112] (and see [113]) 4. The type "classically studied in aircraft and missile systems" [113].

Canter A three-beat gait in which a forefoot and a hindfoot contact at the same time.

Cursor, also known as *courser* or *cursorial. Considered here simply to mean a tendency to run. See debate about its usage in [71], [114], and [115]* 1. A runner, from the Latin *cursus*, and related to the French "course" (race). 2. "slender swift-footed ... types in various phyla" Description of ungulates, [116] (First known usage with respect to legged systems) 3. "Cursorial mammals are those terrestrial quadrupeds that possess vertically-[oriented limbs which move in a parasagittal plane, regardless of the gait being employed." (Incomplete (proposed) definition)[114] 4. " Cursorial animals typically have a narrow stance relative to the height of their center of gravity. This narrow stance gives less inherent stability and more maneuverability. Most quadrupedal mammals having a mass above 5 kg (e.g. the horse (Equus) and dog (Canus)) are of this type. With few exceptions (e.g. the elephant (Hutchinson et al. 2003), etc.), cursorial animals transition from walk to trot to gallop as speed increases (Hoyt and Taylor 1981, Heglund, Taylor and McMahon 1974)." '[69] 5. "It is a fact that the body plans of cursorial mammals universally include placement of the center of mass closer to the line of the shoulders than the line of the hips" [117]

Dimensionless Moment of Inertia "Karl Murphy discovered that the distribution of mass in the body can have a profound influence on the behavior of a running system." [17] 1. $j = \frac{J}{md^2}$ where J is the moment of inertia of the body, m is the mass of the body, and d is half the hip spacing. [17] Note: this is effective in the sagittal plane only. 2. "is a measure of how much the body rotates versus how much it accelerates upward when a vertical force is applied to the hip. When $j < 1$, the body rotates more easily than when $j > 1$." [57, p. 70] 3. "Murphy found that when $j < 1$ the attitude of the body can be passively stabilized in a bounding gait. When $j > 1$, stabilization is not so easily obtained." [17]

Distal 1. Further from the heart, [118]. 2. On legged robots this is refers to the portion of the leg that is furthest from the hip, as well as the body. For instance, the foot is at the distal end of the leg.

Duty Cycle also known as *duty factor.* "of a foot is the fraction of the duration of the stride for which it is on the ground." [119]

Dynamic Stability Within the context of legged locomotion, the ability of characteristic state variables of the system (e.g., body pitch) to return to steady-state periodic motion (e.g. a bound or gallop gait) after the application of perturbations. In addition, the system often has marginal static stability, that is, the ground-projected COM falls close to the boundaries of the support polygon formed by the legs which are in contact with the ground. [50].

Extended Flight During the flight phase the front legs point forward, while the rear legs point backwards, as opposed to the "gathered" or "flexed" phase, in which the legs are pointed in the opposite direction and are found under the body, [79].

Flexed Flight see *gathered flight.*

Four Beat For a given stride four unique ground contacts are distinguishable. In quadrupeds the transverse and rotary gallops, as well as the toelt are four-beat gaits. Refers to the sound made during ground impact in running or walking.

Functional Morphology, see *Biomimesis, Functional.* The approach taken to design in which the mechanism which is to accomplish a particular goal captures the most important task-oriented features of a biological analogue. For instance, in quadrupedal robots such as Scout II the running task can be accomplished without the use of an ankle, therefore no ankle is used.

Gait Stability or *stationary gait stability.* Possibly the first mention of the term can be found in [113] 1. "Suppose that a given *stationary gait* has k continuous charcterisitic parameters. These parameters represent a point g_0 in k space. If the gait is 'stationary,' this point does not move from cycle to cycle. When the system is disturbed, this point moves to a new point g_1 in k space. Then after n steps, if the point g_n approaches g_0 in k space, stability results." [113] 2."... implies that the characteristic features of a gait, represented by a parameter vector, remain within a volume in the parameter space." [112] (and see [113] and [120])

Gathered Flight During the flight phase legs are placed under the body, with the rear legs pointing forwards and the front legs pointing backwards, as opposed to "extended flight" in which the front legs point forward and the rear legs point backwards, away from the body, [79].

Lateral 1. Away from the midline, [118]. 2. On the Scout II and PAW robots the right and left legs in the front form the front lateral leg pair. Likewise, the right and left legs in the rear form the rear lateral leg pair.

Limit Cycle *see related entries: return and Poincaré maps.* A sustained oscillation with "asymptotically stable closed trajectories on a phase plane", [121].

Locomotion "Locomotion results from complex, high-dimensional, non-linear, dynamically coupled interactions between an organism and its environment." [122]

Manoeuvrability "the capacity for rapid and controlled change of speed and direction." [38]

Moment of Inertia, Dimensionless See *Dimensionless Moment of Inertia*

Morphology

The branch of biology that deals with the form and structure of organisms without consideration of function. [123]

Morphology, Functional See *functional morphology*

Natural Dynamics see *passive dynamics*

One Beat For a given stride one unique ground contact is distinguishable. In quadrupeds the pronk is a one-beat gait. Refers to the sound made during ground impact in running or walking.

Passive Dynamics Also referred to as *natural dynamics* or *mechanical intelligence.* Running can be made to be energy efficient if the actuation serves to enhance the passive dynamics of the system. 1. The unforced response of a system under a set of initial conditions. 2. "We believe that the mechanical system has a mind of its own, governed by the physical structure and laws of physics. Rather than issuing commands, the nervous system can only make suggestions, which are reconciled with the physics of the system and task [at hand]" [124]

Parasagittal Plane as opposed to the *sagittal plane.* The vertical plane which is parallel to the *sagittal plane* but does is not equal to it. In other words, it is any vertical plane which runs parallel to, but is offset from, the sagittal plane. Used by Gambaryan, [66], to describe the plane along which legs on animals move during protraction and retraction.

Period One Gait A gait in which the limit cycle converges on one orbit. From one stride to the next the gait is the same.

Period Two Gait A gait in which the limit cycle alternates between two orbits. The gait alternates between one type and another, such as bounding in one stride and pronking in the next.

Phase Plot or *phase plane plot.* Refer to *phase portrait* and *Poincaré map.*

Phase Portrait see also *Poincaré Map.* 1. A plot of trajectories in state space. Use instead of, or to complement, a time domain plot. 2. A two-dimensional diagram used when analyzing periodic motions. Often, the vertical axis is the variable of interest (e.g. body height, hip angle, etc.) and the horizontal axis is time. It is often useful to add points of reference indicating events of interest on the curves such as (in the case of legged locomotion) *liftoff* and *touchdown.* Examples can be found in [125, p. 68] 3. In other cases, the vertical axis (y-axis) is the derivative of the horizontal axis (x-axis) variable. A reference event (impact, apex height during flight, etc.) is denoted by a circle along the curve. In a stable system which results in an orbit-like plot these points are clustered together.

Poincaré Map also known as a *return Map* or (specifically in legged locomotion) a *stride function.* Good explanation specific to legged locomotion in [47, p. 63] "An important conceptual tool for understanding the stability of periodic orbits is the Poincaré map,[[126], [127], [128]]. It replaces an n^{th} order continuous time autonomous system by an $n-1$ th order discrete-time system. The problem of studying the stability properties of a periodic solution of a continuous-time system is thus reduced to the problem of studying the stability of the periodic points of the Poincaré map. In the context of dynamically stable legged systems one can also find the terms stride function, [[129]], or return map, [[130]]. In order to define the return map for a legged system a reference point in the cyclic motion must be selected and then the dynamic equations must be integrated starting from that point until the next cycle. It should be mentioned here that integrating the equations of motion for a legged robot is not a trivial step (as for most real systems). Analytical integration of the dynamics is usually not possible, except for very simple cases. On the other hand, using numerical methods inevitably leads to loss of insight, which is extremely important for identifying which parameters affect the motion of the system. In trying to cope with that problem, many authors use simple mathematical models of the robot, which capture the basic properties that are dominant in the behaviour of the system, e.g. [[131]], [[130]], or they use perturbation techniques to analytically approximate a solution, e.g. [[132]], [[133]]. " [47]

Postural Stability 1. Maintaining the body aligned with the vertical (gravitational) axis. [134] 2. Essentially, the task is to maintain the vertical axis of the body aligned with the gravitational vector; it is an inverted pendulum task.

Preflex as opposed to *reflex.* 1. Actions taken by a system due to its passive (natural) dynamics in response to external perturbations. 2. The reaction of a system due to its passive dynamics is referred to as a "preflex". Depending on the design these preflexes will be enough to keep the system in steady state motion. "Reflexes" are actions undertaken due to sensor-based feedback from the environment are of use in situations

where steady-state operation is not desired, due to maneuvering requirements, large external perturbations, etc. [33]

Protraction As opposed to *retraction.* Raibert refers to this as the "recovery" stage of leg motion. 1. Motion of leg along the *Sagittal* and *Parasagittal* planes, from the back of the animal or robot to the front. Generally, the leg is in the *flight phase* during this motion. 2. Parallel to *Retraction* and perpendicular to *Adduction* and *Abduction.*

Relative Phase "of a foot is the stage of the stride at which it is set down, expressed as a fraction of the duration of the stride following the setting down of an arbitrarily chosen reference foot."[119]

Reflex as opposed to *preflex.* The reaction of a system due to its passive dynamics is referred to as a "preflex". Depending on the design these preflexes will be enough to keep the system in steady state motion. "Reflexes" are actions undertaken due to sensor-based feedback from the environment are of use in situations where steady-state operation is not desired, due to maneuvering requirements, large external perturbations, etc. [33]

Retraction As opposed to *protraction.* Motion of leg along the *sagittal* and *parasagittal* planes, from the front of the animal or robot to the back. Generally, the leg is in the *stance phase* during this motion.

Return Map also known (generally) as a *Poincaré Map* or (specifically in legged locomotion) a *stride function* an alternative name for a *Poincaré map.*

Robust *With respect to control and stability.* Robust: relatively insensitive to disturbances/perturbations.

Running defined by examining exchange between potential and kinetic and not by an aerial phase. 1. "Running or bouncing gaits can be defined by the timing of the mechanical energy fluctuations of the center of mass. During running and trotting gaits horizontal kinetic and gravitational potential energy fluctuations of the center of mass occur in phase" [135, citing Cavagna 1975; Cavagna et al 1976, 1977] 2. "It is important to emphasize that the presence of an aerial phase [for the body] is not necessary for a gait to be classified as a run. The aerial phase of human runners can be reduced to zero by increasing the compliance of the legs (McMahon, 1985; McMahon et al. 1987)." [135]. 3. A gait with a step duty cycle of less than 50%, [38]. McMahon's definition, based on Cavagna's work may not contradict this. 4. "A better criterion[1] for distinguishing between walking and running is the one put forward by

[1]A better criterion than "in running, all feet are in the air at some point in the gait cycle, whereas in walking there is always at least one foot on the ground"

Cavagna et al. (1976). On the basis of observations in humans, they pointed out that in walking, the center of mass is highest in mid-step, when the hip of the stance leg passes over the ankle. In running, by comparison, the center of mass is lowest at mid-step. Thus in walking but not in running, gravitational potential energy is stored in the first half of the walking step as the center of mass rises, and returned in the form of kinetic energy during the second half of the step as the center of mass falls." [40] 5. "The most readily apparent difference between walking and running is the fact that running usually includes an aerial phase, a period when both feet are off the ground. Whether an animal runs on two legs or four, the fraction of one stride cycle occupied by the aerial phase generally increases with speed. A quite different criterion [based on Cavagna's work and which McMahon favours] for distinguishing between walking and running is based on the contact [i.e. stance] phase.... [In] **walking**, the center of mass of the whole body reaches its greatest height above the ground near midstance, the time that the hip of the weight-bearing leg passes over the ankle. The forward velocity of the body is lowest at this moment, and calculations show that the total mechanical energy of the center of mass, including both the gravitational potential energy and the forward kinetic energy, changes little during the period when the swing leg is moving forward (2).[In] **running**, the center of mass reaches its lowest point near midstance, just as the forward velocity is lowest. As a consequence, the total mechanical energy of the body goes through large fluctuations during a contact period." [136] 6. Raibert defines running as requiring ballistic flight in [17, p. 14]: "Running is a special form of legged locomotion that uses ballistic flight phases [of the body] to obtain high speed." *McMahon, etc. don't agree because of exceptions to this rule, like Groucho running*

Sagittal Plane 1. The vertical plane which coincides with the axis of the spine of a vertebrate animal. 2. Divides left and right, [118].

Self Stabilizing as opposed to *active balancing.* Robert Ringrose's work is an example of self-stability while Marc Raibert's robots were active balancers. 1. In legged locomotion the system is inherently stable and needs no sensing to reject minor perturbations. 2. "With proper design the structure and motion of a robot can automatically cause it to recover from minor disturbances even if it cannot detect them." [49]

Specific Resistance As discussed in [18] there are two types of specific resistance: "consumed" based on the power consumed by the system, and "applied" which is based on the power directly applied at the joints to generate motion. $\varepsilon(v) \equiv \frac{P(v)}{mgv}$ where P is the power expenditure, m is the mass of the vehicle , g is the gravitational acceleration constant and v is the vehicle speed.

Stability 1. The robustness of a given outcome to small changes in initial conditions or small random fluctuations. Chaos is an example of a process which is not stable.

[137] 2. A physical system ... is said to be stable if it returns to a stationary state under pertubations of sufficiently small magnitude. It is said to be totally stable if it returns to a stationry state from arbitrary perturbations. [138]

Stable Oscillation ... oscillations that tend toward fixed and well-defined limiting positions are stable oscillations. [138]

Static 1. Common: "stationary; not acting or changing" [139] 2. Physics: "concerned with bodies at rest or forces in equilibrium" [139]

Strain Deformation of a physical body under the action of applied forces. Springs do this.

Stride "is a complete set of leg movements, for example, from the setting down of a particular foot to the next setting down of the same foot."[119]

Stride Cycle also known as the *stride period* "is the time from one foot strike until the next strike of the same foot."[25]

Stride Function see also *Poincaré map* or *return map* 1. "A very useful and classical tool to study the existence and stability of periodic orbits is the Poincaré map or return map, which, in the context of legged locomotion, is also called the stride function. Since the initial work of Koditschek and Buehler, ... a number of authors have used this tool to study the properties of the vertical and forward dynamics of simplified models of monopods, e.g. ... where they demonstrated emergent behaviours that corresponded to animal gaits." [47] 2. "The 'stride function' (McGeer, 1992) is a Poincaré map relating the state during one part of a step with the state during the same part of the next step." [140]

Stride Frequency "is the number of strides taken in unit time."[119]

Stride Length "is the distance traveled in a stride. Thus, mean speed is stride length multiplied by stride frequency."[119]

Stride Period see *Stride Cycle*

Sweep Limit The angle of the hip with respect to the body, φ_{swl}, at which the leg stops until the end of the stance phase. This brake angle limit is used on underactuated robots such as Scout II and PAW in order to allow sufficient vertical leg extension prior to leg takeoff so that the toes clear the ground during protraction. This generally synonymous with takeoff angle, φ_{to} since the leg is to be held at the sweep limit until the leg lifts off the ground.

Three Beat For a given stride only three unique ground contacts are distinguishable. In quadrupeds the canter and the half-bound are three-beat gaits. Refers to the sound made during ground impact in running or walking.

Toelt A four-beat gait similar to the rotary and transverse gallops. See diagram in [119, p. 51] where it is referred to as the "amble".

Two Beat For a given stride only two unique ground contacts are distinguishable. Bipedal running is two beat, as is quadrupedal pacing, trotting and bounding. Refers to the sound made during ground impact in running or walking.

Underactuated The system contains more degrees of freedom (the minimum number of coordinates required to fully describe the configuration of the system) than actuators. The Acrobot, a double pendulum with an actuator applied to the second joint is an example of an underactuated system, [141].

Variable Structure, 1. *E*quations of motion vary due as the structure of the robot (manipulator, wheeled-mobile or legged-mobile) changes from one type of kinematic chain to another. 2."systems characterized by different mathematical descriptions in non-overlapping regions of the state space." [125]

Vestibular Relating to the inner ear. In the context of legged locomotion this is a reference to the sensors in the inner ear that are responsible for balance. In robots, the analogue would be a combination of gyroscopes (rotational sensors).

References

[1] M. G. Bekker, *Introduction to terrain-vehicle systems.* Ann Arbour, MI, USA: University of Michigan Press, 1969.

[2] J. Y. Wong, *Theory of Ground Vehicles.* New York, New York, USA: John Wiley, 3rd ed., 2001.

[3] C. Smith, *Tune to Win.* Motorbooks International, 1978.

[4] K. Iagnemma and S. Dubowsky, *Mobile Robots in Rough Terrain Estimation, Motion Planning, and Control with Application to Planetary Rovers*, vol. 12 of *Springer Tracts in Advanced Robotics.* New York, USA: Springer, 2004.

[5] B. L. Digney and S. Penzes, "Robotic concepts for urban operations," in *Proceedings of SPIE, Unmanned Ground Vehicle Technology IV* (D. W. G. Grant R. Gerhart, Chuck M. Shoemaker, ed.), vol. 4715, pp. 63 – 74, 2002.

[6] B. McBride, R. Longoria, and E. Krotkov, "Measurement and prediction of the off-road mobility of small robotic ground vehicles," in *The 3rd Performance Metrics for Intelligent Systems Workshop (PerMIS'03)*, (Gaithersburg, MD, USA), National Institute of Standards and Technology, 2003.

[7] T. Frost, C. Norman, S. Pratt, B. Yamauchi, B. McBride, and G. Peri, "Derived performance metrics and measurements compared to field experience for the packbot," in *Measuring the Performance and Intelligence of Systems: Proceedings of the 2002 PerMIS Workshop*, National Institute of Standards and Technology, August 2002.

[8] C. Grand, F. Benamar, F. Plumet, and P. Bidaud, "Stability and traction optimization of a reconfigurable wheel-legged robot," *International Journal of Robotics Research*, vol. 233, no. 10-11, pp. 1041–1058, 2004.

[9] A. Mishkin, *Sojourner: An Insider's View of the Mars Pathfinder Mission.* Berkley Publishing Group, 2003.

[10] I. Montpetit and P. Tonietto, "Robots agiles," *Decouverte (Radio-Canada)*, October 2003.

[11] G. Endo and S. Hirose, "Study on Roller-Walker (multi-mode steering control and self-contained locomotion)," in *Proceedings of the IEEE International Conference on Robotics and Automation, 2000.*, (San Francisco, CA, USA), pp. 2808 – 2814, 2000.

[12] T. Estier, Y. Crausaz, B. Merminod, M. Lauria, R. Piguet, and R. Siegwart, "An innovative space rover with extended climbing abilities," in *Proceedings of Space and Robotics 2000*, (Albuquerque, USA), 2000.

[13] S. Hirose, *Experimental Robotics VII*, ch. Super mechano-system: new perspective for versatile robotic system, pp. 281–289. Berlin: Springer-Verlag, 2001.

[14] S.-M. Song and K. J. Waldron, *Machines That Walk: The Adaptive Suspension Vehicle.* Cambridge, Massachusetts: MIT Press, 1989.

[15] J. Bares and D. Wettergreen, "Dante II: Technical description, results and lessons learned," *International Journal of Robotics Research*, vol. 18, pp. 621–649, July 1999.

[16] M. Fujita, "AIBO: Toward the era of digital creatures," *International Journal of Robotics Research*, vol. 20, October 2001.

[17] M. Raibert, *Legged Robots That Balance.* Cambridge, MA, USA: The MIT Press, 1986.

[18] I. Poulakakis, J. A. Smith, and M. Buehler, "Modeling and experiments of untethered quadrupedal running with a bounding gait: The Scout II Robot," *International Journal of Robotics Research*, vol. 24, pp. 239–256, April 2005.

[19] S. Talebi, I. Poulakakis, E. Papadopoulos, and M. Buehler, *Experimental Robotics VII*, ch. Quadruped Robot Running with a Bounding Gait, pp. 281–289. Lecture Notes in Control and Information Sciences, Springer-Verlag, 2001.

[20] D. F. Hoyt and C. R. Taylor, "Gait and the energetics of locomotion in horses," *Nature*, 1981.

[21] M. Hildebrand, "Analysis of asymmetrical gaits," *Journal of Mammalogy*, vol. 58, pp. 131–156, May 1977.

[22] D. P. Krasny, *Evolving Dynamic Maneuvers in a Quadruped Robot.* PhD thesis, Ohio State University, Columbus, Ohio, USA, 2005.

[23] H. M. Herr and T. A. McMahon, "A galloping horse model," *International Journal of Robotics Research*, 2001.

[24] D. W. Marhefka and D. E. Orin, "Fuzzy control of quadrupedal running," in *Proceedings of IEEE International Conference on Robotics and Automation*, (San Francisco, CA), pp. 3063–3069, IEEE International Conference on Robotics and Automation, April 2000.

[25] T. McMahon, "The role of compliance in mammalian running gaits," *Journal of Experimental Biology*, vol. 115, pp. 263–282, 1985.

[26] J. Schmiedeler, *The Mechanics of and Robotic Design for Quadrupedal Galloping.* PhD thesis, The Ohio State University, 2001.

[27] P. Nanua, *Dynamics of a Galloping Quadruped.* PhD thesis, Ohio State University, 1992.

[28] I. Poulakakis, J. A. Smith, and M. Buehler, "On the dynamics of bounding and extensions towards the half-bound and the gallop gaits," in *Proceedings of the 2nd International Symposium on Adaptive Motion of Animals and Machines (AMAM)*, (Kyoto, Japan), pp. 453–458, March 2003.

[29] J. A. Smith and I. Poulakakis, "Rotary gallop in the untethered quadrupedal robot Scout II," in *Proceedings of the 2004 IEEE/RSJ International Conference on Intelligent Robots and Systems (IROS)*, (Sendai, Japan), October 2004.

[30] M. Kanellos, "From medicine to military, machines finally arrive," *CNET News.com*, March 2004. `http://news.com.com/Invasion+of+the+robots/2009-1040_3-5171948.html`.

[31] A. Martin-Alvarez, J. Hillebrand, W. De Peuter, P. Putz, A. Matthyssen, and J. de Weerd, "Walking robots for planetary exploration missions," in *Intelligent Automation and Control: Recent Trends in Development and Applications*, (Montpellier, France), pp. 7–14, WAC'96, Second World Automation Congress, 1996.

[32] T. Steadter, "Robots rolls on rimless wheels," *Discovery News*, October 2005. `http://dsc.discovery.com/news/briefs/20051031/tech_robot_print.html`.

[33] E. Klavins, H. Komsuoglu, R. J. Full, and D. E. Koditschek, "The role of reflexes versus central pattern generators in dynamical legged locomotion," in *Neurotechnology for Biomimetic Robots* (J. Ayers, J. L. Davis, and A. Rudolph, eds.), pp. 351–382, MIT Press, 2002.

[34] U. Saranli, M. Buehler, and D. E. Koditschek, "RHex: A simple and highly mobile hexapod robot," *Int. Journal of Robotics Research*, vol. 20, no. 7, pp. 616–631, 2001.

[35] C. Prahacs, A. Saunders, M. K. Smith, D. McMordie, and M. Buehler, "Towards legged amphibious mobile robotics," in *The Inaugural Canadian Design Engineering Network (CDEN) Design Conference*, (Montreal, Quebec, Canada), July 2004.

[36] K. Automn, M. Buehler, M. Cutkosky, R. S. Fearing, R. J. Full, D. Goldman, R. Groff, W. Provancher, A. A. Rizzi, U. Saranli, A. Saunders, and D. E. Koditschek, "Robotics in scansorial environments," in *Proceedings of SPIE Vol. 5804* (D. W. G. Grant R. Gerhart, Charles M. Shoemaker, ed.), pp. 291–302, 2005.

[37] C. Steeves, "Design and behavioural control of a dynamic quadruped with active wheels," Master's thesis, McGill University, November 2002.

[38] M. Hildebrand, *Functional Vertebrate Morphology*, ch. Walking and Running, pp. 38–57. Cambridge, Massachusetts: Harvard University Press, 1985.

[39] R. M. Alexander, "Three uses for springs in legged locomotion," *International Journal of Robotics Research*, vol. 9, no. 2, 1990.

[40] T. A. McMahon and G. C. Cheng, "The mechanics of running: How does stiffness couple with speed?," *Journal of Biomechanics*, vol. 23, no. Suppl. 1, pp. 65 – 78, 1990.

[41] G. A. Cavagna, H. Thys, and A. Zamboni, "The sources of external work in level walking and running," *The Journal of Physiology*, vol. 262, no. 3, pp. 639–657, 1976.

[42] T. Mitchell, *Machine Learning.* Boston, Massachusetts, USA: McGraw-Hill, 1997.

[43] K. Yoneda and Y. Ota, "Non-bio-mimetic walkers," *International Journal of Robotics Research*, vol. 22, no. 3-4, pp. 241–249, 2003.

[44] E. Thomson, "MIT lab creates robotic dinosaur," *Robotics Online*, 2002. `http://www.roboticsonline.com/public/articles/archivedetails.cfm?id=392%`.

[45] R. Blickhan, "The spring-mass model for running and hopping," *Journal of Biomechanics*, vol. 22, pp. 1217–1227, 1989.

[46] M. Ahmadi and M. Buehler, "The ARL Monopod II running robot: Control and energetics," in *IEEE Int. Conf. Robotics and Automation*, (Detroit, Michigan, USA), pp. 1689–1694, May 1999.

[47] I. Poulakakis, "On the passive dynamics of quadrupedal running," Master's thesis, McGill University, Montréal, Québec, Canada, July 2002.

[48] U. Saranli, *Dynamic Locomotion with a Hexapod Robot.* PhD thesis, University of Michigan, Ann Arbour, 2002.

[49] R. Ringrose, *Self-Stabilizing Running.* PhD thesis, MIT, 1996.

[50] R. J. Full, T. Kubow, J. Schmitt, P. Holmes, and D. Koditschek, "Quantifying dynamic stability and maneuverability in legged locomotion," *Integ. and Comp. Biol.*, vol. 42, pp. 149–157, 2002.

[51] I. Sutherland and M. Ullner, "Footprints in the asphalt," *International Journal of Robotics Research*, vol. 3, no. 2, 1984.

[52] J. Furusho, A. Sano, M. Sakaguchi, and E. Koizumi, "Realization of bounce gait in the quadruped robot with articular-joint-type legs," in *Proceedings of the IEEE International Conference on Robotics and Automation*, (Nagoya, Japan), pp. pp. 697–702, 1995.

[53] H. Kimura, S. Akiyama, and K. Sakurama, "Realization of dynamic walking and running of the quadruped using neural osciallator," *Autonomous Robots*, vol. 72, no. 3, pp. 247–258, 1999.

[54] J. G. Nichol and K. J. Waldron, "Biomimetic leg design for untethered quadruped gallop," in *Proceedings of the International Conference on Climbing and Walking Robots (CLAWAR)*, (Paris, France), pp. 49–54, September 2002.

[55] S. Kirsner, "They're robots? those beasts!," *The New York Times*, September 16 2004. `http://www.nytimes.com/2004/09/16/technology/circuits/16robo.html?ex=12%53073600&en=b5c3b3d3ce4bfeba&ei=5088&partner=rssnyt`.

[56] F. Iida, G. J. Gomez, and R. Pfeifer, "Exploiting body dynamics for controlling a running quadruped robot," in *Proceedings of the 12th International Conference on Advanced Robotics (ICAR05)*, (Seattle, WA, USA), pp. 229–235, July 2005.

[57] M. H. Raibert, H. B. Brown, M. Chepponis, J. Hodgins, J. Kroechling, J. Miller, K. N. Murphy, S. S. Murthy, and A. Stentz, "Dynamically stable legged locomotion," Tech. Rep. CMU-LL-4-1985, The Robotics Institute, Carnegie Mellon University, Pittsburgh, PA, 1985.

[58] M. D. Berkemeier, "Modeling the dynamics of quadrupedal running," *International Journal of Robotics Research*, vol. 17, no. 9, pp. 971–985, 1998.

[59] I. Poulakakis, E. Papadopoulos, and M. Buehler, "On the stable passive dynamics of quadrupedal running," in *Proceedings of the IEEE International Conference on Robotics and Automation (ICRA) 2003.*, pp. 1368–1373, 2003.

[60] J. Schmiedeler and K. Waldron, "The mechanics of quadrupedal galloping and the future of legged vehicles," *International Journal of Robotics Research*, vol. 18, pp. 1224–1234, December 1999.

[61] A. Formalsky, C. Chevallereau, and B. Perrin, "On ballistic walking locomotion of a quadruped," *International Journal of Robotics Research*, vol. 19, no. 8, pp. 743–761, 2000.

[62] P. S. Freeman and D. E. Orin, "Efficient dynamic simulation of a quadruped using a decoupled tree-structure approach," *International Journal of Robotics Research*, vol. 10, no. 6, pp. 619–627, 1991.

[63] L. R. Palmer and D. E. Orin, "3D control of a high-speed quadruped trot," *Industrial Robot*, vol. 33, no. 4, 2006.

[64] M. H. Raibert, H. Brown, M. Chepponis, E. Hastings, J. Koechling, K. N. Murphy, S. S. Murthy, and A. Stentz, "Dynamically stable legged locomotion progress report: October 1982 - october 1983," Tech. Rep. CMU-RI-TR-83-20, Robotics Institute, Carnegie Mellon University, Pittsburgh, PA, 1983.

[65] J. G. Nichol and K. J. Waldron, "Biomimetic leg design for untethered quadruped gallop," 2002.

[66] P. P. Gambaryan, *How Mammals Run – Anatomical Adaptations.* John Wiley & Sons, 1974.

[67] M. Gates and A. Barber, "The tolt," *ToltNews.com*, February 2003. `http://www.toltnews.com/aboutice.html`.

[68] S. Renous, J.-P. Gasc, V. L. Bels, and R. Wicker, "Asymmetrical gaits of juvenile crocodylus johnstoni, galloping australian crocodiles," *Journal of Zoology*, vol. 256, pp. 311–325, 2002.

[69] J. G. Nichol, L. R. Palmer, S. P. N. Singh, D. E. Orin, and D. E. Waldron, "System design of a quadrupedal galloping machine," *International Journal of Robotics Research*, vol. 23, no. 10-11, pp. 1013–1027, 2004.

[70] D. P. Krasny and D. E. Orin, "Generating high-speed dynamic running gaits in a quadruped robot using an evolutionary search," *IEEE Transactions on Systems, Man and Cybernetics, Part B*, vol. 34, pp. 1685–1696, August 2004.

[71] M. T. Carrano, "What, if anything, is a cursor? categories versus continua for determining locomotor habit in mammals and dinosaurs," *Journal of Zoology*, vol. 247, pp. 29–42, 1999.

[72] J. P. Schmiedeler, D. W. Marhefka, D. E. Orin, and K. J. Waldron, "A study of quadruped gallops," in *Proceedings of 2001 NSF Design, Service, and Manufacturing Grantees and Research Conference*, (Tampa, FL), NSF Design, Service, and Manufacturing Grantees and Research, January 2001.

[73] R. M. Alexander, *Elastic Mechanisms in Animal Movement.* Cambridge University Press, 1988.

[74] E. Muybridge, *Animals in Motion.* Dover Publications, 1957.

[75] I. Halvorsen, "The sleipnir runestone," *Runes, Alphabet of Mystery*, August 2002. `http://www.sunnyway.com/runes/sleipnir.html`.

[76] J. R. Duffy, "Icelandic horse connection, gaits of the icelandic horse," *Icelandic Horse Connection*, February 2001. `http://gaits.iceryder.net/`.

[77] B. Firman, "Paso fino - the world of paso fino horses on paso pedigree.com," January 2005 (visited URL). `http://www.pasopedigree.com/Articles/LargoPorFavor.html`.

[78] M. Ashley-Ross, "Introduction to locomotion (walking and running I)," No date available. `http://www.wfu.edu/~rossma/bio322/locomotion1.ppt` (Classroom presentation).

[79] M. Hildebrand, "Motions of the running cheetah and horse," *Journal of Mammalogy*, vol. 40, pp. 481–495, November 1959.

[80] D. W. Marhefka, D. E. Orin, J. P. Schmiedeler, and K. J. Waldron, "Intelligent control of quadruped gallops," *IEEE/ASME Transactions on Mechatronics*, vol. 8, pp. 446 – 456, December 2003.

[81] R. Ringrose, "Self-stabilizing running," in *Proceedings of the 1997 IEEE International Conference on Robotics & Automation*, (Albuquerque, NM, USA), pp. 487–493, 1997.

[82] D. P. Krasny and D. E. Orin, "Evolution of dynamic maneuvers in a 3d galloping quadruped robot," in *IEEE International Conference on Robotics and Automation (ICRA)*, (Orlando, FL, USA), May 2006.

[83] H. Herr, *A Model of Mammalian Quadrupedal Running.* PhD thesis, Harvard University, Cambridge, MA, USA, January 1998.

[84] R. Battaglia, "Design of the scout ii quadruped with preliminary stair climbing," Master's thesis, McGill University, May 1999.

[85] J. A. Smith and I. Sharf, *The PAW v.2.1 User Manual.* McGill University, Montreal, Quebec, Canada, November 2005.

[86] M. de Lasa, "Dynamic compliant walking of the scout ii quadruped," Master's thesis, McGill University, 2000.

[87] S. Talebi, "Compliant running and step climbing of the Scout II platform," Master's thesis, McGill University, Montreal, Quebec, Canada, November 2000.

[88] D. Papadopoulos and M. Buehler, "Stable running in a quadruped robot with compliant legs," in *Proceedings of the 2000 International Conference on Robotics and Automation (ICRA)*, (San Francisco, California, USA), pp. 444 – 449, 2000.

[89] Anonymous, *Maxon Motor High Precision Drives and Systems (Catalogue).* Burlingame, California, USA: Maxon Precision Motors, Inc., 2001.

[90] Anonymous, *Maxon Motor Components and Systems (Catalogue).* Burlingame, California, USA: Maxon Precision Motors, Inc., 1997 - 1998.

[91] D. McMordie, "Towards pronking with a hexapod robot," Master's thesis, McGill University, Montreal, Quebec, Canada, July 2002.

[92] J. Angeles, *Fundamentals of Robotic Mechanical Systems - Theory, Methods, and Algorithms.* Springer-Verlag, second ed., June 2002.

[93] D. McMordie, C. Prahacs, and M. Buehler, "Towards a dynamic actuator model for a hexapod robot," in *Proceedings of the International Conference on Robotics and Automation*, (Taipei, Taiwan), pp. 1386 – 1390, September 2003.

[94] C. Steeves, M. Buehler, and S. Penzes, "Dynamic behaviors for a hybrid leg-wheel mobile platform," in *Proceedings of SPIE Vol. 4715*, (Orlando, FL, USA), pp. 75–86, April 2002.

[95] Anonymous, *Material Contact Properties (ADAMS Solver).* MSC.ADAMS, 2004. `http://ti.mb.fh-osnabrueck.de/adamshelp/solver/f_hlp/subtopics/contact_%material_properties.htm`.

[96] Anonymous, *MSC.ADAMS ADAMS/View Solver Settings - Dynamic.* MSC.ADAMS, 2004. `http://ti.mb.fh-osnabrueck.de/adamshelp/view/view_hlp/newstart.html?sim%_set_panel_dynamic.htm~mainFrame`.

[97] S. Kim, J. E. Clark, and M. R. Cutkosky, "iSprawl: Design and tuning for high-speed autonomous open-loop running," *The International Journal of Robotics Research*, vol. 25, pp. 903 – 912, September 2006.

[98] N. Neville, "Bipedal running with one actuator per leg," Master's thesis, McGill University, Montreal, Quebec, Canada, October 2005.

[99] G. Gabrielli and T. H. von Karman, "What price speed?: specific power required for propulsion of vehicles," *Mechanical Engineering*, vol. 72, no. 10, pp. 775–781, 1950.

[100] J. Yong, R. Smith, L. Hatano, and S. Hillmansen, "What price speed - revisited," *Ingenia*, vol. 22, pp. 46 – 51, March 2005.

[101] R. M. Alexander, "Models and the scaling of energy costs for locomotion," *The Journal of Experimental Biology*, vol. 208, pp. 1645 – 1652, 2005.

[102] D. J. M. Sampson, *Active Roll Control of Articulated Heavy Vehicles.* PhD thesis, University of Cambridge, 2000.

[103] D. Papadopoulos, "Stable running for a quadruped robot with compliant legs," Master's thesis, McGill University, Montreal, Quebec, Canada, April 2000.

[104] M. Raibert, "Trotting, pacing and bounding by a quadruped robot," *Journal of Biomechanics*, vol. 23, pp. 79–90, 1990.

[105] T. A. McMahon, *Muscles, reflexes, and locomotion.* Princeton, N.J., USA: Princeton University Press, 1984.

[106] D. Campbell and M. Buehler, "Preliminary bounding experiments in a dynamic hexapod," in *Experimental Robotics VIII* (B. Siciliano and P. Dario, eds.), vol. 5 of *Springer Tracts in Advanced Robotics*, pp. 612–621, Springer-Verlag, 2003.

[107] R. Altendorfer, D. Koditschek, and P. Holmes, "Stability analysis of legged locomotion models by symmetry factored return maps," *International Journal of Robotics Research*, vol. 23, no. 11, pp. 979–1000, 2004.

[108] A. Goswami and V. Kallem, "Rate of change of angular momentum and balance maintenance of biped robots," in *Proceedings of the 2004 IEEE International Conference on Robotics & Automation*, (New Orleans, LA, USA), 1994.

[109] J. G. Nichol, *Design for Energy Loss and Energy Control in a Galloping Artificial Quadruped.* PhD thesis, Stanford University, July 2005.

[110] M. Cutkosky, "Biomimetic robotics," 1999. `http://www-cdr.stanford.edu/biomimetics/`.

[111] E. Z. Moore, D. McMordie, M. Buehler, U. Saranli, D. E. Koditschek, and R. J. Full, "Design and control of an autonomous hexaped runner," 1999. `http://www.cim.mcgill.ca/research/1999AnnualReport/html/node119.html`.

[112] M. Vukobratovic, A. A. Frank, and D. Juricic, "On the stability of byped locomotion," *IEEE Transactions of Biomedical Engineering*, vol. 17, pp. 25–36, January 1970.

[113] M. Vukobratovic and A. A. Frank, "On the gait stability of biped machines," *IEEE Transactions on Automatic Control*, pp. 678–679, 1970.

[114] B. R. Stein and A. Casinos, "What is a cursorial mammal?," *Journal of Zoology*, vol. 242, pp. 185–192, 1997.

[115] K. Andersson, *Aspects of locomotor evolution in the Carnivora (Mammalia).* PhD thesis, Acta Universitatis Upsaliensis, 2003.

[116] W. K. Gregory, "Notes on the principles of quadrupedal locomotion and of the mechanism of the limbs in hoofed animals," *Annals of the New York Academy of Science*, vol. 22, pp. 267–294, 1912.

[117] K. J. Waldron and J. G. Nichol, "Architectural issues in running machines," in *Proceedings of ROMANSY 2004*, (St-Hubert, Quebec, Canada), June 2004.

[118] Anonymous, "Glossary of terms associated with the footmaxx system," *Clinician's Corner*, 2004. `http://www.footmaxx.com/clinicians/glossary.html`.

[119] R. M. Alexander, "The gaits of bipedal and quadrupedal animals," *International Journal of Robotics Research*, vol. 3, pp. 49–59, Summer 1984. Special Issue: Legged Locomotion.

[120] M. Vukobratovic, "Re: Question about ZMP paper." Personal correspondance, May 2004.

[121] D. Pelinovsky, "Van der pol nonlinear oscillaator," 2002. `http://dmpeli.math.mcmaster.ca/Matlab/CLLsoftware/Vanderpol/Vanderpol.h%tml`.

[122] R. J. Full and D. E. Koditschek, "Templates and anchors: Neuromechanical hypotheses of legged locomotion on land," *J. of Experimental Biology*, vol. 202, pp. 3325–3332, 1999.

[123] Anonymous, "morphology - definitions from dictionary.com," 2006. `http://dictionary.reference.com/browse/morphology`.

[124] M. H. Raibert and J. A. Hodgins, "Legged robots," *Biological Neural Networks in Invertebrate Neuroethology and Robotics*, 1993.

[125] M. Ahmadi, *Stable Control of a One-legged Robot Exploiting Passive Dynamics.* PhD thesis, McGill University, Montreal, Quebec, Canada, 1998.

[126] J. Guckenheimer and P. Holmes, *Nonlinear Oscillations, Dynamical Systems and Bifurcations of Vector Fields.* Springer-Verlag, 1983.

[127] H. Khalil, *Nonlinear Systems.* Prentice Hall, third edition ed., 2001.

[128] Y. Kuznetsov, *Elements of Applied Bifurcation Theory.* New York: Springer-Verlag, 2nd ed., 1998.

[129] T. McGeer, "Passive bipedal running," tech. rep., Simon Fraser University, Centre For Systems Science, Burnaby, B.C., Canada, 1989.

[130] D. Koditschek and M. Buehler, "Analysis of a simplified hopping robot," *International Journal of Robotics Research*, vol. 10, no. 6, pp. 587–605, 1991.

[131] R. M. Ghigliazza, R. Altendorfer, P. Holmes, and K. D. E., "Passively stable conservative locomotion," *SIAM J. of Applied Dynamical Systems*, vol. 2, no. 2, pp. 187–218, 2002.

[132] M. Berkemeier, "A model of quadrupedal running-in-place in the plane," in *Proc. of the IEEE Int. Conf. on Decision and Control*, pp. 3581 – 3586, 1996.

[133] R. T. M'Closkey, J. Burdick, and A. F. Vakakis, "On the periodic motions of simple hopping robots," in *Proc. of the IEEE Int. Conf. on Systems, Man and Cybernetics*, pp. 771 – 777, 1990.

[134] H. Hemami and V. S. Cvetkovic, "Postural stability of two biped models via lyapunov second method," *IEEE Transactions on Automatic Control*, 1977.

[135] R. J. Full and M. S. Tu, "Mechanics of a rapid running insect: Two-, four- and six-legged locomotion," *Journal of Experimental Biology*, vol. 156, pp. 215–231, 1991.

[136] T. A. McMahon, G. Valiant, and E. C. Frederick, "Groucho running," *Journal of Applied Physiology*, vol. 62, pp. 2326–2337, 1987.

[137] E. Weisstein, *CRC Concise Encylopedia of Mathematics.* Chapman and Hall, CRC, second ed., 2002.

[138] James and James, *Mathematics Dictionary.* Chapman & Hall, fifth ed., 1992.

[139] D. Thompson, ed., *The Concise Oxford Dictionary of Current English.* Oxford University Press, ninth edition ed., 1995.

[140] A. L. Schwab and M. Wisse, "Basin of attraction of the simplest walking model," in *Proceedings of DETC'01 ASME 2001 Design Engineering Conferences and Computers and Information in Engineering Conference*, (Pittsburgh, PA, USA), September 2001.

[141] M. Berkemeier and R. S. Fearing, "Tracking fast inverted trajectories of the underactuated acrobot," *IEEE Transactions on Robotics and Automation*, vol. 15, pp. 740 – 750, August 1999.

This has been a Team Smuth Production.